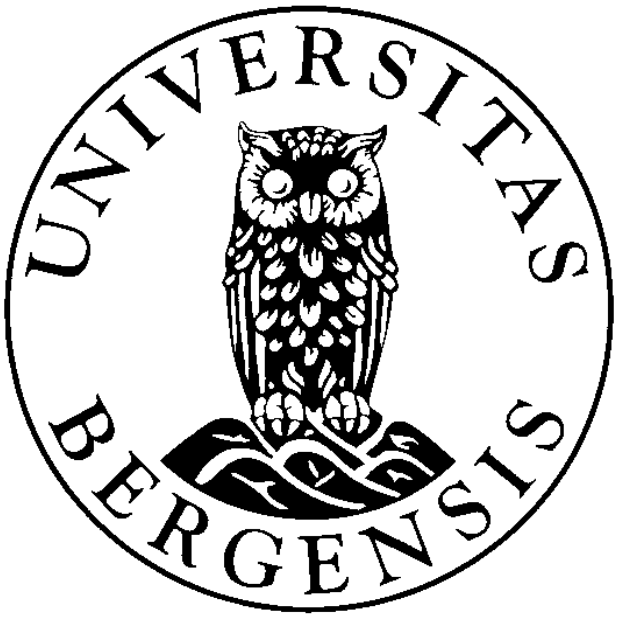

Visualization and interpretation of methane hydrate growth and dissociation in synthetic porous media

Master Thesis in Reservoir Physics

By

Josef Flatlandsmo

Department of Physics and Technology
University of Bergen

December 2015

Summary

Sedimentary natural gas hydrates might play an important role in the future energy mix and the impact of methane release from natural gas hydrates can be significant also with respect to climate change. Vast amounts of methane gas are trapped in the subsurface permafrost and in submarine environments below sea floors. To understand the mechanisms of formation and dissociation on pore scale is fundamental to explain phenomena on core scale and making hydrate simulators on field scale. The three scales combined, will provide valuable data and understanding for field planning and testing. The experimental work presented in this thesis is visual observations conducted in a 2D silicon wafer micro-model with a one-to-one representation of the Berea sandstone pore network using a vertical pore depth of 25µm. In this thesis the overall objective was to characterize hydrate formation and dissociation on pore scale by direct visualization. The second objective was to identify the limiting factors for hydrate formation and growth in the micromodel and compare these to bulk properties.

Hydrate formation attempts has been done both with vacuumed and non-vacuumed water. This to mimic the oxygen and nitrogen levels in reservoir and surface conditions respectively and tracing the three-phase-equilibrium line in both cases. No significant difference was found.

Thin film interference was used to determine the thickness of the water and hydrate film. This turned out to be limited by wavelength of the visual light spectrum. Water films were found to be thinner than 140nm and the hydrate films to be thicker than 1500nm.

The experimental setup was modified to enable live view monitoring of the micro-model and fluid flow through all four ports. A new cooling-chamber was constructed allowing a more efficient temperature control and quicker heating/cooling of the still water surrounding the micro-model.

During fixed pressure and variable temperature experiments, it was found that even at conditions well within the hydrate equilibrium line, growth did not necessarily commence spontaneously. However, a disturbance in the fluids by pressure regulation was a key factor. Therefore, the degree of which turbulence and flow promotes hydrate formation in a porous medium by high flowrates has been studied. This was done at 145, 130 80 and 55 bars of differential pressure and temperature range from 0.6-11°C, with vacuumed and non-vacuumed distilled water. 21 formation runs with high flow rate through the model to initiate the visual growth were done and in 21 of 21 attempts visual hydrate formation occurred within 4 minutes**.** This method of initiating hydrate growth turned out to be very effective making the stochastic nature of nucleation insignificant.

In every instance the hydrate was observed to grow as a black film inwards in the gas phase that subsequently turned more transparent upon further growth. Due to the difference in refractive index of hydrate and gas the hydrate film appears as black while re-soaking in water makes it more transparent. Growth into the water phase has not been observed. After flow, hydrate grew evenly from thin water films retaining on flat surfaces inside the micro-model, while growth from a static situation led to a hydrate film advancing through the gas phase from the interface to the center.

Dissociation experiments with temperature change and fixed pressure and vice versa were conducted. The methane hydrate was observed to appear as a layer within the micro-model. The dissociation was observed mainly to occur along the edge of the hydrate film upon pressure reduction. Contact with a free gas phase seemed to be a necessity for quick heat and mass transport leading to melting. Immobile water surrounding the hydrate films acted as a hindrance for dissociation. When heating the system at constant pressure, methane released from the hydrate were more evenly spread and occurred at the hydrate film edge as well as within the hydrate layer. This may be explained by heat transport through the matrix and silicon wafer.

Acknowledgements

First of all I want to thank my supervisor Associate Professor Geir Ersland. He has let me be quite independent in the experimental work so that my personal ideas and approaches could be applied. His relaxed way of being, kept the threshold very low for stepping by his office for small technical and scientific talks.

Without Professor Arne Graue this research would have not been possible, and for that I am very thankful. I would also like to thank Assoicate Professor Martin Fernø for good advices and helping me keep the right focus in this thesis.

Thanks to Chief Engineer Rachid Maad for fixing damaged equipment and thanks to the personnel at the mechanical workshop for making parts to my experimental setup.

My family deserves a big thank you for being so supportive and interested in what I have been doing.

I would like to thank fellow students in the reservoir physics group for a good atmosphere, productive working environment and making these years memorable. I especially want to thank Erik Vadla for helping me out in the lab and Erik Andreas Guldberg for questions regarding the chemistry and behavior of fluids.

Writing a thesis demands a lot dedicated work and focus. In my opinion this is not possible without a home where there is laughter and joy. I have been so lucky to have good people around me to cheer me up with music and good times. I want to give my gratitude to MøhlensprisBanden. What a gang!

Table of Contents

1 Fundamentals 1

1.1 The water molecule 1

1.2 Hydrogen bonds 1

1.3 Comparison of Properties of Hydrates and Ice 3

1.4 Water Solubility of Natural Gases 4

1.5 Nucleation 4

1.6 Labile Cluster Nucleation Hypothesis 8

1.7 Stochastic Nature of Heterogeneous Nucleation 10

1.8 The Memory Effect Phenomenon 11

1.9 Driving Force and limiting factors of Nucleation 12

1.10 Cavities 12

1.11 Cavity filling 14

1.12 Hydrate appearance and film/shell growth at the water-HC interface 15

1.13 Hydrate Formation in Porous Media 17

1.14 Mass transfer in hydrate system 20

1.15 Hydrate inhibition 21

1.16 Geometrical Optics and Snell`s Law 21

1.17 Total inner reflection 22

1.18 Thin Film Interference 23

2 Literature survey 25

2.1 Methane Hydrate formation in porous media 25

2.2 Methane Hydrate Dissociation 27

2.3 Micro capillary network in hydrate films 28

3 Experimental setup, Procedures and Materials 29

3.1 The high pressure micromodel 29

3.2 Assembly of the model 33

3.3 Apparatus 35

3.4 Uncertainty of the thermometer, pressure transducer and pump 35

3.5 The valves 36

3.6 Vacuuming the water 36
3.7 Setup A 38
3.8 Experimental Procedure for setup A 39
3.9 Setup B 40
3.10 Procedure for filling the high pressure pump 41
3.11 Procedure for filling the “reservoirs” and micro-model 41
4 Water films, hydrate films and micro-model properties 42
4.1 Color and sharpness of images 42
4.2 Thin water films 44
4.3 Formation and dissociation by temperature control with setup A 46
4.4 Why hydrate films appear black 49
4.5 Water transport during hydrate film formation 52
4.6 Why hydrate films tend to get transparent in the middle of the pore first 52
5 Experiments and results 55
5.1 Hydrate formation setup A 55
5.1.1 Successful hydrate formation setup A 55
5.1.2 Hydrate formation attempts setup A 55
5.2 Hydrate formation Setup B 55
5.2.1 Foreign Particles 56
5.2.2 Formation attempts by decrease of temperature and fixed pressure 56
5.2.3 Formation attempts by gas injection at fixed temperature and pressure with vacuumed and non-vacuumed distilled water 57
5.3 Hydrate formation characteristics in the micro-model 59
5.4 Hydrate appearance at different pressures 60
5.5 The memory effect 64
5.6 Water displacement upon hydrate crystallization 65
5.7 Layered hydrate 66
5.8 Finding the equilibrium line 67
5.9 Dissociation 70
5.9.1 Dissociation by pressure decrease 70

5.9.2 Dissociation by heating 71
5.10 Cementation 71
6 Conclusions 72
7 Future Work 74
8 Appendix 75
8.1 Experimental table values for three-phase-equilibrium line. 75
9 Bibliography 77

Introduction

Natural gas hydrate is a crystalline non-stoichiometric compound where its constituents are natural gas and water. The water molecules can organize into a cage like structure due to the special properties of hydrogen bonding, and trap a gas molecule inside the cage. These structures can be made in the laboratory and exists in nature in vast amounts all around the world. They are typically found in the permafrost regions and in offshore sediments. When gas is introduced to water within high a pressure and low temperature range the conditions are set for transforming the two fluids into a solid crystalline structure.

Natural gas-hydrates are an unconventional energy source. An increasing interest for NGH`s has led to the discovery of 220 gas-hydrate deposits around the world. In total, the potential reserves found so far are over $1.5 \times 10^{16} m^3$. If 15% of these known deposits were commercially producible it could provide the world with energy for the next 200 years with today`s energy consumption (Makogon, et al., 2007). The world's energy use has almost doubled since 2000 and millions of people have been lifted out of poverty, still there are 240 million people without access to electricity and there are underlying reasons to expect continued rapid growth in energy demand (Agency, 2015). Methane gas is known to be the cleanest energy bearer of fossil fuels leaving only CO2 and water as combustion products whilst other heavier fossil fuels, especially coal, produce a lot of aerosols upon combustion. The main constituent gas in gas-hydrate deposits is methane. In the lack of a better and greener way to get energy, NGH is considered as a near futuristic energy source and its gas as an export product by some countries, especially China, North-Korea and Japan.

The two most commercial production techniques of interest regarding NGH are pressure depletion and CO2-CH4 exchange. The pore scale physics of these two methods is not fully covered but essential for further development and progression. Performing hydrate formation and dissociation in a micro-model where the two processes are made visual will give invaluable information. Gas-Hydrate studies have been conducted by several but the stochastic nature of its formation leads to very time consuming experiments. The work in this thesis has been centered around the primary hydrate formation mechanisms on pore scale.

1 Fundamentals

1.1 The water molecule

The water molecule, H_2O, consists of two hydrogen atoms and one oxygen atom in a nonlinear arrangement. The molecule has four valence electrons which forms two lone pair orbitals. The pair of electrons that are shared with the protons results in two positive charges from the protons. The other pair causes two negative charges around the oxygen molecule. The force balance will form molecule with a permanent dipole and 4 charges. (Sloan & Koh, 2008).

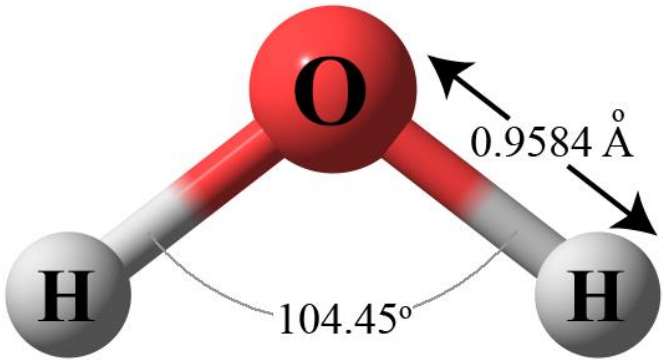

Figure 1: The water molecule. The distance between one of the hydrogen atoms and the oxygen atom is 0.9584 Å. The angle between the hydrogen atoms is 104.45 degrees and causes the whole molecule to be a dipole. Picture from (Anon., u.d.)**.**

1.2 Hydrogen bonds

The water molecules donate two hydrogens and accept two in addition through hydrogen bonding, where the four hydrogen bonds are arranged in a tetrahedral structure locally around one molecule. Comparing the strength of hydrogen bonds in water with those in HF and NH_3, one finds that although the hydrogen bonds in HF are stronger the solid crystal structure is weaker than that of hexagonal ice. The same goes for NH_3. This is due to the hexagonal network H_2O creates while NH_3 and HF cannot arrange such structures. Having such a strong structure, ice has the highest melting point of the three. The intramolecular covalent bonds are much stronger (102kcal/mol) than the hydrogen bonds (0.3kcal/mol) and consequently the geometrical shape of the H_2O molecule stays about the same in liquid form and solid form (Stillinger, 1980).

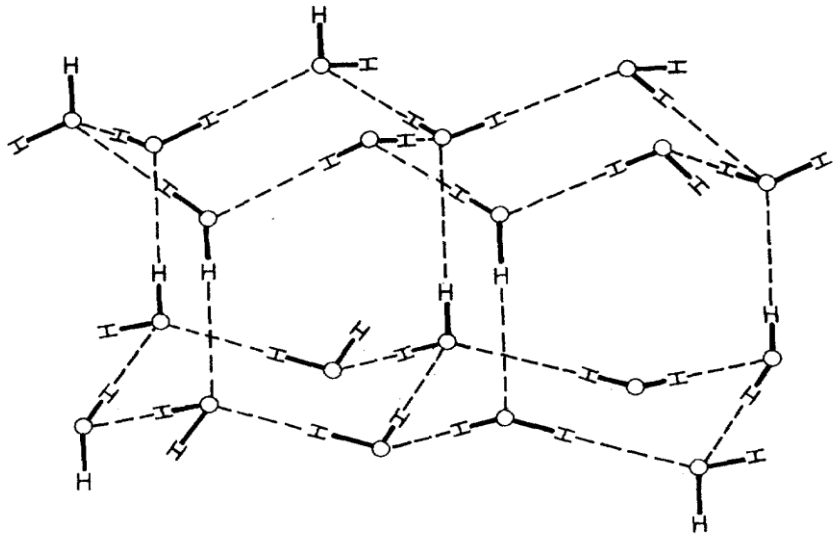

Figure 2: The structure of hexagonal ice. Hydrogen bonds are shown as dashed lines while the intramolecular covalent bonds are shown as solid lines (Stillinger, 1980).

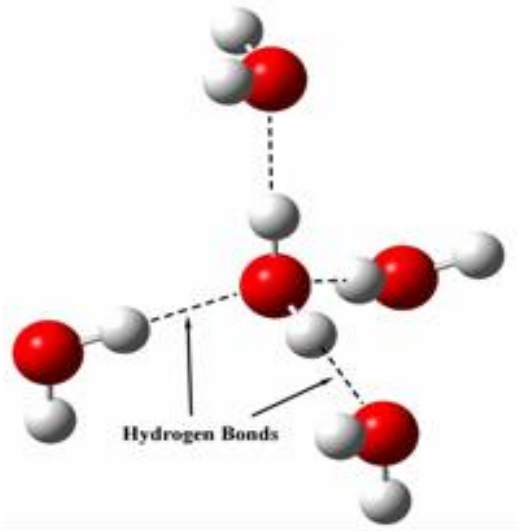

Figure 3: Showing the tetrahedral arrangement of the hydrogen bonds around a water molecule. The two negative charges of the dipole on the oxygen atom attract one hydrogen atom each while the two positive protons bonds to an oxygen atom of two other molecules. Picture from (Millam, et al., u.d.).

1.3 Comparison of Properties of Hydrates and Ice

On average, hydrogen bonds in hydrate are 1% longer than in ice and the O-O-O angles differ with 3.7° in sI and 3.0° in sII from the ice tetrahedral structure. Water molecules reorient themselves about a fixed point in ice structure around one order of magnitude slower then they diffuse. Hydrate water molecules on the other hand, reorient about 20 times faster than they diffuse. Comparison of hydrate water molecules and ice water molecules in terms of diffusivity yields that the hydrate water molecules diffuse two orders of magnitude slower than in ice. Due to the lower density of hydrogen bonded water molecules, reorientation of water hydrate molecules is about on half of those in ice (Sloan & Koh, 2008).

The mechanical strength of hydrate is found to be higher than that of ice. Ice creep and deformation rates are higher due to coordination of crystalline defects, which are generally governed by the diffusivity of the water molecules. Thermal expansion coefficient has also been found to be higher in hydrate than for ice. The suggested explanation for this, rooted in molecular dynamics calculations and free energy calculations, is due to inharmonic behavior in the water lattice. Collisions of the guest molecule with the cage wall, weakens the hydrogen bonds between the water molecules in the surrounding cage making it more sensitive to temperature changes.

This study is based on visual observations through a microscope. Methane gas, hydrate and water are the constituents in the micro-model and are made visible with light perpendicular to the model. Understanding how the light travels through the different media is crucial for interpretation of the results. Methane hydrate structure I refractive index was found to be 1.346 while for natural gas hydrate structure II a refractive index of 1.350 was determined. These numbers will not always be the case since the hydrate cages are only partially filled to some varying extent (Bylov & Rasmussen, 1997). In comparison refractive index of water, ice and methane is 1.333, 1.31 and 1.000444, respectively (EngineeringToolBox, u.d.). The refractive indexes of glass and silicon are also needed for the discussion regarding light interference and are n_{glass} =1.55-1.62 (EngineeringToolbox, u.d.) and $n_{silicon}$=3.44 (Chandler-Horowitz & Amirtharaj, 2005). Bylov & Rasmussen (1997) points out that if the difference in refractive index of water and gas hydrate is small, visual detection of the hydrates can be difficult in their setup.

1.4 Water Solubility of Natural Gases

Many gases can form hydrate but the process is very pressure and temperature dependent which is closely connected to the solubility. Gas molecules need to be in the aqueous water phase for hydrate to form. Due to the non-polarity of natural gases such as hydrocarbons, He, H_2 and Ne, the solubility in water is very small. H_2S is a bent molecule similar to water. Hydrogen sulfide (H_2S) has a polar nature and therefore also more soluble in water, approximately 70 times more soluble than methane at 298K and atmospheric pressure (Sloan & Koh, 2008). CO_2 is linear and non-polar and about 30 times more soluble in water than methane. H2S is considered as an extreme hydrate former. Nitrogen and oxygen are the main constituents of air therefore their solubility is worth mentioning. At 0°C and atmospheric pressure nitrogen and oxygen has a solubility of 0.03 [g gas/kg water] and 0.07 [g gas/kg water], respectively while methane is in between at 0.04 [g gas/kg water] (EngineeringToolbox, u.d.).

1.5 Nucleation

Hydrate nucleation is the process where small hydrate crystals cluster together in order to achieve the critical size. Once the critical size is achieved further growth of the hydrate can commence without dispersing. “One may define the induction time as the period necessary for the appearance of the very first hydrate cluster of super nucleus size (such a cluster is capable of spontaneous overgrowth to a macroscopic size)” (Kashchieva & Firoozabadi, 2003). There are calculations and experimental work on how large the critical size is. A key factor in these calculations is the driving force, which can be defined as the difference in experimental value and theoretical equilibrium value of fugacity, chemical potential, Gibbs free energy, supersaturation or temperature (sub-cooling). Usually in experiments, pressure and temperature are controlled and are directly affecting the driving forces mentioned. Experimentally, (Nerheim, et al., 1994) found that the critical size varied from 2 -80 nm in structure II gas hydrates depending on the driving force. The higher the driving force the smaller the critical size. They used Photon Correlation Spectroscopy and varied the pressure and temperature.

Methane and ethane hydrates were investigated by (Englezos, et al., 1987). They calculated the critical size to be ranging from 30-170 nm and the film thickness (a diffusive film of water surrounding the nucleus) to be at least three orders of magnitude larger. This size ratio suggests that further growth is continued as homogenous nucleation, they argue. Computer simulations

Homogeneous nucleation is a 3-dimensional solidification process in the absence of impurities. It takes place in the bulk water phase and will therefore not be heat transfer limited but limited by mass transfer. The mass transfer limitation is especially relevant for low soluble gases such as methane (Kvamme, 2014). Since the number of molecules needed to form a super nucleus is

larger than simultaneously colliding molecules, the collisions need to happen in a sequential manner. Before reaching the critical size, the clusters may either grow or shrink as a result of density and composition fluctuations (Sloan & Koh, 2008).

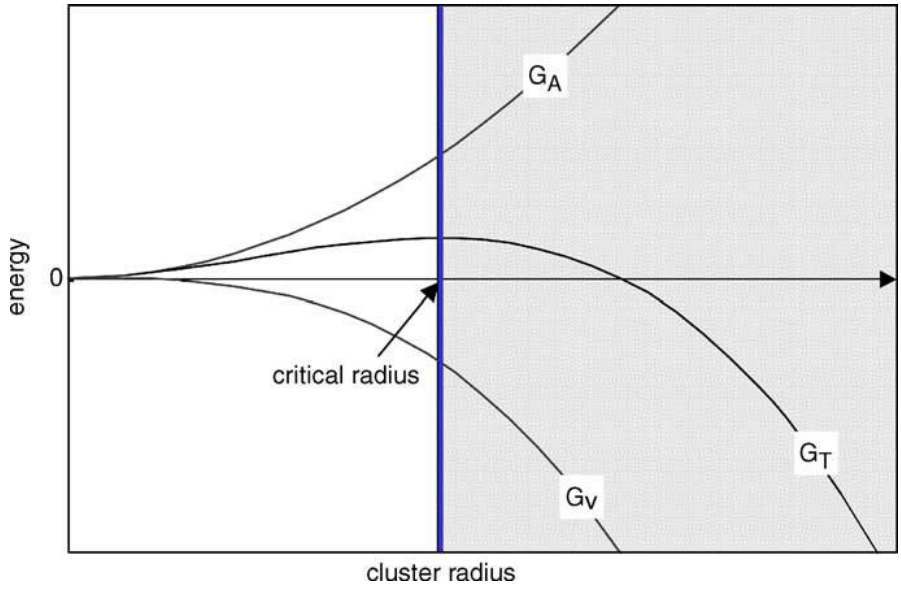

Figure 4: Gibbs free energy for spherical crystal. Indices A,V and T meaning Area, Volume and Total, respectively (Turner, et al., 2005).

The nucleation is governed by the minimization of Gibbs free energy and is a battle between the surface excess free energy and the volume excess free energy (Sloan & Koh, 2008). Mathematically this is expressed as

$$\Delta G = \Delta G^{surface} + \Delta G^{phase\ trans.} = 4\pi r^2\gamma + \frac{4}{3}\pi r^3 \rho_N^H \Delta g^{phase\ trans.} \leq 0 \qquad (1\text{-}1)$$

where ΔG is the total energy as given by G_T in figure 4, γ is the interfacial free energy [J/m^2], r is the crystal radius [m], ρ_N^H is the molecular density [mole/m^3] and $\Delta g^{phase\ trans.}$ Is the intensive change in Gibbs free energy related to the phase transition [J/mole]. The favorable negative free energy change from the phase transition must overcome the penalty from creating new surface area. The critical size has been predicted from data simulation to be a couple of nanometers and can be reach within nanoseconds (Kvamme, 2014).

To obtain the critical size from classic theory one differentiates equation (1.1) and setting the result equal to zero.

$$r_c = -\frac{2\gamma}{\rho_N^H \Delta g^{phase\ trans.}} \tag{1-2}$$

The critical radius is dependent on the interfacial free energy (the same as interfacial tension but expressed as [N/m]). Pressure and temperature dependency of the interfacial tension between methane and water have been investigated by Sachs & Meyn (1994). At 25°C the interfacial tension varied between 70.57 mNm^{-1} at 1.036 MPa (10.36 bar) to 60.96 mNm^{-1} at 10.394 MPa (103.94 bar). This shows that the lower the interfacial tension the more soluble methane becomes in water. It follows from equation (1.2) and (1.3) that the critical radius is decreased and the Gibbs free energy barrier lowered.

Homogeneous nucleation is practically impossible to achieve in a porous media. Due to the convex meniscus (positive radius measured from center of nonwetting fluid), nonwetting fluids have a higher internal pressure in a porous than surrounding fluid and a higher vapor pressure and solubility than the same substance in bulk conditions. Therefore the level of supersaturation needed for nucleation is lower in heterogeneous nucleation than homogeneous (Clennell, et al., 1999). Considering nucleation from a free energy point of view it is more favorable to grow a hydrate or ice crystal on a 2 dimensional surface than in 3 dimensions. Heterogeneous nucleation occurs in the presence of a foreign particle or a surface and smaller supercooling temperature is needed compared to homogeneous. In mathematical terms this is expressed as

$$\Delta G'_{crit} = \Phi \Delta G_{crit} \tag{1-3}$$

where Φ is a fraction between 0 and 1 making $\Delta G'_{crit}$ for heterogeneous nucleation smaller or equal to homogenous nucleation. Φ is related to the angle of contact between hydrate crystal and surface through a defined mathematical expression (Sloan & Koh, 2008).

Therefore, heterogeneous nucleation is most likely what happens in nature (Sloan & Koh, 2008). Clennel et. Al (1999) argues that homogenous nucleation is very unlikely to occur inside a porous media with small pores due to capillary effects and limited diffusional properties, but rather in large pores or open fractures where the nucleation is limited by the critical nucleus size. “Given the r^3 relationship between pore radius and volume and the sensitive dependence of nucleation probability on the numbers of freely associating molecules [Adamson and Gast,

1997], it seems that pore size could exert a very strong constraint on nucleation even when the pores are much larger than the critical size for homogeneous nucleation" (Clennell, et al., 1999).

Nucleation and disintegration of clusters are stochastic processes and so achieving the critical size is a stochastic process. That is why visual growth of hydrate crystals is not predictable. Gas hydrates usually grow on the surface between gas and liquid. There are two reasons for this:

1. Gibbs free energy for nucleation is lower at the interface.
2. The concentration of hydrate former is much higher in the interface.

The concentration of hydrate guest molecule at the interface can be as high as 0.15 mole fraction. However, the water mole fraction in the gas phase is lower than 0.05 and the mole fraction of hydrocarbons in the aqueous phase is never greater than 0.001 (Sloan, 1998). In a porous system there are a lot of contact surfaces between medium and fluids and many interfaces between the fluids. This might increase the probability of making the induction time shorter than for a bulk system containing only one interface.

The *Labile Cluster Nucleation Hypothesis* and the *Nucleation at the Interface Hypothesis* are both models of hydrate growth at the vapor-liquid interface. The following are based upon the description of the nucleation hypothesizes from (Sloan & Koh, 2008). An explanation of coordination number and hydration number is needed for further reading:

Coordination number: The number of water molecules, fixed in a cage structure, surrounding a guest molecule. In a perfect hydrate crystal the neighboring guest molecules share the water molecules that make up the cages and the coordination number.

Hydration number: The ratio of the total number of water molecules to guest molecules. For full occupancy in sI methane hydrate hydration number is 5.75.

1.6 Labile Cluster Nucleation Hypothesis

- Pure water exists without any guests. Because of the special hydrogen bonds between the water molecules, water creates a labile ring structure of pentamers and hexamers.
- When a guest molecule is introduced water forms a labile cluster around it.
- The clusters then combine to form unit cells. Cavity 5^{12} and $5^{12}6^2$ require a coordination number of 20 and 24 respectively to form sI. To form sII coordination numbers of 20 and 28 are needed due to the $5^{12}6^4$ cavity. Nucleation of either structure cannot happen if labile clusters of both coordination numbers are not present. In the case of only one cage type, hydrogen bonds need to be broken and reassembled in a manner that favors both coordination numbers.
- An energy barrier has to be overcome in order to transform the cluster from coordination number 20 to 24. In the case of methane gas this barrier is high for two reasons 1) the stability of methane in a $5^{12}6^2$ cage is low and 2) the $5^{12}6^2$ cavities outnumber the 5^{12} by a factor of three. Since methane cannot stabilize the large cavity in sII (unless very high pressure) the transformation from 20 to 28 has a too high energy barrier.

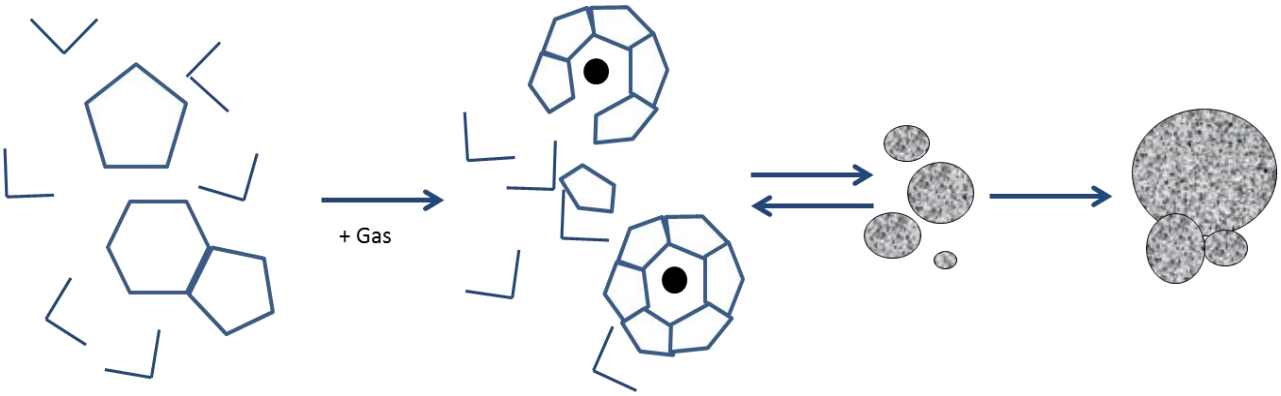

Figure 5: Schematic of Model of Hydrate Cluster Growth based on Sloan (1998).

In Figure 5 a cycle of hydrate growth and At 1 the system is pressurized and guest molecules are dissolved in the water and short lived cages are formed. Temperature is decreased and critical size is achieved at 2. Catastrophic nucleation and growth occurs at B resulting in a pressure decrease due to consumption of guest molecules. Heating system again and gas hydrate will dissociate and gas release will bring back the pressure to point A.

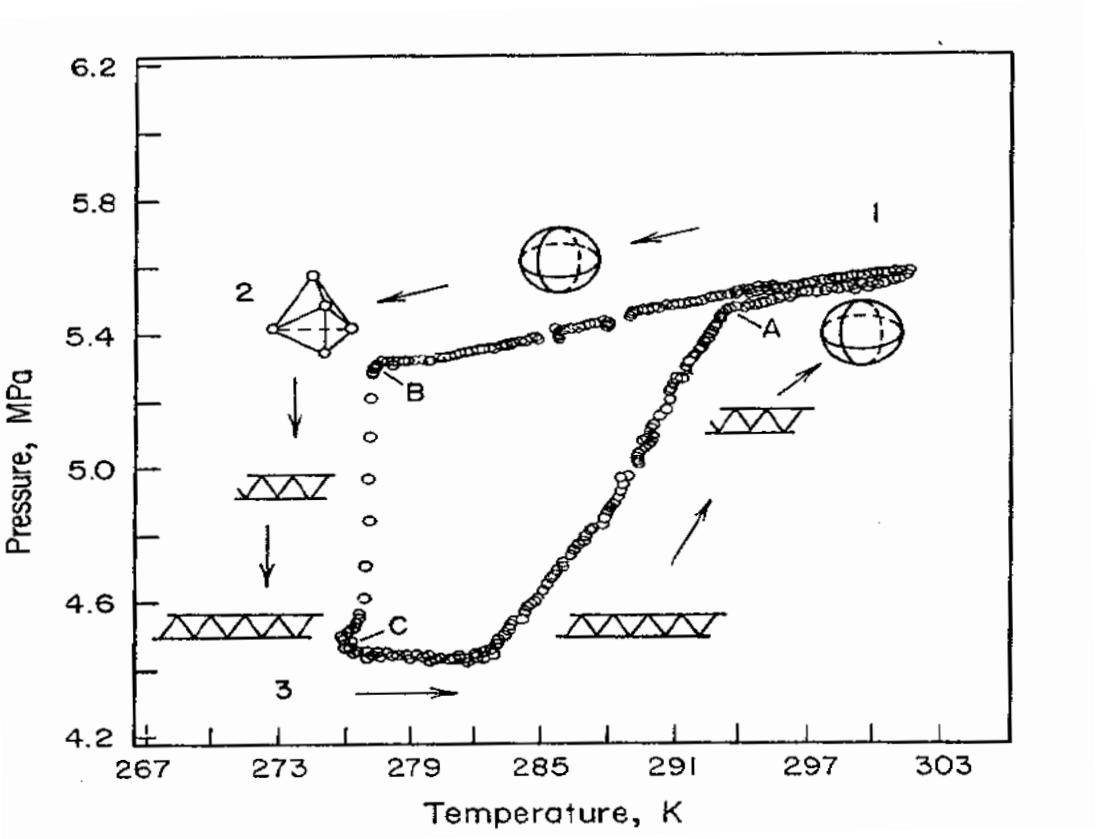

Figure 6: Hydrate Labile cluster growth mechanism on a pressure-temperature trace (Sloan, 1998).

Nucleation at the interface hypothesis

- Gas that is near the interface is adsorbed.
- The adsorbed gas migrates to a location suitable for diffusion and then the water forms partially cages at first and then forms complete cages around guest molecule.
- Clusters then grow to overcome the critical size. This can happen by two mechanisms. Cages get additional water and guest molecules or clusters connect.

Based on simulations of homogenous nucleation of CO_2 hydrate, a new hypothesis, the local structuring theory, is proposed to explain nucleation. Gibbs free energy calculations of homogenous nucleation have showed that it is more thermodynamically favorable for labile clusters to disintegrate than to agglomerate at the interface between CO_2 and water. The main point of this theory is that guest molecules group together locally because of thermal fluctuations and the number exceeds that of a critical nucleus. This results in a hydrate nucleus of critical size or greater (Sloan & Koh, 2008).

1.7 Stochastic Nature of Heterogeneous Nucleation

Experimental evidence shows that the nature of hydrate induction is stochastic. It varies with the driving force and apparently dependent upon whether the temperature is held constant or at constant cooling rates. When the system is set to a constant temperature the process is more stochastic. At a constant cooling rate the hydrate growth occurs within a narrow range of temperature (around $2^{\circ}C$ by some experiments) (Sloan & Koh, 2008). Bishnoi & Natarajan (1993), reported that at pressures above 3,5 MPa induction times are far more reproducible. The induction time seems also to be dependent on the experimental setup, apparatus, agitation (cavitation and turbulence), surface area of the system, the rate of heat and mass transfer, history of the water and the presence of foreign particles. (Sloan & Koh, 2008).

Two curves divide stability regions into three parts; labile region, metastable region and stabile region. The induction time takes place in the metastable zone. It is the time from the system enters the metastable region to the time where solid formation occurs. The line CD is not a definite line, therefore the small horizontal lines, this because it has only been calculated and not determined experimentally for hydrates (Sloan & Koh, 2008).

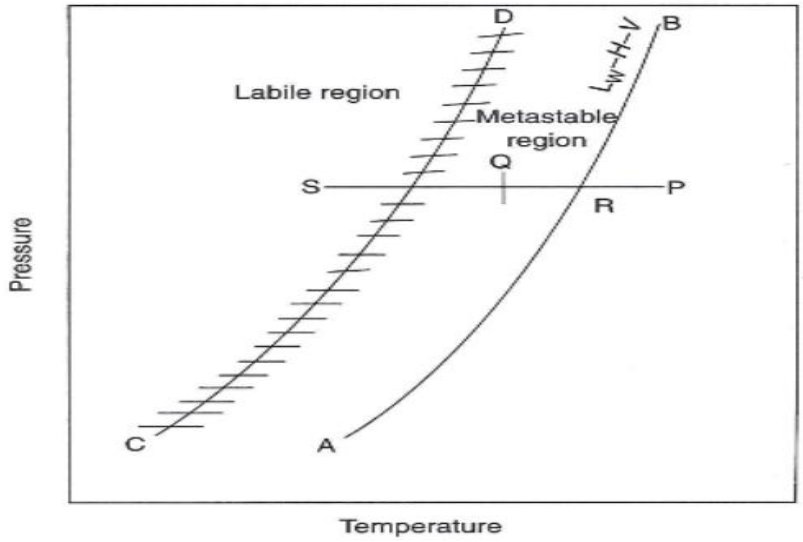

Figure 7: Hydrate formation as a function of subcooling relative to the equilibrium line (AB) and the spinodal line (CD; supersaturation limit) The pressure axis is logarithmic. (Sloan & Koh, 2008).

To the right of the stability line AB no hydrate can form. Once the system enters the metastable region the likelihood of hydrate formation increases the closer it gets the curve CD due to higher driving forces. To the left of CD the system is supersaturated and the conditions for spontaneous crystal growth are set.

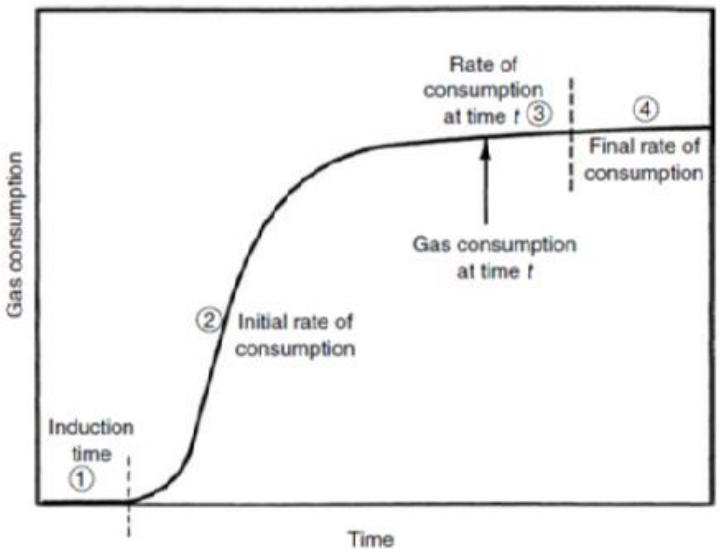

Figure 8: Gas consumption as a function of time. Pressure and temperature held constant (Sloan & Koh, 2008)

1.8 The Memory Effect Phenomenon

The memory effect is a well-established term amongst hydrate researchers yet not fully understood. Melted hydrate water, crystallize and grow hydrate by a much shorter induction time than water that has been in hydrate structure. To destroy the memory effect, a sufficient temperature at a certain pressure outside the stability curve for a sufficiently long time is required. The memory effect is undoubtedly something at a molecular level and there are two main hypotheses to this date. 1) Dissolved gas remains in solution after hydrate has melted. 2) Partial cages remains in water or whole hydrate crystals and nucleuses remain in water after hydrate has melted. A recent experiment with Cyclopenthane, the authors (Lourdes Martinez de Baños, et al., 2015) of the article "*Droplet-based milli fluidics as a new tool to investigate hydrate crystallization: Insights into the memory effect*" observed that, where there were cp emulsions in the water droplets the hydrate crystallized easier and first.

In an experiment to find the refractive index of gas hydrate the memory effect was also studied. On the contrary to many experiments done by others, the agreement of shorter induction time with water that have already been crystallizing hydrate, did not match. Instead it was found that the rate of hydrate growth was slower in the water with no hydrate history while the induction time was not affected (Bylov & Rasmussen, 1997).

1.9 Driving Force and limiting factors of Nucleation

In general the driving force of hydrate nucleation is the total molar change in Gibbs free energy given by

$$\Delta g^{exp} = \Delta g^{rx} - \Delta g^{pr} \quad (1\text{-}4)$$

with superscripts rx, pr and exp meaning reactants, product and experimental respectively. Δg^{exp} is a function of the chemical potential μ, the fugacity ƒ, temperature T and pressure P. In the experimental setup here the pressure and temperature are controlled. Experiments have shown that above 20MPa subcooling, ΔT (temperature difference between hydrate stability temp and experimental value), is the main driving force (Sloan & Koh, 2008).

Hydrate formation is an exothermic process and the produced heat has to be transported away. Since water has about 30 times higher thermal conductivity than air (Ormestad, 2009), it is reasonable to believe that approximate numbers also goes for water and methane. Thermal conductivity of silicon is over 130 times higher than in water at the experimental temperatures is this work, ranging from 0-30^{o}C. In other words, most of the heat from the reaction is transported away through the matrix and the silicon wafer, given that it is a static situation of no fluid movement and mass transport. This is elaborated in section 3.1.

When a hydrate film is formed the transportation of gas and water through the film is strongly limited. Therefore, the growth will slow down very rapidly once the hydrate film has formed (Hauge, et al., 2015).

1.10 Cavities

When hydrate is formed, guest molecules get trapped in cavities. The cavities are cage like structures built up by only water molecules. The simplest cavity is formed by one structure, a pentagon, and has 12 sides therefore a pentagonal dodecahedron and labeled 5^{12}. In structures I,II and H there are 5 constituent cavities (Sloan & Koh, 2008). Given in the table below, the structures with accompanying cavities are given.

Table 1-1:Table showing some characteristics of cavities in the different Hydrate structures. Table based on model from (Sloan & Koh, 2008)

Hydrate Crystal Structure	**I**		**II**		**H**		
Cavity	**Small**	**Large**	**Small**	**Large**	**Small**	**Medium**	**Large**
Description	5^{12}	$5^{12}6^2$	5^{12} $5^{12}6^4$		5^{12} $5^{12}6^8$		$4^35^66^3$
Number of Cavities/Unit Cell	2	6	16	8	3	2	1
Average Cavity Radius, Å	3,95	4,33	3,91 4,73		3,91[a] 5,71[a]		4,06[a]

a) Estimates of structure H Cavities from geometric models

As seen from the table cavity 5^{12} is present in the three structures and therefore referred to as the basic building block. Since the pentagons are linked together through the sides, only 20 molecules are needed to build up the cavity and not 60 as indicated by 5*12. This is also true for the remaining four cavities and they are illustrated in figure 1.

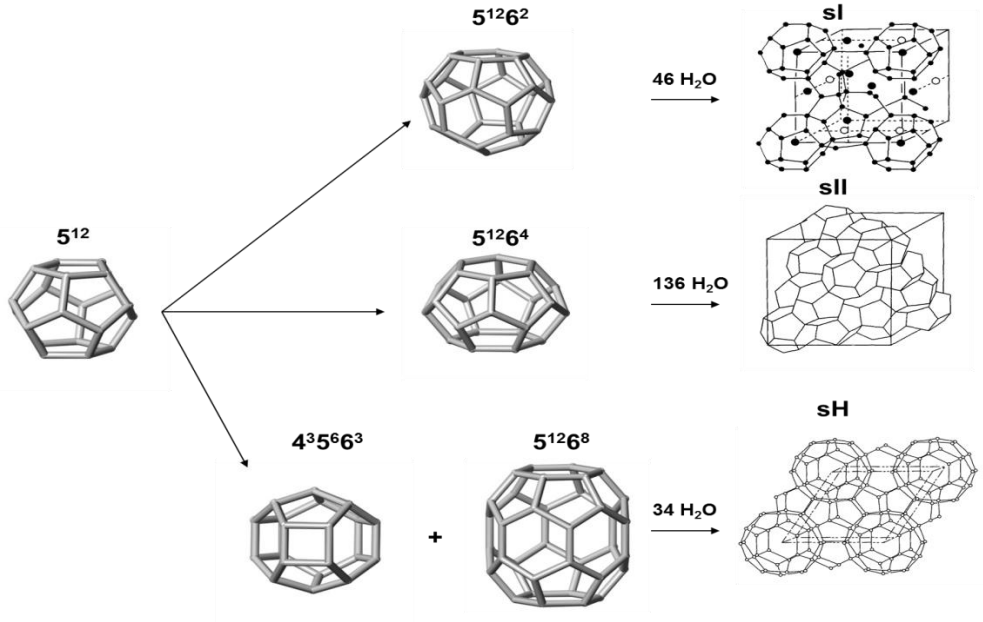

Figure 9: The five different cavities from Table 1 and the composition of cages in s1,s2 and sH illustrated (BIRKEDAL, 2013).

1.11 Cavity filling

The cavities in structure I,II and H are capable of trapping only one guest molecule. This is under usual pressures dealt with under hydrate formation in nature (Sloan, 1998).

A few important points concerning cavity filling from (Sloan, 1998):

- Below 3,5 Å ,the guest molecules are too small to stabilize any cavity. Above 7,5 Å the guest molecules are too large to fit in to any of the cavities in structure I or structure II.
- Some molecules can only stabilize the large cavities, for example: ethane can stablilize the $5^{12}6^2$ while iso-butane stabilizes the $5^{12}6^4$ cage.
- When a guest molecule stabilizes a small cavity it also stabilizes the large cavity of that structure.
- Since 1983 it`s been known that the smallest guests (argon, krypton, nitrogen and oxygen) rather form hydrate of structure I than structure II.

Very small guest molecules like Ar, Kr, N2 and O2 can be trapped together in the same cage if it is a large sized cavity (Taylor & Kwan, 2004).

1.12 Hydrate appearance and film/shell growth at the water-HC interface

The lower the driving force upon hydrate formation, the smoother and stronger (can take more shear forces) the hydrate film/crystal is. The fluid permeability increases with increasing driving force (Daisuke, et al., April, 2006). See graph below.

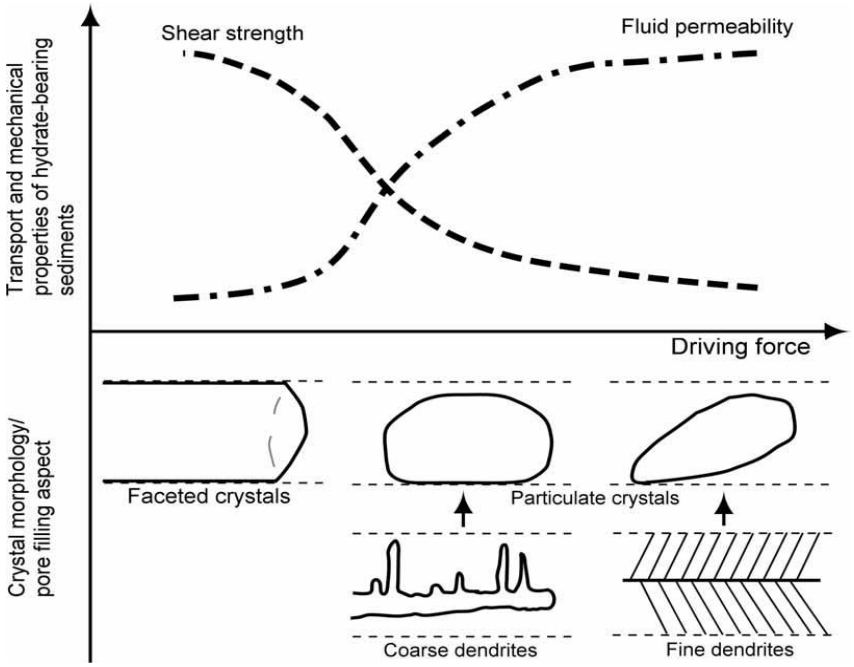

Figure 10: The fluid permeability increases with increasing driving force (Daisuke, et al., April, 2006)

In an experiment with three water droplets surrounded by pressurized methane gas and conditions for high driving forces (274,6 K and 2150 kPa above three-phase hydrate equilibrium pressure) it was observed that: Higher driving forces results in more unstructured hydrate and chaotic growth pattern. The surface was rough and needle like structures appeared to be growing into the gas phase (Servio & Englezos, 2003).

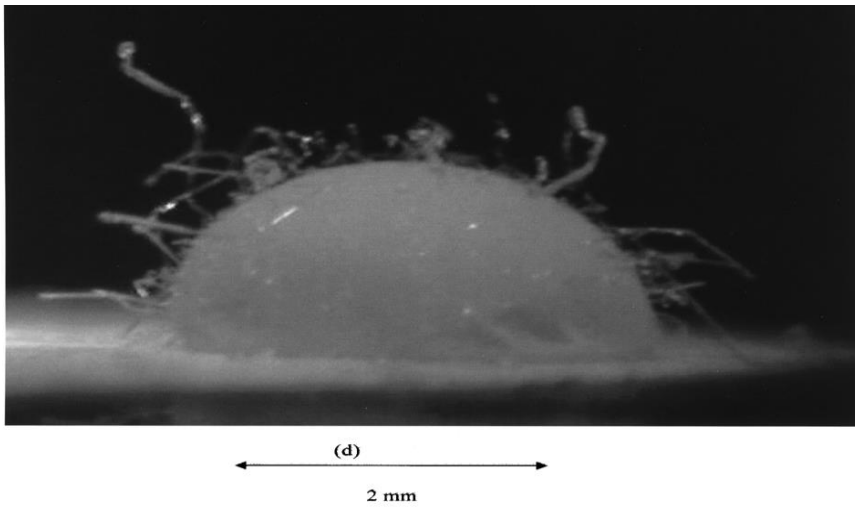

Figure 11: Water droplet with methane hydrate structures on surface under high driving forces 10 min after nucleation (Servio & Englezos, 2003)

Englezos and Servio observed that the hydrate structure evolvement could be divided into three stages for this experiment. Up to 10 hours after nucleation the needle-like crystals grew in size and thickness. The second stage involving collapse of the needle-like structures. In the third stage (after 10-15 hours up to a couple of days) the water droplet got an indent. The indent or collapse is considered as a proof that water is still converted to hydrate and that hydrate also grows into the water phase.

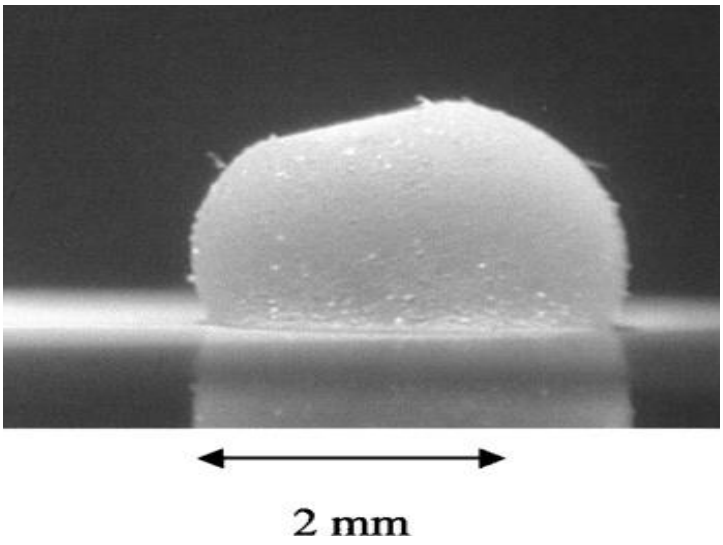

Figure 12: CO2 hydrate surface collapse after 20 hours. The indent is considered as proof of water continuously being converted to hydrate (Servio & Englezos, 2003).

1.13 Hydrate Formation in Porous Media

Gibbs phase rule yields how many intensive variables or degrees of freedom that must be specified in order to achieve equilibrium in a system. It is given by

$$F = C - P' + 2 \tag{1-5}$$

Where, *F* is the number of intensive variables, *C* the number of components and *P'* the number of phases. In a methane-water system the number of components equals 2. When an inhibitor is introduced, the number of components is added by one. In a system containing liquid water, hydrate and gas, the number of phases can be several due to adsorbed phases on different solid surfaces such as hydrate crystals, different minerals and metals. When local pressure and temperature are set the system is over-determined and equilibrium cannot be achieved. Thus, the hydrate in a porous media will be in a semi-stable state where the existence of different hydrate compositions is possible (Kvamme, 2014). However, in a two phase equilibrium system with water and hydrate where all the gas is dissolved in the water phase, the addition of salt can promote hydrate growth. Salt decreases the solubility of methane in water, making the amount of gas required to form hydrate lower (Zatsepina & Buffet, 1998).

The hydrate formation is directly connected to the activity of water where activity being a measure of chemical potential normalized to a reference state (Clennell, et al., 1999). Partial ordering and adsorption onto hydrophilic mineral surfaces reduce the water activity. When the activity is reduced the temperature of formation is depressed at a given pressure or the pressure of formation is higher at given temperature. The capillary forces in a porous media reduce the water activity and create an inhibition of hydrate nucleation with respect to that in a bulk medium. Thus, laboratory experiments on bulk hydrate may not be directly used as models for hydrate in porous media (Handa & Stupin, 1992).

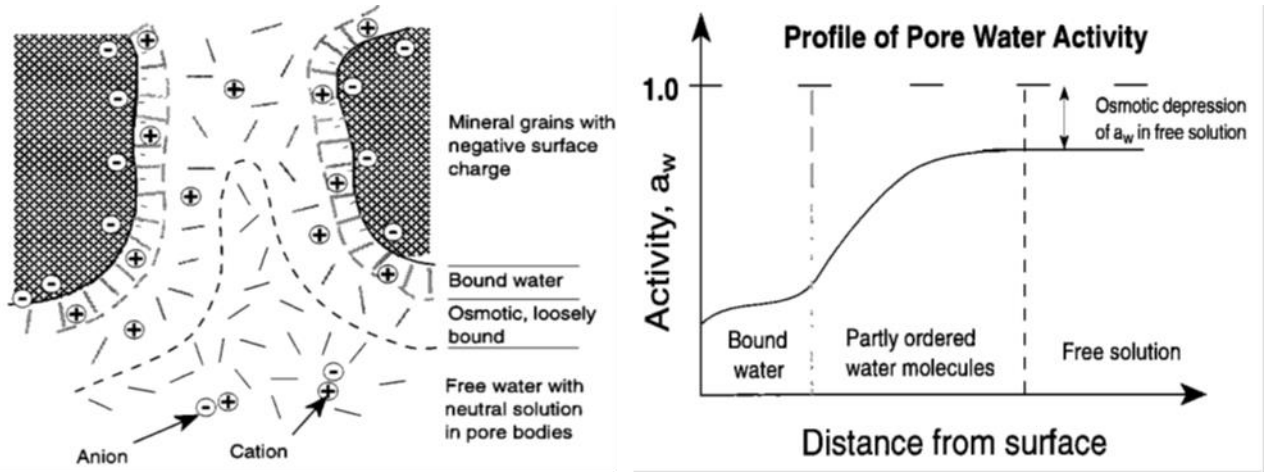

Figure 13: Shows the different water layers in a pore and pore throat with a negative mineral grain surface. The pore water is the wetting phase and bounded water layer ranges from 5-50 nm thick and will not participate in hydrate nucleation (Clennell, et al., 1999).

"Inside porous media the thermodynamic potential of chemical components can change with respect to bulk conditions as a consequence of (1) Molecular interactions at the pore walls, usually attraction of the fluid molecules by hydrophilic mineral surfaces and (2) The energy required to maintain capillary equilibrium" (Clennell, et al., 1999).

Undercooling of water inside a porous media is a thermodynamic effect which is unrelated to supercooling which is due to difficulties in nucleation kinetics. Water freezes at a lower temperature than in bulk conditions. Undercooling is attributed to the curved ice-water interfaces that increase the free energy of pore ice relative to bulk ice (Everett, 1961). It is only significant for very fine grained media such as clay and silt.

When two immiscible fluids or phases (can be ice or hydrate) are in contact with each other and one encloses the other entirely, forming an object as close as possible to a sphere due to minimization of interfacial energy, the capillary pressure is given by the Laplace Equation

$$P_c = P_{nw} - P_w = \gamma\left(\frac{1}{R_1} + \frac{1}{R_2}\right) \tag{1-6}$$

Where *nw* and *w* indices is non-wetting and wetting, respectively.

Equation (1-6) says that when two different fluids/phases are present in a porous medium or a tube and the curvature for the drops/bubbles/globules is positive, then the fluid/phase will have higher internal pressure than the surrounding fluid/phase, weighted by the interfacial tension. The smaller the pore is (smallest curvature of the interface) the higher the internal pressure. When a solid surface is introduced, a mechanical equilibrium between the phase-interfaces is established and the angle of contact needs to be multiplied with equation (1-6) in order to find the capillary pressure. This is the case for gas and hydrates in a water wet media such as sandstone when water is present.

Some important points from Clennel, et al (1999):

- Bounded water will not participate in the hydrate. When salt is present the bounded water layer becomes thicker.
- Non-wetting fluids in a porous medium have greater activity, higher equilibrium vapor pressure and greater solubility in solvents with respect to the same substance in bulk.
- Hydrate formation is inhibited in a fine grained porous media (typically silt and clays with tens of nanometers pore size) especially when gas saturation is high. The gas forces the free water away leaving the lower activity water (some of it is adsorbed by the mineral surface) left in the pores.
- Capillary supersaturation: At thermodynamic equilibrium the chemical potential of aqueous methane has to be the same as chemical potential of methane bubbles (free gas) which leads to a supersaturation of methane in the water phase. This counteracts capillary inhibition of hydrates in pores and promotes hydrate formation.

The mobile phases in a porous medium will rearrange into a configuration of minimum surface energy. This is a local and not a global effect. Therefore, one locality may affect a neighboring locality leading to a rearrangement there. Transitions of these local stable states may proceed in a discontinuous manner with abrupt jumps in saturation and phase pressures. The thermodynamic state of the phases will depend on the capillary pressures, wettability, phase saturations and saturation history due to hysteresis (Gaydos, et al., 1993).

(Gaydos, et al., 1993) gives a comprehensive discussion on why the regular Gibb`s phase rule, equation (1-5), is not applicable in capillary systems and deduces new relations which takes into account the different phases that can coexist in a porous medium. They conclude that the breakdown of Gibb`s phase rule is closely linked to the mechanical equilibrium conditions in a capillary system, such as capillary pressure and wettability.

As a starting point of hydrate formation conditions the values of hydrate bulk conditions was used as a reference. The three phase equilibrium line was plotted by values given from the program CSMGem (Mines, 2009). It is given below in Figure 14.

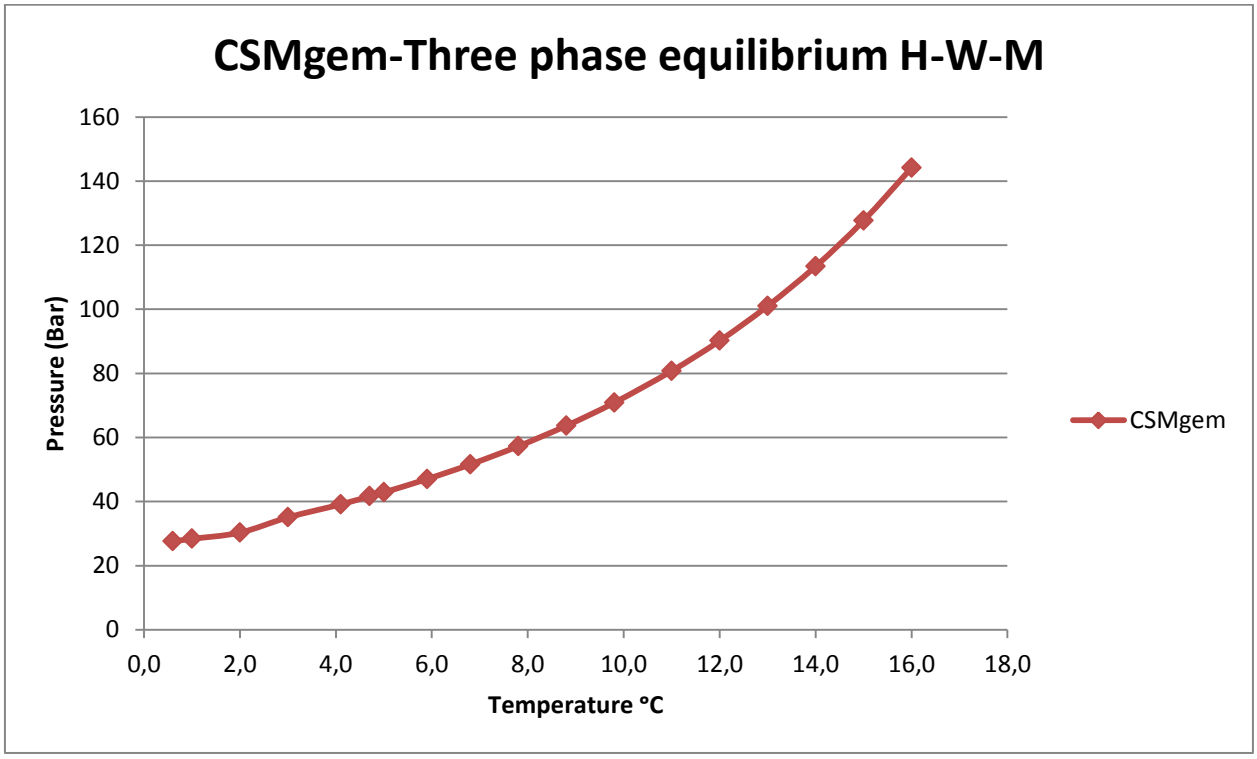

Figure 14: Three phase equilibrium line of Hydrate, water and methane gas from CSMgem. This was used as a reference.

1.14 Mass transfer in hydrate system

Investigating how the hydrate films and crystals develop after growth has commenced, yields valuable information of the mass transfer in a pore-network. Mass transfer supporting hydrate growth in a porous system relies on two mechanisms. Water and gas can be transported directly by macroscopic movement or by diffusion through hydrate films and the fluid phases.

The first and second law of thermodynamics implies that the lowest free energy regions of non-equilibrium hydrate film will grow at the cost of less stable neighboring regions. This is under the constraint that a direct supply of guest and/or host molecules is limited by the low mass transfer rates through the hydrate film (Hauge, et al., 2015).

1.15 Hydrate inhibition

Understanding the inhibiting factors on hydrate growth makes it easier to point out sources of error and improvement regarding experimental hydrate formation. One may divide hydrate inhibitors in three different parts: thermodynamic, kinetic and anti-agglomerates. Thermodynamic inhibitors shift the equilibrium line in P,T diagrams towards higher pressure and lower temperature by reducing the chemical potential. The system always seeks the minimum energy state and the molecules neutralize the chemical potential difference by mass transportation to the phase of the lower potential. Methanol, salts and monoethylene glycol are examples of thermodynamic inhibitors (Sloan & Koh, 2008). Nitrogen can act as an inhibitor, at least lowering the thermodynamic drive for hydrate formation (Kvamme, 2015)

Kinetic inhibitors and anti-agglomerates can prevent hydrate formation. Kinetic inhibitors are low molecular weighted polymers and they bond to the hydrate surface, known as sterical blocking, to prevent further growth (Kvamme, 2014). Anti-agglomerates hinder agglomeration of hydrate particles by surface active agents that reduces the adhesion forces (Sloan & Koh, 2008).

1.16 Geometrical Optics and Snell`s Law

This thesis is based on visual observations with the use of a microscope. To interpret the images correctly a fundamental understanding of how the light travels through the different media is needed. Approaching the task from this point of view led way to explaining why the hydrate film appears a black layer and using thin film interference to detect thin water films inside the model.

Fermat`s principle says that when a beam of light is to travel from point A to point B it will take the path of the shortest period of time, independent of A and B being in two different media. In geometrical optics it is adequate to consider light as rays, and three fundamental laws can be formulated to represent it:

- In a homogenous medium, light will spread as straight rays.
- At a plane surface between two media some of the light will be reflected.
- At a plane surface between two media some of the light will be refracted into the next medium (Lillestøl, et al., 2006).

From this, Snell`s law arises for an incident ray and a refracted ray. In mathematical terms Snell`s law is formulated as

$$n_1 sin\Theta_1 = n_2 sin\Theta_2 \quad (1\text{-}7)$$

Qualitatively, Snell`s law implies that when a ray of light is refracted into a medium with higher refractive index, the angle of refraction is smaller than the angle of incident. The refractive angle in a medium with lower refractive index is larger than the angle of incident. See Figure 15: Snell`s law exemplified with $n_1<n_2$.

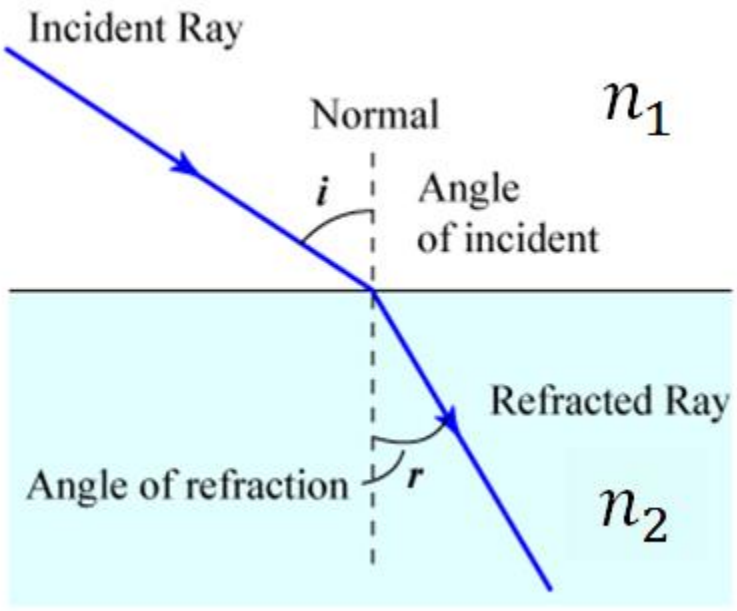

Figure 15: Snell`s law exemplified with $n_1<n_2$.

1.17 Total inner reflection

A consequence of Snell`s law when $n_1>n_2$ (1 referring to the medium of incident and 2 the medium of refraction), is that at a certain critical incident angle Θc, the light will be totally reflected. This occurs at the maximal value of Θ_2, $sin\Theta_2=1$

$$n_1 sin\Theta_c = n_2 \tag{1-8}$$

Since $\Theta_2>1$ is impossible, the light will be totally reflected (Lillestøl, et al., 2006).

1.18 Thin Film Interference

In this thesis the experimental work consist mainly of hydrate formation and dissociation in a micro-model. During these experiments it has been observed interference patterns in water films and hydrate films which can give valuable information on growth rate or dissociation rate and the thickness of films.

In sufficiently thin films of different materials, interference patterns from the reflected beams are possible to detect visually. Thin film interference has numerous applications one of which is to measure thickness of the film or separation between two media. Three important things have to be pointed out:

1. The wavelength of light transmitted through a medium with refractive index n_a is $\lambda_n=\lambda/n_a$. The refractive index tells us how much the light will be bent from one medium to another, how much light will be reflected and how much the speed and the wavelength will be reduced with respect to its vacuum values.
2. Light in a medium with refractive index n_a, reflected from a surface of a medium with refractive index $n_{b,}$ where $n_a<n_b$, will get a phase shift of π. When $n_a>n_b$, there is no phase shift.
3. If the film is too thin there is no interference pattern. If the film is too thick many wavelengths will have the constructive and/or destructive interfering at the same thickness and thereby now pattern is detectable (Brandon & Kaplan, 2008). Visible light is in the range of 380-800nm according to Miyawa & Schulman (2001). This gives a limitation of the thickness of the films to be observable.

Six scenarios that are relevant in this thesis concerning thin film interference are illustrated below in Figure 16, Figure 18, : and are:

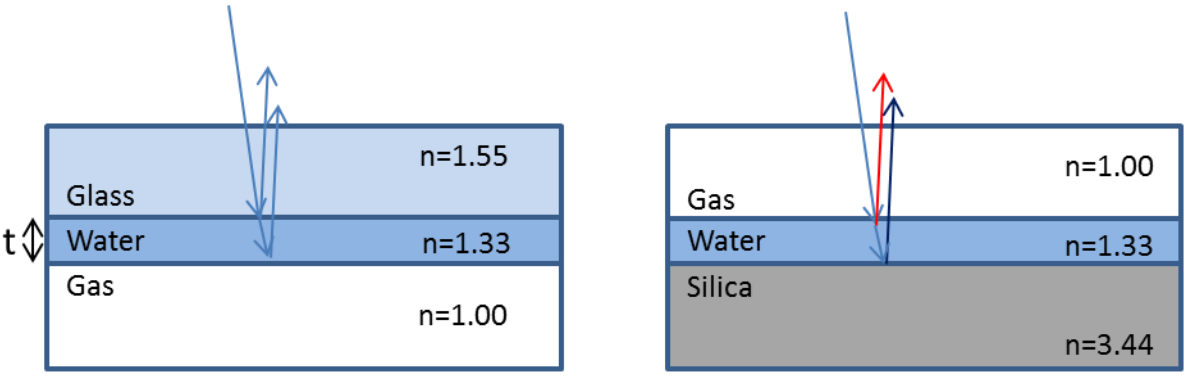

Figure 16: To the left case number 1 and case 2 to the right. The red arrow symbolizes a phase shift of π, whereas the dark blue a double phase shift. The model is seen from the side.

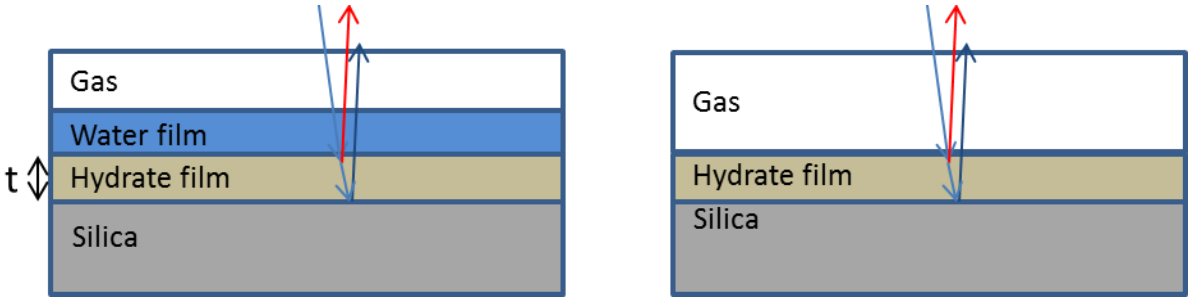

Figure 17: Hydrate film growing from the silicon wafer surface with water or gas on top.

The mathematical expression for constructive interference will be the same for all four scenarios since a double phase shift of 2π gives the same expression as no phase shift. Constructive interference in these four examples is given by:

$$t = \frac{\lambda * m}{2n_{water}} \tag{1-9}$$

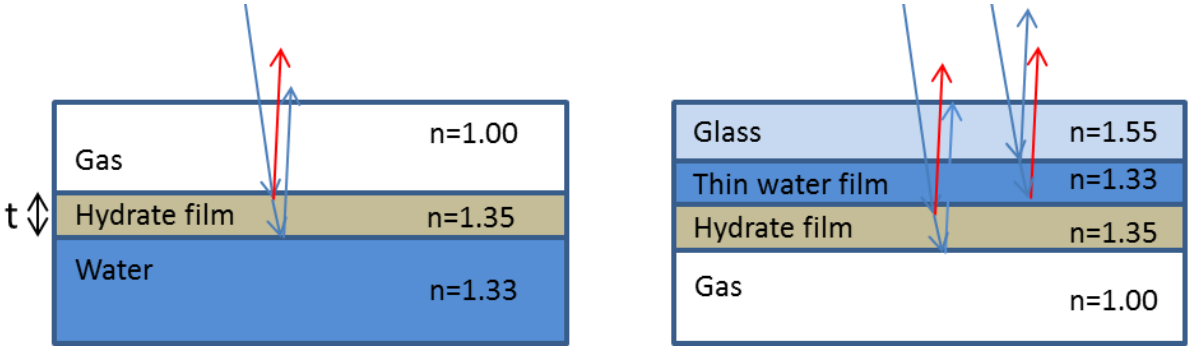

Figure 18: The hydrate film can emerge from gas to water interface (left) or from a thin water film, which adheres onto the glass surface, to gas interface. As seen on the model to the right, there are two possibilities in which an interference pattern occurs. Red arrow symbolizes phase shift.

Three possible scenarios are given for constructive interference when a thin hydrate film has formed, in Figure 18. In all three cases the expression for constructive interference will be

$$t = \frac{\lambda * (2m - 1)}{4n_{hydrate}} \tag{1-10}$$

Where *m* and *2m-1* are 1, 2, 3… and symbolize if it is the first interference maxima, second, third… . The interference pattern will repeat itself but the numerical distance between larger numbers is small and therefore the pattern will get blurry and vanish as the maxima's overlap.

2 Literature survey

2.1 Methane Hydrate formation in porous media

The hydrate formation in micro-models in this thesis is similar to Tohidi, et al. (2001), but a more realistic pore network resembling a 2D profile of Berea sandstone was used. Their model had an etched pore network consisting of up to 50µm deep channels and width > 50µm. The pore network was open to the surrounding gas and was put in a pressure vessel and pressurized by the surrounding gas to 40MPa (very high pressure). They saw visually that hydrate formed at the liquid-gas interface as well as from dissolved gas in water. The also noticed that hydrate formed within the center of pore spaces, rather than on the grain surfaces. Hydrate cementation of/between grains only occurred for the smallest grain sizes or where most of the pore space was filled with hydrate. At high clathrate saturations there was still a thin water film on the grains.

The effect of capillary inhibition on methane hydrate growth due to small pores size was investigated by Turner, et al., (2005) and Uchida, et al. (2004). Turner, et al. (2005), observed on their sensitivity analysis that for pore sizes greater than 0.12µm the temperature shift was less than 0.2% or -0.55K at 273.15K and below the uncertainty of the thermocouple. They concluded that their results showed no difference between a porous network of average pore radius 550Å and bulk system regarding hydrate equilibrium data.

With pressures of 40-60 bar Uchida, et al. used Berea sandstone for investigating capillary inhibition of hydrate growth. The Berea sandstone grain size ranged from 50µm to 200µm and had a mean grain size of 115.6 µm. They also used glass beads of uniform diameter of 20µm and 100µm. They concluded that the maximum pore size that give rise to a negative temperature shift were about 50µm for sand and sandstone, 100µm for 100µm glass beads, and 10µm for 20µm glass beads. The surface texture of the different materials did not significantly affect the hydrate equilibrium conditions but the pore size distribution did. Therefore glass beads serves as good medium for studying hydrate. They also observed that hydrate formed in the largest pores first. However, most of their measurements were within the uncertainty range when investigating their data.

Methane hydrate growth and formation were observed in glass micro-models by Katsuki, et al. (2007). The micromodels were made out of two glass plates that had straight channels of 10µm width in a grid pattern with 20µm interval. Methane gas was dissolved in the liquid water at 1 K above the methane-hydrate-liquid equilibrium pressure and temperature before entering the model. They observed pressure decreases of 0.1-0.8MPa during the experimental runs. They attribute these pressure losses to methane gas consumption by hydrate growth and temperature decrease. They however, pointed out that the actual degree of pressure loss is not clear due to possible plugging of the tubing connecting the pressure transducer. They reported

hydrate film growth at the methane-water interface and hydrate crystal growth into the gas phase. The hydrate films before ageing appeared black and coarse but an explanation to this was not given. Faceted crystals seemed to be cementing to the channel walls. Ageing, smoothened the coarse surface of the crystals. Particulate and dendritic crystals did not attach to the channel walls and were formed at higher driving forces.

Very interestingly Jiang, et al. (2010) found that cooling rate was a significant factor of the induction time. The faster the cooling rate the shorter the induction time, but the lower the conversion of methane gas to hydrate. They used loess with grain size of 10-100µm with a mean of 35µm and deionized water. They vacuumed the cell containing the loess before injecting the fluids.

Methane hydrate formation in bulk conditions, with a flat methane-water interface, were conducted by Sun, et al. (2010). The morphology and growth rate of the hydrate crystals was very dependent on the driving forces, see Figure 19 below. The surface itself grew as a single crystal at lower driving forces and with a polycrystalline structure at higher driving forces. They also observed, from a single methane bubble experiment, that initially the surface is coarse but smoothened on ageing and further growth.

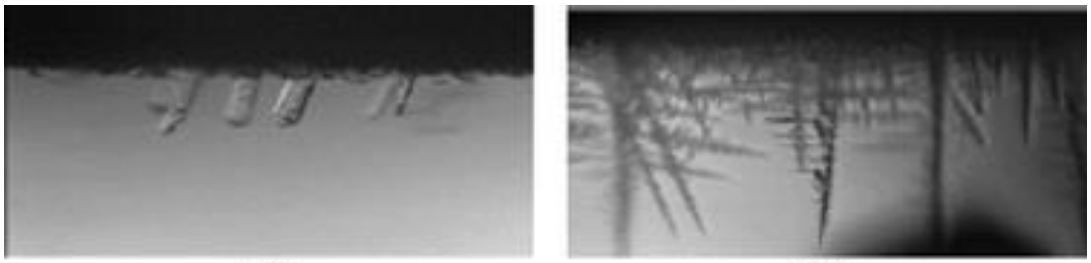

Figure 19: a) smaller driving force 6.9MPa and 273.5K. Columnar hydrate crystals growing into the water phase from the methane water boundary. b) A higher driving force of 9.7MPa and 273.3K. Dendritic crystals growing into the water phase from the methane-water boundary (Sun, et al., 2010).

Methane hydrate film crystals and morphology was studied experimentally by Ohmura, et al. (2005). They observed that irrespective of the system-pressure the methane hydrate was initially formed at the interface and then the hydrate grew into the liquid water from the film. The water was saturated with methane prior to hydrate formation. At 273.5K, hydrate formed under pressures from 6-8MPa hydrate crystals with skeletal, columnar morphology were formed and dendritic crystals for pressures of 10MPa.

2.2 Methane Hydrate Dissociation

To investigate a possible shift in the three phase equilibrium line hydrate formation at equilibrium conditions was done in this thesis. Capillary inhibition and the effect of vacuuming the water was the main goal in this thesis. The experimental data could hopefully be comparable to CSMGem values and a dissociation study by Yang, et al. (2001) and Katsuki, et al. (2008). Yang, et al. (2001) did a visual study in a high pressure view vessel (bulk conditions) and the average deviation with theoretical values was 2.1%.

2-1: Dissociation data by Yang, et al. (2001) from a high pressure view cell.

Temperature (K)	Pressure (Bar)
276.5	3.68
278.5	4.19
279.7	4.90
281.3	6.07
282.2	6.55
283.0	7.13
283.8	7.73
284.5	8.33
285.8	9.55
286.3	9.66

Katsuki, et al. (2008) performed a visual observation of methane hydrate dissociation in glass micro-models by increase in temperature and decrease of pressure. The glass micromodels were the same as used in the formation and growth study from 2007. They observed that the dissociation front in both cases could not be determined. Methane bubbles formed on the surface of the hydrate crystals formed into slugs filling the whole pore volume in a matter of seconds or diffused through liquid water to a free gas phase. The hydrate crystals that were in contact with the gaseous methane melted first.

2-2: Dissociation data of Katsuki, et al. (2008).

Type of dissociation	Temperature	Pressure
Temperature increase	288.2K	12.2 MPa
Temperature increase	288.0K	10.2 MPa
Pressure decrease	Constant 284.7 K	9.8 MPa
Pressure decrease	Constant 274.5 K	2.0 MPa

They conclude that for methane bubbles not appearing on the hydrate face, the methane is dissolved in a water film on the hydrate and transported through this film or through liquid water due to a concentration difference with the methane-water interface. They assume that the surface of the hydrate crystal has the three phase equilibrium temperature while the methane-water interface has a higher temperature. Thereby, the solubility of methane is lower on the methane-water interface creating the concentration difference.

- From this survey some questions naturally arose and answers and comparison to these was under focus throughout this work.
- Did this synthetic pore-network shift the three-phase-equilibrium line?
- Would there be a visible difference in structure and growth of hydrate crystals under different conditions?
- Why was the hydrate film black/dark and why did it become transparent upon ageing?
- Would there be visual cementation of hydrate crystals to the matrix?
- What was the effect of vacuuming the water?
- What factors promote hydrate growth in this porous media?
- Would there be visual differences in hydrate dissociation regarding pressure decrease versus temperature increase?

2.3 Micro capillary network in hydrate films

This part of the literature study was done to get an "up to date" and better understanding of mass transfer through hydrate films. This is only referred to once in the thesis. Most importantly was it done to know that models for mass transfer through hydrate films were rooted in theoretical models.

Several models exist that explains mass transfer through hydrate films thereby "*Hydrate in suspension models" "Micro-perforated plate models" and "Permeable solid-plate models".* These models are discussed by Radhakrishnan, et al. (2003). Based on a theoretical study by molecular simulations they found a model that predicts the diffusivity of CO_2 in the hydrate phase accurately. DAVIES, et al. (2010) on the other hand did a study on mass transfer through methane hydrate films with isotopic tracers and Raman focal spectroscopy. They found that the methane hydrate film contained gas filled pores, which provided pathway for gas migration supporting *"Micro-perforated plate models"*. These pores annealed over time and increased the mass transfer resistance. They conclude that their results indicate that movement of the water within the hydrate film is controlling the hydrate growth.

3 Experimental setup, Procedures and Materials

All experiments were conducted in a laboratory at the Institute for Physics and Technology at the University of Bergen. Two main setups have been used in the experimental work one of which was already in place and set up by former PhD and master students. Using a microscope and a "2D model" of a pore network which can withhold high pressures, it is possible to study pore effects, flow and hydrate growth visually. A slight modification was done before the initial experiments, though. An extra pc-screen for live view monitoring was brought in place, making it easier to detect the start of visual hydrate growth in the micromodel.

3.1 The high pressure micromodel

Only one type of micro-model has been used during the experiments. It is produced by Pharmafluidics, have an operating pressure in the range 0-150 bars is 1.7 mm thick and characterized as a high pressure model. It Consist of two main parts that are anodic bonded together. The silicon wafer is etched with a pore network and a glass wafer on top to cover and seal the network (Hornbrook, et al., 1991). Anodic bonding is used to avoid an intermediate layer and is able to bond hydrophilic and hydrophobic silicon surfaces equally effectively. High voltage and temperature (several hundred volts and 200-500°C) causes a diffusion of oxygen atoms through the glass to the interface between the silicon wafer and the glass wafer and forms a siloxane (Si-O-Si) layer which acts as a "glue". These oxygen atoms stem from a chemical bond with alkali-metals which are impurities in the glass. While the oxygen atoms are attracted to the positive side of the applied electric field, the alkali-metal is diffused to the negative and opposite side due to its positive ionic state (Wallis & Pomerantz, 1969). This oxide layer gives the model a strongly water wet behavior (Buchgraber, et al., 2012).

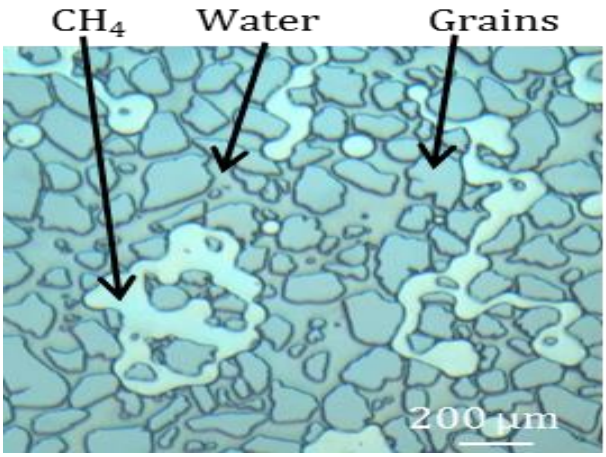

Figure 20: A typical view in the model under the microscope where the lower right corner shows a dimension length of 200µm. Modified from Hauge, et al. (2015). Knowing that the model is water-wet and the convex curvature of gas in a gas-water system it is easy to classify the white areas as free methane phase.

Linear thermal coefficients of silicon and borosilicate is 3.0 [10^{-6}m/(m*K)] and 3.3 [10^{-6}m/(m*K)], respectively (EngineeringToolbox, u.d.), (Azom, 2011). Similar and low thermal linear expansion coefficients, minimizes the risk of cracking upon temperature changes.

A simplified construction procedure based on (Hornbrook, et al., 1991) is given below.

- A thin section of the porous medium was photographed with high enough magnification to capture details of the grains and voids. This image was then turned into a black and white negative picture.
- The image was digitally manipulated to ensure that continuous flow paths exist. In 2D view of a porous network grain contacts will appear as a blocked pore throat.
- An image mask used to transfer the flow paths onto the silicon wafer was applied.
- The silicon wafer was coated with a photo-resist material and the coated side was put into contact with the image mask. Ultraviolet light was then shined through the image mask and destroyed the photo-resist material which exposed the flow patterns in terms of clean silicon surface. The flow patterns was now of desired depth. A DRIE (Deep Reactive Ionic Etching) technique was used to etch the model, causing the pore walls to be vertical and ensured the same width in a vertical profile of a pore.
- 4 holes were drilled on the backside of the silicon wafer (called ports), enabling access to the pore network. Finally the two wafers were anodic bonded together.

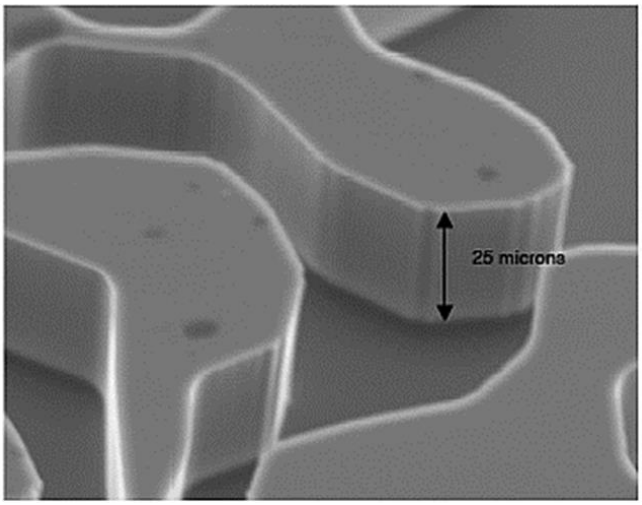

Figure 21: The vertical walls due to DRIE (Deep Reactive Ionic Etching), ensures the same width in a vertical profile of a pore. SEM (scanning electron microscopy) was used to measure the etching depth (Rangel-German & Kovscek, 2006). Note that this image was not of the same pore network as the models used in the experimental work, but the same etching method was used and therefore it illustrates the precision and depth of the flow channels.

Due to the vertical walls, that otherwise would have been curved, the porosity is larger than for the Berea sample. For the purposes of this thesis only a rough estimate of the total pore volume is needed. Pore volume is given by

$$V_P = L * W * H * \Phi \tag{3-1}$$

Where, L, and W, is the length and width of the pore network, H being the etching depth and Φ is the porosity. The pore network has the dimensions as indicated by Figure 22.

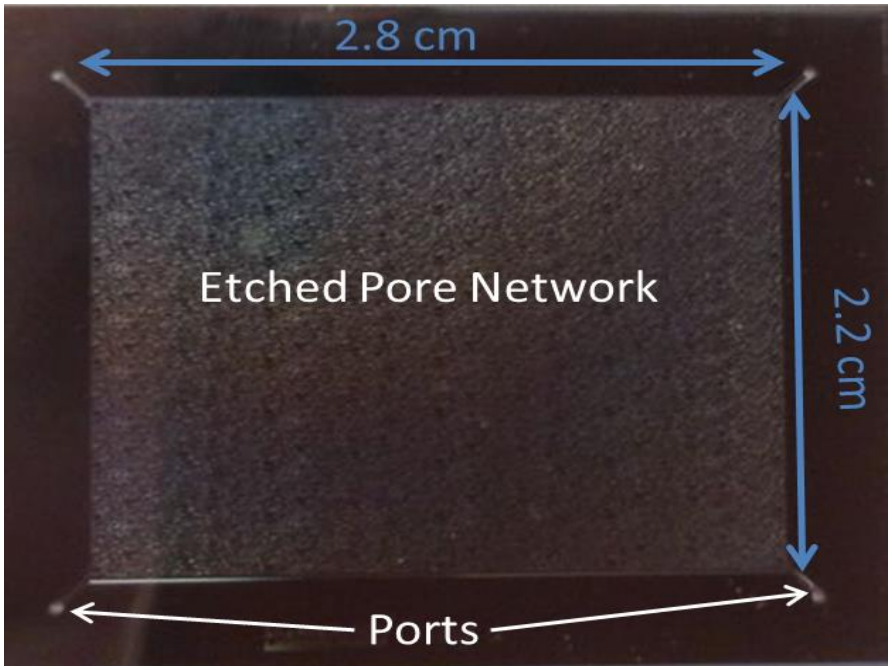

Figure 22: High Pressure Micromodel with etched pore network.

These measurements were done with a caliper. Using the most upper values, beyond the uncertainties, ensures that the calculated volume is higher than the real physical number. Using equation (3-1), but assuming a porosity of 60% (Høyland, 2014), one finds that P_v= 0.00924 ml. That is, a volume less than 0.01 ml. In comparison the, 1/16 tubing has a volume of ca 0.5ml per meter. Care was taken when saturating the model with gas and water, as traces of air or any other substance potentially could partly fill the model, and possibly be a cause of hydrate inhibition.

An elaborate discussion on the thermal properties was needed to understand the heat transport through the model as one cannot measure the temperature inside the micro-model directly. Thermal conductivity coefficients for water, borosilicate, silicon and aluminum is 0.609 (at 27°C), 1.14, 156 (at 27°C) and 237 [W/(m*K)] respectively (Azom, 2011), (Semiconductor, u.d.), (Lillestøl, et al., 2006) .

The general heat transport equation is given by

$$\rho c \frac{\partial T}{\partial t} = \boldsymbol{\nabla} \cdot (\kappa \boldsymbol{\nabla} T) \tag{3-2}$$

Where is κ the heat conductivity, ρ is the density and c the specific heat capacity. The solution of this partial differential equation for a one dimensional problem is given by

$$T(x) = T_0 + T_S cos \frac{\pi x}{L} \exp(-\frac{t}{\tau}) \tag{3-3}$$

Where, τ is known as the time constant for cooling/heating, L is the length of the material in the heat flow direction, T_0 is the known temperature on the outside of the surface while T_s is the temperature in the middle of the material (Lillestøl, et al., 2006).

$$\tau = \frac{\rho c L^2}{\kappa \pi^2} \tag{3-4}$$

Equation (3-3) yields the temperature as a function of depth in a plate. If the temperature inside the model is lower than the surroundings the second term is valued negative. Since the width and length of the micromodel is so much larger than the thickness it is reasonable to assume that a time dependent heat flow relation can be reduced to a one-dimensional problem, therefore using equation (3-3). When comparing the heat conductivity coefficients one finds that, water inside the model and the glass, will act as isolators while the heat flow will mainly be through the silicon wafer. The silicon wafer is 0.6mm thick. Using this together with density of 2.33 [g/cm^3], specific heat capacity 712 [J/(kg*K)] (Haynes, et al., 2015) and heat conductivity κ=156 [W/(m*K)]. Equation (3-4) yields $\tau \approx 3.95*10^{-3}$ seconds. Meaning that after $3.95*10^{-4}$ seconds the temperature difference is reduced according to, $T_\tau = \frac{Tstart}{e}$. For the aluminum frame of 4mm thickness τ is calculated to be 0.02 seconds, with c=900 [J/(kg*K)], κ=237 [W/(m*K)] and 2.70 [g/cm^3] (Lillestøl, et al., 2006).

In addition a consideration of the heat transfer coefficient is needed. In between the model`s backside and the aluminum frame there is a thin water layer. Impossible to measure when the

two frames are screwed together and the rubber packings squeezed. This layer is definitively smaller than one millimeter. Using 1mm as an upper limit and c=4186 [J/(kg*K)] one arrives at approximately 0.7 seconds. Thus, the water layer in between the model and the frame is the limiting factor. For ten periods of τ_{water} (7 seonds) the temperature difference is practically zero. This means that the temperature difference of the inside of the model and the still water is, in this experimental work, negligible as an uncertainty. Note that changing the temperature of the still water takes several minutes for every 0.1°C upon cooling, a little faster upon heating.

3.2 Assembly of the model

To assemble the model six main steps were required. The picture sequence in Figure 23 is explained by the following:

1. The bottom aluminum frame was placed facing up and the nano-tubing guiders were pushed into position.
2. The black rubber packings were placed in their countersinks on the nano-tubing guiders.
3. The micro-model was carefully put in place and simultaneously one made sure it rested only on the rubber packings.
4. The frame was held up against a light source to confirm that all four holes in the guiders went clear of the rubber packings and let light through.
5. The top aluminum frame was put in place and the 9 screws were finger tightened. Then, 1Nm of torque was applied with a momentum key on the screws. Opposing screws were tightened in pair to ensure that the model was pressed vertically down. More than 1Nm was not recommended due to increased risk of cracking the model when put under pressure.
6. The nano-tubes were connected finger tight in the guiders. The model was then ready to be connected to 1/16” steel tubing. Pressure and flow testing was necessary before using it experimentally to check for leakage and permeability.

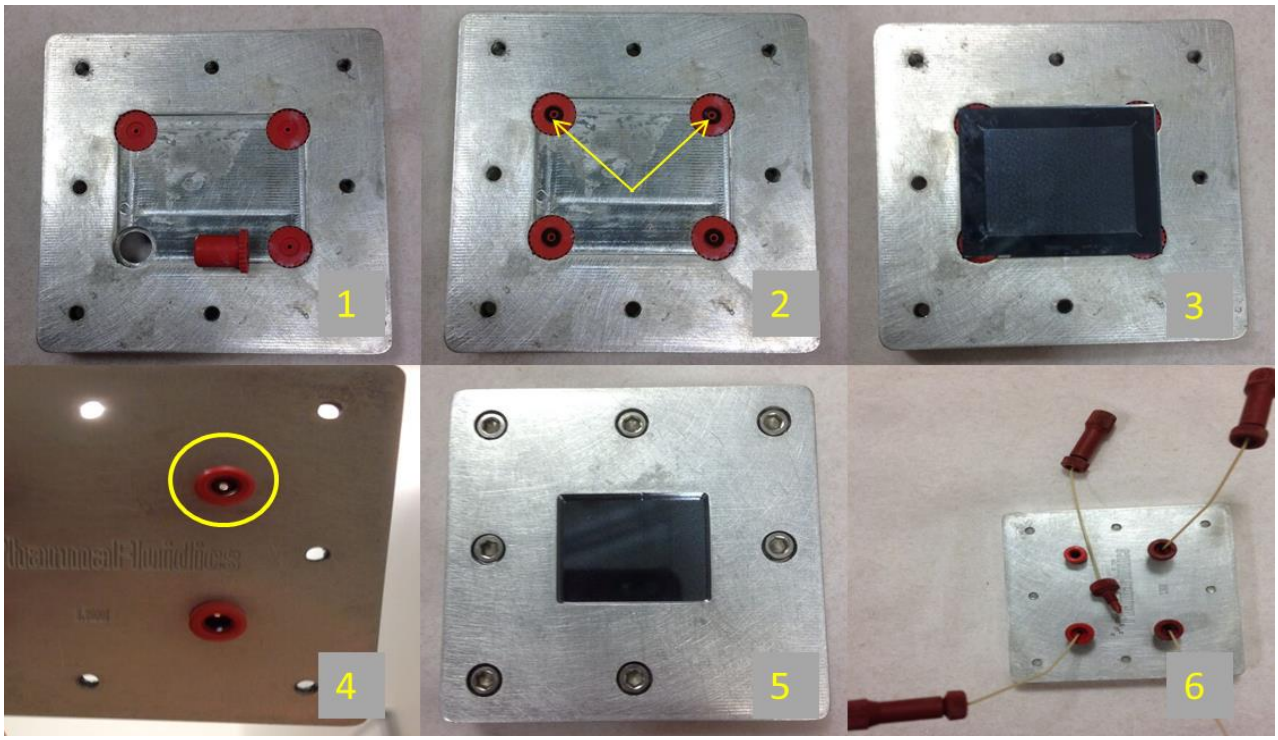

Figure 23: Mounting sequence of the micro-model. 1) nano-guiders were placed. 2) Rubber packing on the guiders was put in place. 3) The micro-model was the positioned into the aluminum frame. 4) Making sure the rubber packing was not blocking the nano-guiders. 5) Top frame mounted on. 6) Nano tubes connected.

3.3 Apparatus

The list of materials and equipment below was the same in Setup A and Setup B, but there was one exception. The lid on the cooling chamber was not sealed and fastened so if the flow of cooling liquid was too large it would flow over the edges. This was a limiting factor of how cold the still water and model could get. In setup B the chamber was replaced with one that was sealed up and could withhold enough pressure to run the low temperature bath on maximum flow.

Constituents of the experimental setup:

- Quizix Q5200 Pump System (40ml cylinders)
- 1/16" and 1/8" tubing, valves and fittings from Swagelok
- Genspec Standard ESI usb Transducer: 0-400 Bar ± 0.25%
- Lightsource: Photonic LED F1 Cold light 5500K
- Nikon Digital Camera D70100
- Propylene glycol based antifreeze by Camco
- Nikon SMZ1500 microscope
- HH506RA Multilogger Thermometer by Omega engineering
- Thermo Scientific Neslab RTE 17 low temperature bath
- Self-designed Chamber for cooling liquid
- Methane gas from YaraPraxair, Purity ≥99.5%
- Distilled water

3.4 Uncertainty of the thermometer, pressure transducer and pump.

The temperature measurements showed to be the biggest uncertainty. The thermometer was tested with 2 different pins and against 4 other thermometers. The average temperature of these measurements was used ± 0.6°C which was the biggest offset. The calibration of the thermometer is a rather hard task to do and the equipment needed was not at hand.

Three pressure transducers were used, two of which were part of the pump and one single that was used for calibration and control measurements on some experiments. Although, the transducers on the pump were calibrated accurately, during the experimental runs the fluctuations were significant. Therefore an uncertainty equaling the largest fluctuations at stable situations of 0.1Bar was used. The uncertainty of the calibrating transducer was given as ±0.25% by the manufacturer.

3.5 The valves

The valves and metal tubing were delivered by Swagelok. The two way valves had only one option, either opened or shut. The three-way-valves had three options as described by Figure 24.

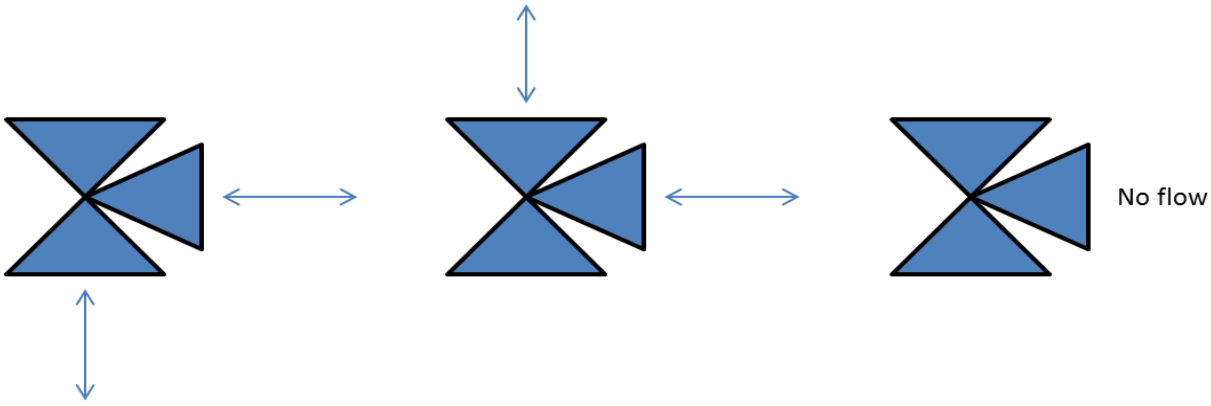

Figure 24: Showing the flow options in the three way valves. Notice that flow through the two vertical inlets at the same time was not possible.

3.6 Vacuuming the water

It became clear during the initial experiments that an evacuation of the distilled water used for hydrate formation was necessary. Nitrogen and methane has about the same solubility in water at STP while oxygen has about the double. In reservoir conditions there is no oxygen (or very small amounts) present. Also, oxygen is consumed by living organisms and the concentration drops rapidly from the surface of lakes and the ocean. Biodegradation of organic material below the seafloor, in sumps and source rocks etc. is anaerobic (Selley, 1998).

At thermodynamic equilibrium the chemical potential of the components has to be equal in the aqueous and gaseous phase. According to Henry`s law the amount of gas dissolved in water for a dilute solution is proportional to the partial pressure in the gaseous phase. Hence, higher partial pressure leads to increased concentration. This is achieved in two ways either by increasing the total pressure or having only one type of gas present. By evacuating the water and then introducing it to methane gas the methane concentration will increase in the water, which in turn might promote hydrate formation.

For vacuuming the water the system in Figure 25 was used.

Figure 25: Set-up for vacuuming water with transition-valve to the experimental pump.

1. The O-rings were greased up, the containers were put together with the clamp and valve 2 was shut.
2. The water was set under a pressure of less than 2mbar by a vacuum pump for ten minutes. This was sufficient to minimize the dissolved air gases.
3. Valve 1 was closed.
4. The rubber tubing was then released from the vacuum flask.
5. Valve 2 was then connected to the high pressure pump and cylinder A was filled.
6. All volumes from cylinder A to valve three in Figure 27 were flushed with water to ensure a minimum of air in this part of the setup.

When filling the pump with vacuumed water the vacuum system was turned upside down in order to get water through the tube.

3.7 Setup A

The micromodel was connected to the pump via 1/16" tubing. The model was placed in still water that was cooled down by the cooling liquid through the aluminum barrier. In order to get clear and focused view of the pores upon magnification by the microscope, the water surface had to be absolutely still. The microscope could get out of focus in two different ways when the camera was set to interval pictures for a longer period of time (10 hours +):

1. The objective might creep a little down.
2. The cold still water condensed moist from the air resulting in an elevation of the water surface.

Cylinder A was filled with water and B with methane gas. Two of the ports in the model were closed, as indicated by the *x* marks in Figure 26, permitting only diagonal flow. It is not possible to measure the temperature within the model directly, but the thermometer was put in the still water right under the model. In a steady state situation (no temperature change) it is reasonable to assume that the temperature inside the model equals the still waters temperature.

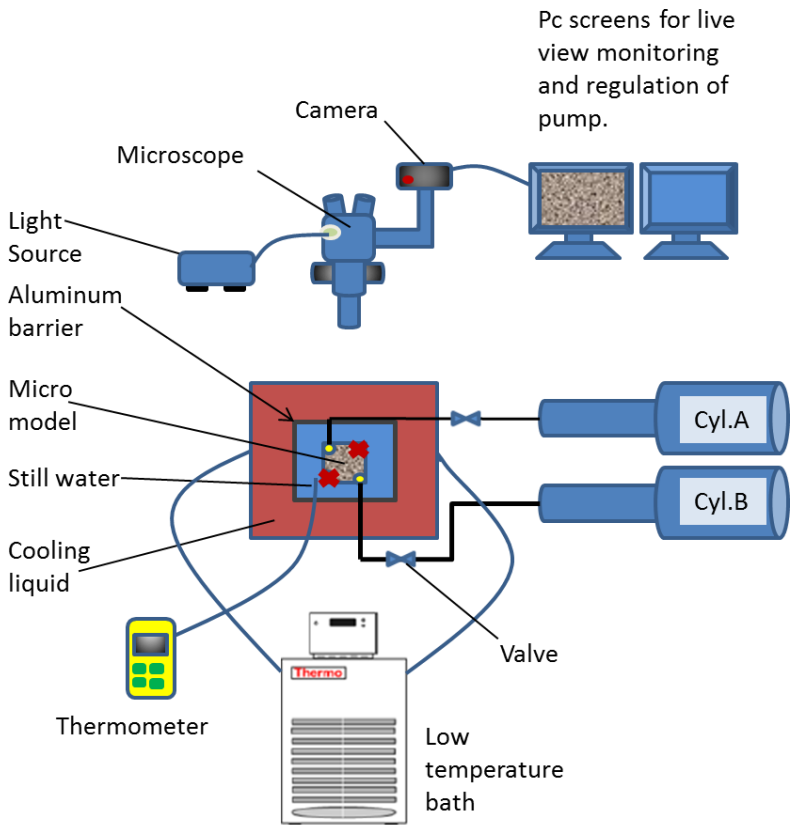

Figure 26: Experimental setup A.

3.8 Experimental Procedure for setup A

The model had been resting on constant pressure 80 Bar and 0.7°C for 3 weeks. Noting that the bath was set to -1.5°C, but because of heat loss through the tubing and chamber, the temperature in the still water and model is always higher. The flowrate from the bath had to be adjusted not to overflow the cooling chamber. This strongly reduced the cooling capacity. The pump was working in *independent constant pressure mode*, practically meaning that the pistons work independently and will retract and extend all the time by small amounts to withhold 80 Bar.

1) The bath temperature was set to 10 degrees.
2) Camera was set to take pictures at preset intervals, while carefully monitoring the model. When something of interest happened (hydrate growth, fluid movement) camera was set to record in video mode.
3) When the system had stabilized its temperature (depending on the room temp) usually around 12°C it was left for approximately two hours.
4) The bath was then set to -1.5°C, aiming for still water temperature of 0.7°C
5) When cooling the system the model was monitored continuously in order to record hydrate growth on video.
6) At a stabile temperature of the still water the camera was set to take pictures at intervals of 2 hours to document the development during the subsequent days.

3.9 Setup B

The new cooling chamber was mounted and the valve regulating the flowrate of cooling liquid was disconnected to maximize the flowrate and the cooling effect. This led to a temperature decrease of the still water and to a desired temperature of 0°C - 1°C. For rapid cooling regular ice cubes was put in the still water.

All ports of the model were put in use as indicated by Figure 27. Two "reservoirs" consisting of coiled tubing, acting as a heat exchanger was placed diagonally in the still water. With such low flow rates used, the coiled tubing of approximately 1 meter cooled the water/gas down to still water temperature when reaching the model. The ideas behind is to flow gas or water to visualize gas flow with hydrate present and, induce more hydrate growth by adding more gas when it has been totally consumed, stir up the fluids in the model to promote critical nucleation if hydrate does not form. One problem encountered from the first experiments is plugging. The nano-tubes, the steel tubing or in the ports is plugged by hydrate and inhibits flow through the model. This is most likely due to a mix of gas and water slugs. As seen in the model and described by theory the hydrate growth appears at the interface between the phases. By a certain procedure, to be described in section 3.10, it was possible to avoid these alternating slugs. The reservoirs would then be totally filled with only one phase, all the way through the ports, to prevent plugging.

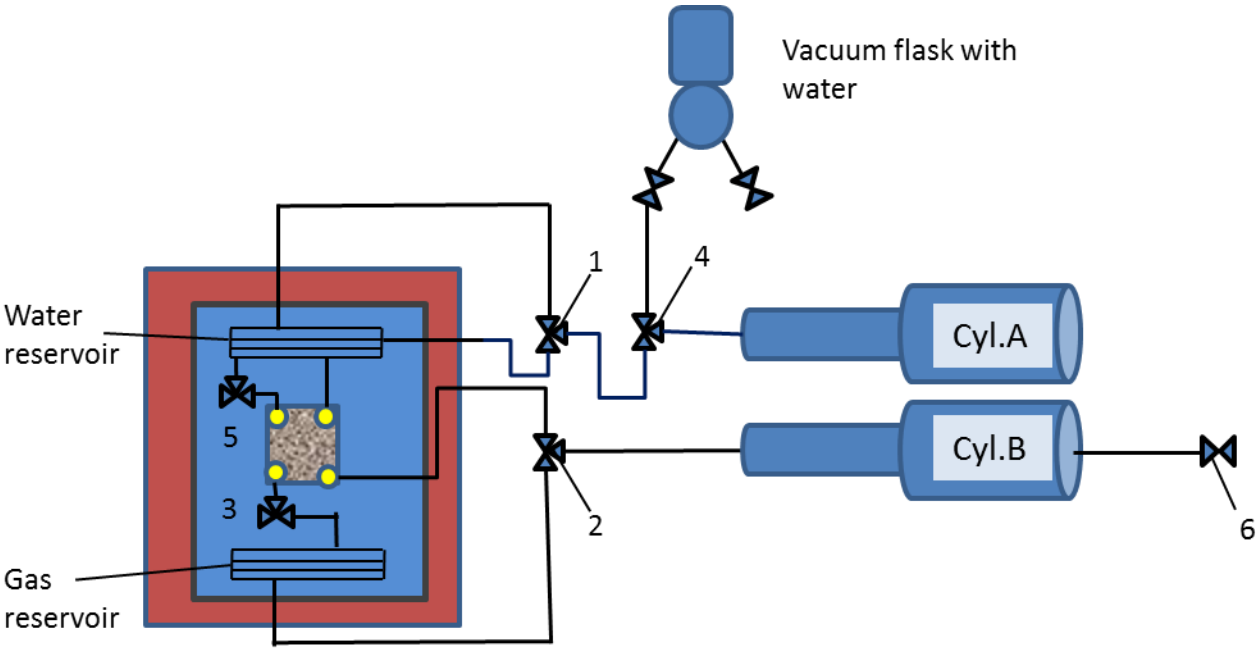

Figure 27: Setup B. Equipment from setup A is left out for clarity in the figure. Three way valves are used to control flow through reservoirs and model.

3.10 Procedure for filling the high pressure pump

1) The pump was emptied by setting the pistons to maximum extension with the open end of valve 3 to atmospheric pressure.
2) Valve 1 and 2 was shut.
3) Water was introduced via valve 4.
4) The piston in cylinder A was retracted and the whole volume was filled with water.
5) Cylinder B was then filled with methane gas via valve number 5.

3.11 Procedure for filling the "reservoirs" and micro-model

1) To fill the reservoirs valve 1 and 4 was opened, water flushed through the model to atmospheric pressure out of valve 3. Valve 5 altered between open and shut making sure both inlet tubes to the model was filled with water. To avoid communication between the cylinders in the next steps, valve 1 was shut.
2) The outlet to atmospheric pressure in valve 3 was shut and the pathway from the gas reservoir to the model was opened. Valve 2 altered between the two model inlets to flush the tubes and model with methane. The methane was vented out to atmospheric pressure small seeps at a time, to ensure that the volumes let out being out of flammable range.
3) Then the model was pressurized with methane through the methane reservoir to 10-20 bars below the pressure desired for the experiment. The reason for water flushing first was that the port into the model by valve 3 needed to be filled with methane to avoid an interface that may result in plugging.
4) Valve 1 was opened up without pressure difference across the valve (to avoid fluid flow).
5) The remaining 10-20 bars were pressurized with the water from cylinder A. This to ensure enough water in the model. This way of pressurizing the model makes it easier to get a more controlled water to gas ratio.
6) Valve number 1 was closed shutting of cylinder A. Valve 2 was opened without differential pressure from model to cylinder B. The model was then ready for a temperature decrease and the pressure regulated with methane from cylinder B.

4 Water films, hydrate films and micro-model properties

To make the reader familiar with how the results are presented, chapter 4 will deal with the interpretation of the micromodel. How hydrate appears in the microscope and how to identify the different phases are explained.

4.1 Color and sharpness of images

The pictures to document this work are of different colors. Explanations to why that is are given below.

1. The camera settings were of major importance. The blender opening controlled how much light that would pass into the camera and adjust the brightness of the picture. The default settings made the photos taken more blue and bright while the video was darker and more red/purple. This was adjusted when experiments were conducted with setup B, but automatic adjustments were continuously done by the camera so that the color settings changed. The water height above the model also influenced the brightness due to loss of intensity, absorption and spreading. This can be seen in Figure 29.
2. When the micro-model was pressurized, the fluids would try to split the model and put tensile forces to the glass and the silicon wafer. This might change the absorption and refractive characteristics of the silicon wafer. The thickness of the siloxane layer might change or the surface of the silicon can be affected of this. Going further into this material is outside the scope of this thesis but the reader is encouraged to read the following articles for more information (Mirshafieyan & Guo, 2014), (Kim, et al., 2011). It is hard to determine the significance of this effect here.

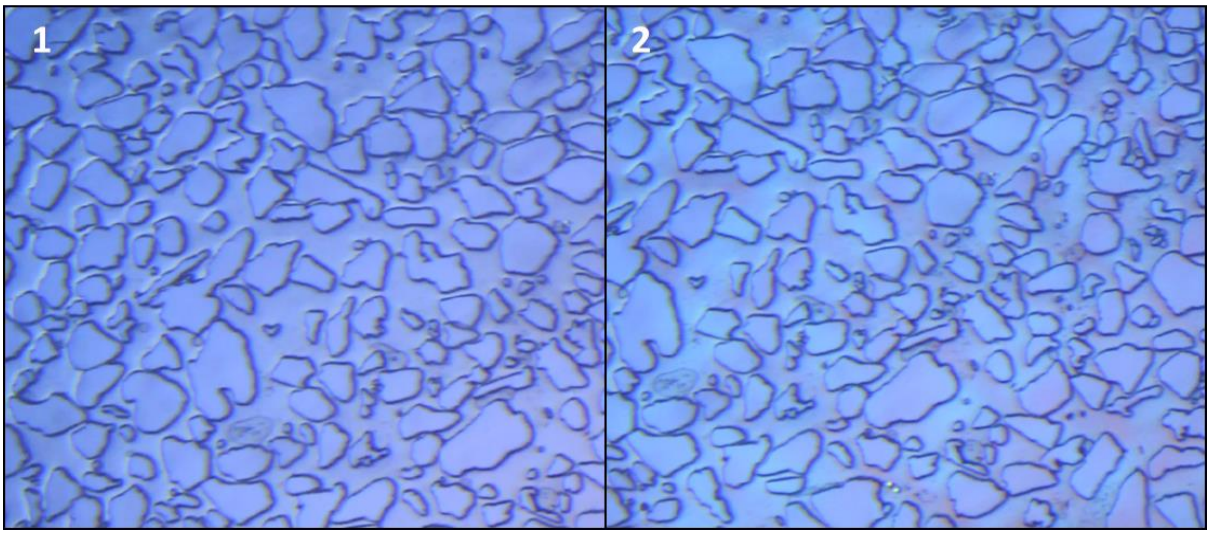

Figure 28: A pattern of pink areas appears for pressures above 100Bar (second picture). The pattern is much more visible in the microscope than in this picture. This pattern might be caused by surface changes on the silicon wafer.

3. The reflected light rays were very sensitive to the angle of the model. Two main cables/fibers from the light source entered the microscope. These were again divided into many fibers. One of the main cables gave the red end of the visible spectrum and the other the blue part. When the light rays omitted from these overlap each other the reflected light appeared as white day light, or a color temperature of 5500K which is the surface temperature of the sun. The model might bulge a little due to the pressure and changes the angle of the silicon wafer slightly. The two main light beams came from opposite sides through the lens resulting in different angles of incident and thereby different angles of reflection. So at certain angles only one of the beams would be reflected back into the lens. See Figure 29. This effect together with point number 1 is most significant to the quality and color of the photos.

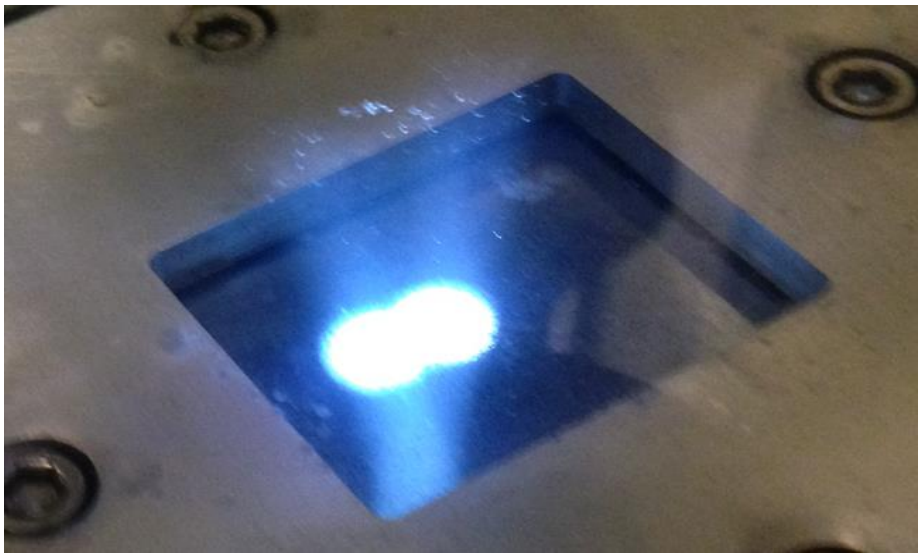

Figure 29: The two beams of light from opposite sides are easily seen when the microscope is out of focus. Dust, particles and some bacterial growth dirties up the water making the intensity of the reflected light lower.

The clearness and focus of the images was also very dependent on the water height above model surface. The water contains impurities the spreads light away but is also a dispersive media in it self (Lillestøl, et al., 2006). For getting the best images a thin water layer is favorable. Upon magnification the images would still look sharp. A thin water layer would also mean a larger temperature gradient close to the model from the surrounding air which in turn leads to very inaccurate temperature measurements. More accurate temperature measurements were chosen over sharpness of the images.

4.2 Thin water films

During flow of either gas or water thin water films attaches to the glass or silicon wafer inside the gas phase. Constructive interference patterns are observed and the rings of different colors corresponds to the different maxima`s, see Figure 30. By using equation (1-9), m ranging from 1 to 5 and the wavelength from 380 to 800 one finds that the films are between 140nm to 1500nm thick. They disappear after approximately 2 minutes. It is interesting to see that the films are thinnest at the edges. This points to film drainage from the edges which should mean that the film is getting thinner. This is indeed verified by Figure 31 and by the edges of the films which are blue.

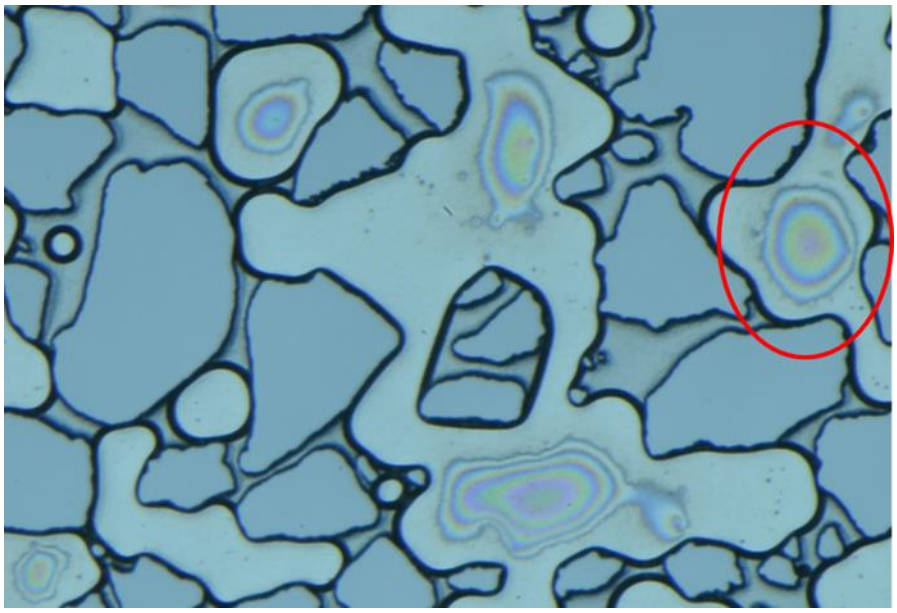

Figure 30: The water films are thinnest at the edge and more planar in the middle. The blue color of the edge tells us that its thickness is around 140nm.

By looking at Figure 30, one notice that the space between the bands of same color is smaller the closer it is to the edge of the film. In the middle of the film a larger area of the same color is seen. This is because the film is more planar in the middle with same thickness while the film curves towards the edge and getting increasingly thinner.

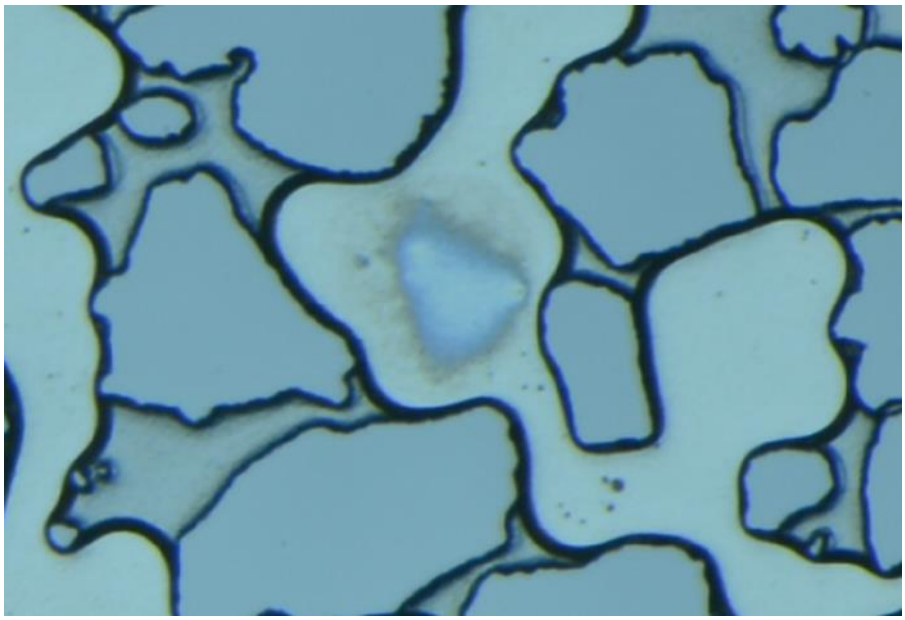

Figure 31: The thinnest possible film to be observed, around 140 nm thick. It is the remnants of the interference pattern highlighted with red in Figure 30, approximately one minute after it formed. This, together with the grey diffuse area that spreads away from the water film shows that water has drained away. The water films were undetectable after 2 minutes.

4.3 Formation and dissociation by temperature control with setup A

The following experimental work is not something that is weighted as a big part of the results. It was more of a "play-around" to get a feel of the system, to get the first visual observations on hydrate and the memory effect, typical errors, get to know the pump and low temperature bath, what not to do, how to detect plugs. From this experience the experiments with setup B could be planned and a much better control on the parameters was achieved. The pressure and temperature measurements of formation and dissociation were very inconsistent due to plugging and leakage. Therefore these values are excluded. It was however a very time consuming part of the thesis to familiarize with the equipment, working out procedures and pressure testing it.

Six successful hydrate dissociation and formation experiments were done with setup A by temperature increase and decrease at constant pressure. The micro-model was not substituted during these. The system had been resting at 0.6°C and 80 bars for 3-4 weeks. Some hydrate crystals were still in the model but mostly there was free water and gas, see Figure 32. During the subsequent experiments a small leakage from the model was identified. The pump and tubing had a pressure of 80bar but the pressure inside the model was unknown since the tubing was plugged with low/un-permeable hydrate. The remaining hydrate crystals, free gas and free water imply that the conditions inside the model are close to three-phase equilibrium.

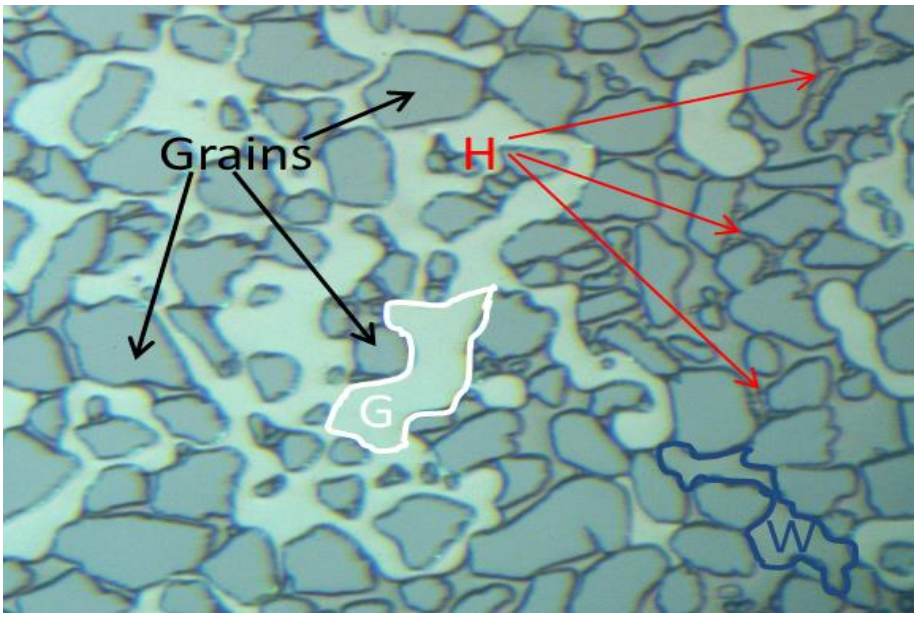

Figure 32: An example of the light gas phase is marked with white, some of the water is marked blue and hydrate is seen by following the red arrows. This color-classification will be used throughout to identify the various phases. To not lose track of the phases, knowing that the model is water-wet, one can study the curvature of the interface to differentiate between the phases.

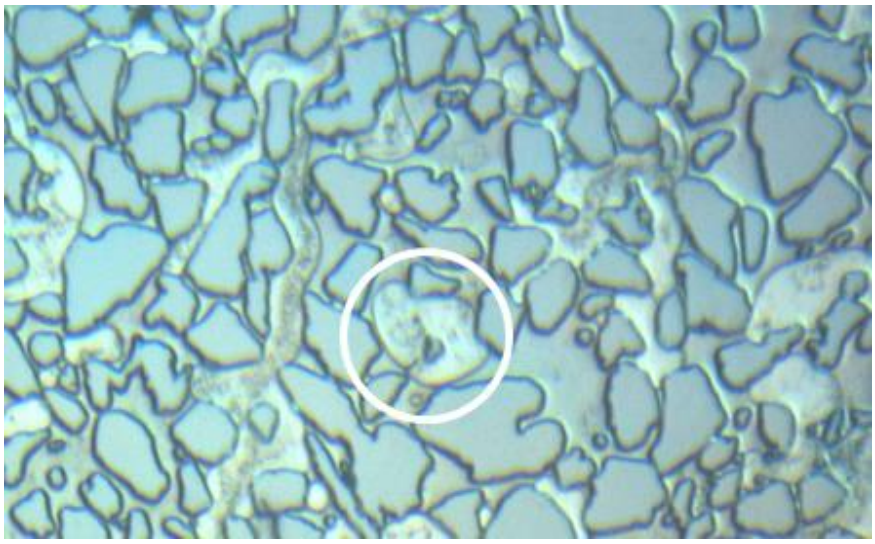

Figure 33: Gas bubbles seek to be of spherical shape to minimize the surface-energy. The black dots in the gas phase are very small water droplets adsorbed to the glass or silicon surface. They appear after water and gas flow through the model.

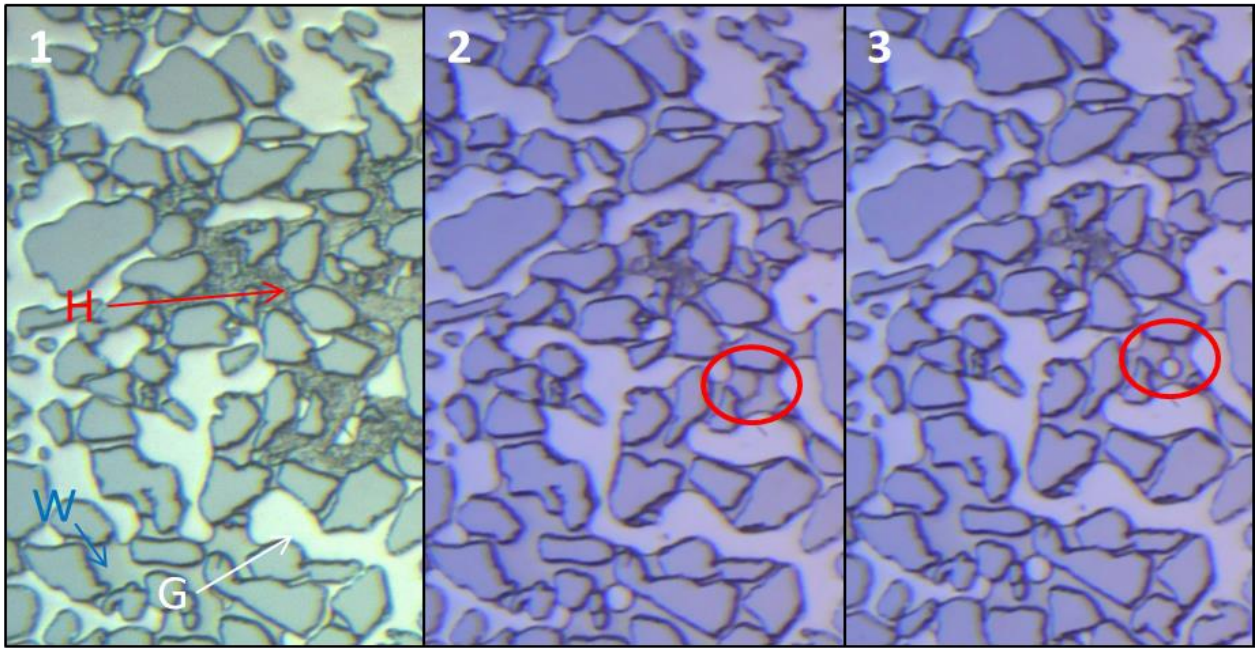

Figure 34: From picture 1 to 3, shows the development from 1°C to 5.5°C. Hydrate starts to melt and free methane gas forms as a bubble at the surface of the hydrate (red circle). The pressure is unknown due to leakage, but from section 0 and dissociation data from appendix 8.1 the pressure should be in the range of 40-60bar.

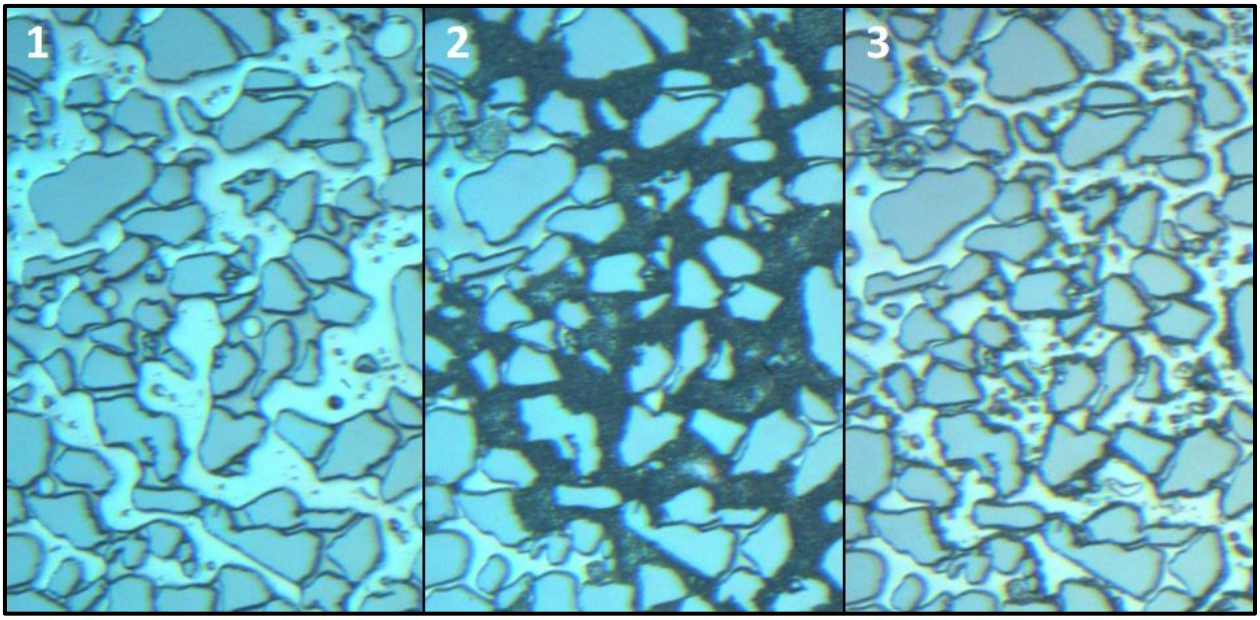

Figure 35: Redistribution has occurred due to plug melt and pressure pulse, comparing picture 3 from Figure 34 with picture 1 here. After the plug melt the pressure reaches 80bar again and temp 7.5-9.5°C and a hydrate film starts to grow. The hydrate film appears as black although it is actually white. The last picture shows the model at 12°C. Still some hydrate left but most of the water has been redistributed to another part of the model, leaving the field of view to contain a lot of gas. The black dots in the gas phase in picture 1 are small water droplets retaining to the glass and silicon surfaces of the model.

4.4 Why hydrate films appear black

When reading through the literature on hydrate in micro-models the discussion on why hydrate films appear black under the microscope was not found. The simple answer is that little to no light is reflected back to the microscope where hydrate is present. This happens only when there is gas on the hydrate film and the hydrate film is of a certain thickness (>1500nm). This has been verified by visual observations; see Figure 36, Figure 37 and Figure 38. The value of 1500nm is calculated by equation (1-9) with m=1 and λ=800nm, from observations of Figure 45, meaning first interference maximum for red light.

Spreading of light:

The difference in refractive index between water and hydrate is 0.013, which is a small difference. To visually distinguish them is difficult because very little light is reflected on the surface according to point 1 in section 0. One example of how different substances or states of matter can be hard to distinguish visually is when clear water-ice (without bubbles) is submerged in liquid water.

Hydrate-gas difference regarding refractive index, or water-gas difference if we assume that a thin film of water is covering the hydrate crystals, is 0.333 or 0.346 respectively. The following argument will be the same in both cases. This means that the light will be bent significantly according to Snell`s law and a good portion will be reflected. The problem is that the hydrate film is coarse and has many faces in different angles, and at high driving forces even dendritic crystals are grown. The light that is reflected from the surface will spread in many directions, and since the system is very sensitive to perpendicularity of the focused item with the microscope as reference frame, the reflected light rays will not find their way back into the narrow area of field of view on the lens. The refracted light rays are reflected by the silicon wafer. These rays will, due to the coarseness of the hydrate film, have too big of an angle to eventually reach the observers eyes or camera. The small amount of light that reaches the camera is of insignificant intensity. When the hydrate film is exposed to water instead of gas, the light rays will travel almost straight through and thereby will not bent or spread. Note that, if the hydrate film is very thin (hundreds of nanometers) or planar it is transparent. This is because thin hydrate films cannot be very coarse and planarity will allow for parallel light rays.

If these hydrate films are made visible in daylight they would have appeared as white just like snow/ice crystals. The difference is that snow and hydrates in bulk are lighted from every possible direction and angles and spreads the light in every possible direction, whereas here the hydrate in the model is lighted from two single directions/angles.

It has to be mentioned in this discussion that destructive interference leading to no light being reflected also can be a part of the answer to why the hydrate film appears as black. However, if we were to illuminate the model by only one wavelength this would be relevant but since the light source has the whole visible spectrum it is not an effect that is observed.

Total inner reflection:

Light might also get "trapped" inside the by total inner reflection, see 1.17. This will contribute by a small amount because the light will eventually escape and will be spread according to the discussion above.

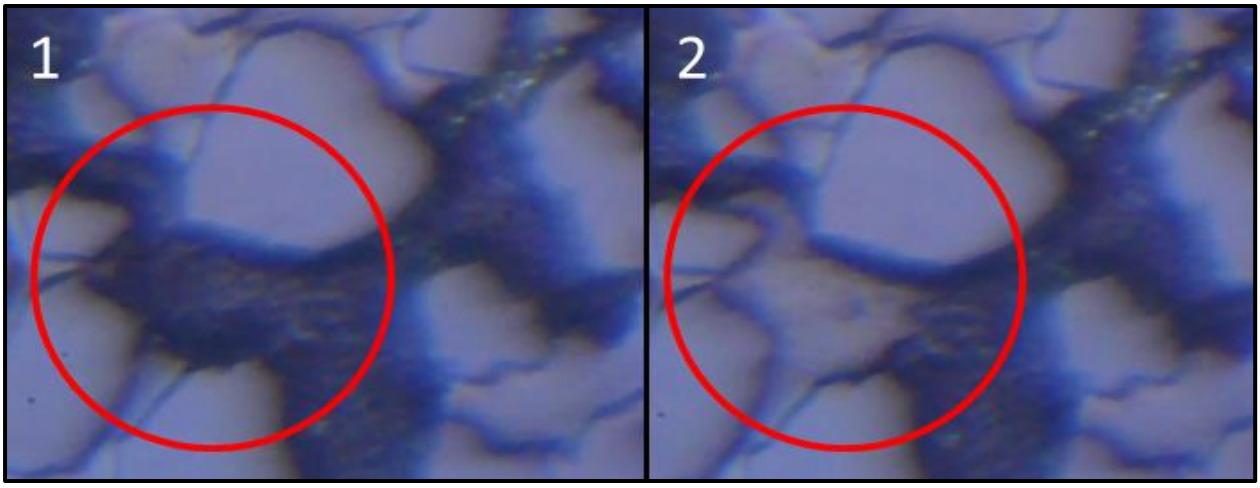

Figure 36: In picture 1, a hydrate film is in contact with gas. Within a very brief moment (in the fraction of a second) the black area highlighted in red, disappears in a fashion very similar to the rearrangement of free gas in a gas-water system. This is considered as evidence that hydrate film in contact with gas appears as black. However, the hydrate film need to be developed and of a certain thickness. The pictures are still photos from a video during hydrate formation at 3.9°C and 50bar.

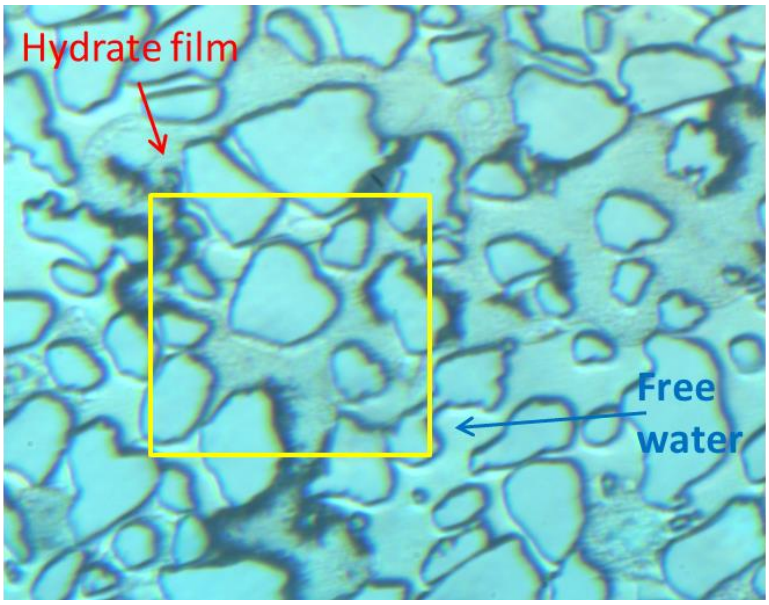

Figure 37: When water has replaced the consumed gas the small difference in refractive index between the hydrate and water makes it transparent. The yellow rectangle encloses the area that is shown in Figure 36.

The final evidence of a black hydrate film due to the refractive index difference between gas and hydrate/water is seen below. Hydrate had been forming for 2 minutes at 0.9°C and 145bar when gas injection was successfully conducted with 5 bar differential pressure, 145bar in gas reservoir and 140bar in water reservoir.

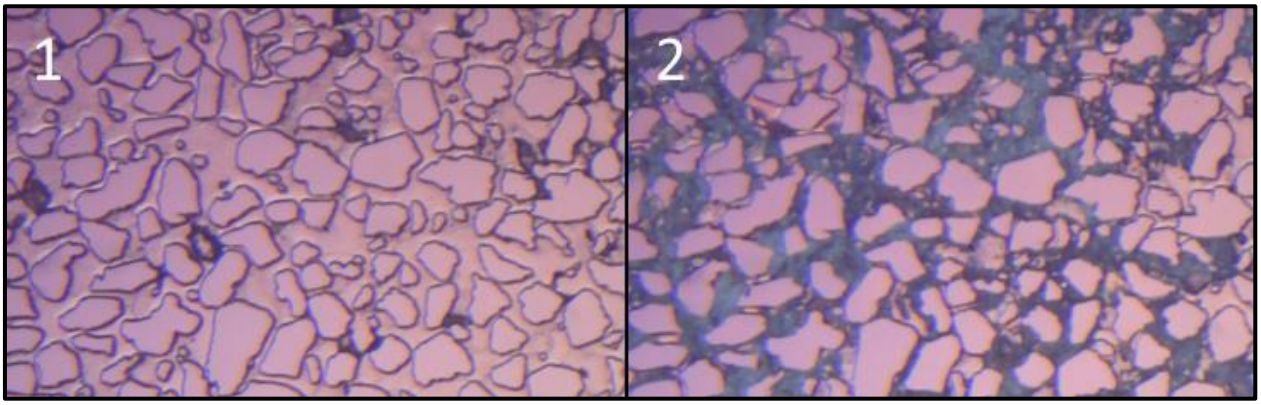

Figure 38: A hydrate film has already been formed in the left picture. A successful gas injection was done proving the theory and explanation of section 0 regarding spreading of light on the hydrate film.

Summing up this discussion; the coarseness of the hydrate film and its refractive index difference with gas, spreads and bends the light rays so that they are not reflected back into the microscope. This is why the hydrate film appears black.

4.5 Water transport during hydrate film formation

It is clear from the hydrate formation experiments that a hydrate film grows into the gas phase. From Figure 30 and Figure 31 we see that the water films in the gas phase seems to drain away. How thick they are after drainage has commenced fully is unclear and is not possible to observe in this setup. By Clennell et al. (1999), a bounded water layer ranges from 5-50 nm and will not participate in hydrate formation. If a thin water film, from the glass surface, the silicon wafer or both is participating in hydrate crystalization there still must be a water transport along the hydrate film to support the continued growth. We also know from Figure 31, that the water film is less than 140 nm. This is not likely to be enough to consume the alle the gas that fills the pore during hydrate growth. As seen in Figure 37 and Figure 39 and all the other formations conducted, the hydrate will continue to grow as long as there is supply on free gas and free water within hydrate stable conditions. The hydrate film is water-wet and coarse creating a good surface for water transport due to wettability and possibly micro capillary effects, see section 2.1.

4.6 Why hydrate films tend to get transparent in the middle of the pore first

It has been observed directly that most of the hydrate in this work appears as films and not fully grown in depth of 25µm. To detect if the hydrate grows to fill the vertical profile of the pores is impossible to do with this setup.

When studying the pictures in Figure 39 and knowing that the picture to the right is later in time within hydrate forming conditions, one obvious question arises. Why does the black hydrate film tend to get transparent in the middle of the pores first? The two pictures are typical and the same development of transparency happens every time.

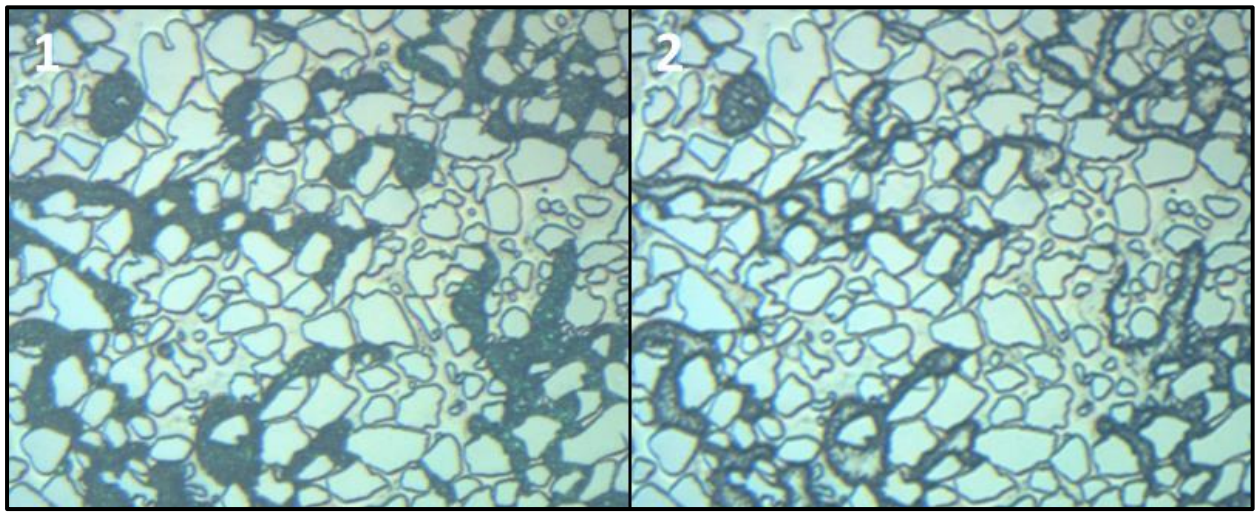

Figure 39: In picture 2, the hydrate film has grown to cover the whole gas filled areas. Picture 2 is taken about one hour later. On clearly see that hydrate film starts to get transparent in the middle of the gas filled areas wile it stays black at the grain contacts.

Since the pores get transparent in the middle first, by discussion 0 one knows that water has to be transported there. The gas bubble is consumed by hydrate formation and thereby the pressure decreases. When the pressure is sufficiently low the gas will rearrange to obtain a lower energy state of the interface and to increase its inner pressure again to achieve equilibrium with its surroundings. These rearrangements has been observed and can happen in a blink of an eye or slowly. The water transport takes places along the hydrate film or through it via micro pore channels as mentioned in 1.14. The transported water cannot be in contact with the glass, hydrate film and silicon wafer at the same time because then it would be transparent. This means that the hydrate film, water and gas have to be layered vertically. The gas gathers along the grain contact due to the upwards curvature of the water-gas interface, gravity segregation and since the hydrate film is more gas wetting than the top glass. It is more likely that gas bubbles will stay in contact with the hydrate film than the glass, so when it snaps/divides it will be attracted to the grain. This cannot be verified but is a possible explanation. Even though the gas-water interface before hydrate formation is almost vertical as shown in Figure 41, the hydrate film is horizontal.

How the exact configuration of this looks like and the mechanism of this development is beyond the scope of this thesis and cannot be verified here, but one knows that the black edges shown in Figure 39 is indeed gas.

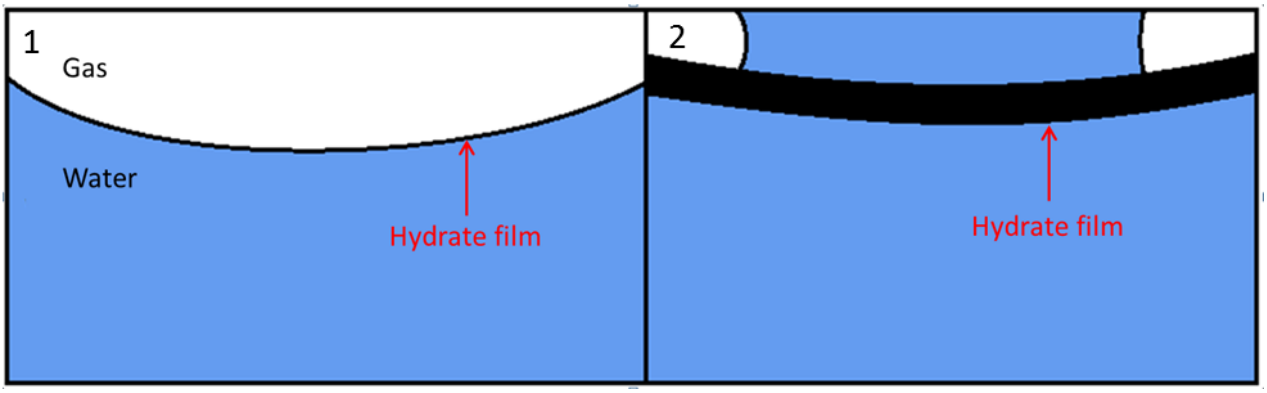

Figure 40: The hydrate film grows and consumes gas. When the pressure in the gas phase is sufficiently low it will rearrange and contract to achieve equilibrium pressure again. The gas rather stays at the edge where it can be in contact with the hydrate film since it is more gas wetting. Water is transported to the middle either via on the film, through the film or both. The hydrate film is simplified for illustrative purposes, and will be coarse and have columnar and/or dendritic crystals into the water phase as seen in Figure 19.

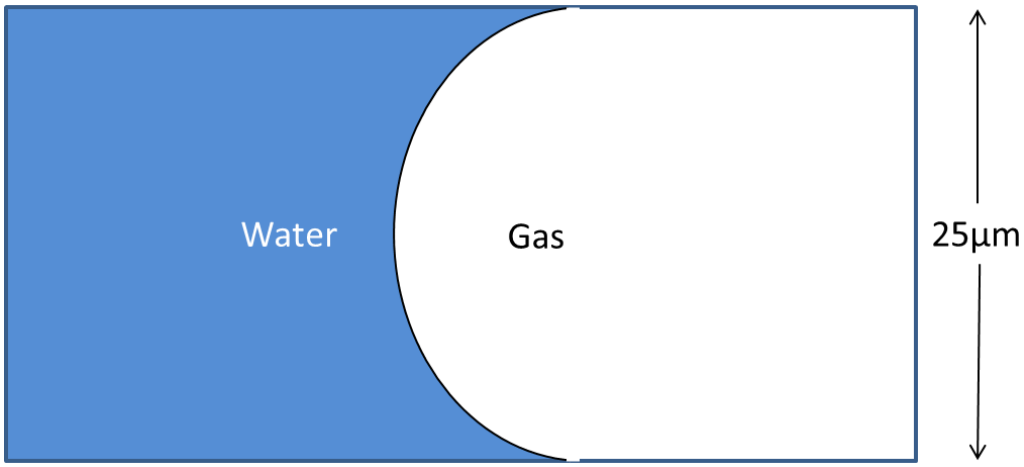

Figure 41: The water-gas interface before hydrate formation. It is almost vertical due to the small vertical distance. The reason why the interface looks black and thick in the microscope from above is because of the slight curvature illustrated here with side-view.

5 Experiments and results

5.1 Hydrate formation setup A

5.1.1 Successful hydrate formation setup A

Six hydrate formations were conducted with memory effect as described in 4.3.

5.1.2 Hydrate formation attempts setup A

There were 4 unsuccessful attempts of hydrate formation with setup A after replacing the model. The pressure was kept constant at 80bar and the temperature varied. Between every attempt the water was changed and the model flushed through with methane gas and water. It has to be mentioned that between attempt 1 and 2 the low temperature bath had to be changed. The cooling capacity of the new bath was not quite as good so the temperature were around 2°C above the first attempt. The final temperatures are averages since the room temperature changes due to ventilation system turning off for the night. The specifics are given in the table below.

5-1: Formation attempts with non-vacuumed distilled water, setup A.

No.	Pressure (Bar)	Starting temp. (°C)	Final temp. (°C)	Cooling Time (minutes)	Time at final temp. (days)	Formation
1	80	15	1.5	95	3	No
2	80	21	3.5	210	6	No
3	80	15	3.3	210	10	No
4	80	21	3.3	210	14	No

5.2 Hydrate formation Setup B

The main objective in this thesis was to identify the most significant sources of error to why hydrate did not form, even though the conditions were well within the three-phase-equilibrium line. Keeping in mind that agitation, turbulence, apparatus, surface area and foreign particles are factors affecting the induction time in addition to pressure, temperature and possibly rate of temperature change (see 1.7), formation attempts with setup B were done with some of these as variables.

Surface area of the gas-water interfaces were almost impossible to control in the micro-model, due to the small volume of it. Apparatus stayed the same throughout setup B. Therefore these two parameters were not tested.

5.2.1 Foreign Particles

The idea that foreign particles might contribute to hydrate formation stems from the same reason why rain droplets starts to grow on aerosols or other pollution particles, why crystallization of ice, salt etc. can be initiated by introducing a new surface and creating a kink site. Since distilled water was used throughout this work, 3 experimental runs were conducted where regular tap water was used. The water was not vacuumed for comparison with the results in table 5-1.

5-2: Formation attempts with regular tap water by decrease of temperature with setup B.

No.	Pressure (Bar)	Starting temp. (°C)	Final temp. (°C)	Cooling time (min).	Time at final temp. (days)	Formation
1	80	21	1.5	80	3	No
2	80	21	0.9	105	6	No
3	80	21	1.1	80	7	No

5.2.2 Formation attempts by decrease of temperature and fixed pressure

In the tables below the 4 experimental runs are summarized. The column of "time for system at final temperature" is the time where the experiments were executed or hydrate formation started. From studies done by others the induction time should be far less than the ones experienced here. The cooling time was heavily reduced in the runs with vacuumed water. The low temperature bath and cooling liquid were kept at lowest possible temperature. Ice blocks were used additionally to cool the system even faster. From these four runs there seems to be no effect from the cooling rate as the two hydrate formations started 12 and 6 hours after reaching the final temperature. Even though the cooling time was reduced to half the time it still was relatively long. A cooling time of less than 10 minutes is desired in future experiments, but is not possible with this setup.

5-3: Formation attempt by decrease of temperature with non-vacuumed distilled water. Notice the pressure of 140bar.

No.	Pressure (Bar)	Starting temp. (°C)	Final temp. (°C)	Cooling time (min).	Time at final temp. (hours)	Formation
1	140	21	1.5	80	12	Yes
2	140	21	0.4	105	48	No

5-4: Formation attempt by decrease of temperature with vacuumed distilled water.

No.	Pressure (Bar)	Starting temp. (°C)	Final temp. (°C)	Cooling time (min).	Time for temp. (hours)	Formation
1	140	30	0.4	45	14	No
2	140	30	0.4	45	6	Yes

Analyzing the results from table 5-1, 5-2, 5-3 and the high pressure of 140bar does promote hydrate formation. The induction time does not correspond to a trend, having formation at 12 hours and 6 hours but not within 48 and 14 hours from table 5-3 and 5-4.

5.2.3 Formation attempts by gas injection at fixed temperature and pressure with vacuumed and non-vacuumed distilled water

So far in the experiments the likelihood of forming hydrate was very low. This was the biggest issue regarding this thesis. In order to conduct dissociation or CH_4-CO_2 exchange experiments in a micromodel, for later research purposes, the presence of hydrate in the first place is obviously a need. Knowing the stochastic nature of hydrate formation, was it possible to get some kind of control of the conditions for growth? It was upon testing flow and turbulence that the breakthrough came. When reading through the literature, it has been mentioned that agitation might have an effect on hydrate formation in bulk experiments. Experiments where this parameter has been isolated in a porous medium has not been described by anyone known to the author but touched upon by Hauge, et al. (2015) in form of pressure pulses. However, their pressure pulses did not cause flow. 21 experiments were done in this work and all showed hydrate formation, see table 5-5 and 5-6.

These 20 experiments were done in a row and a repetitive procedure was followed.

1) The model was flushed through with water to the point were only water was visible. The water went out to atmospheric pressure and the valve kept open.
2) Cylinder B, containing methane gas, was pressurized to the desired pressure.
3) Valve to cylinder B was opened creating a differential pressure through the model to atmospheric pressure equal to the pressure inside cylinder B.
4) After a quick methane flush the model was re-pressurized to the desired level. The pressure drop was typically 2-5 bars.

This caused a lot of agitation and turbulence inside the model. In all runs for 130 bars and up hydrate formation occurred instantly. For pressures of 75-80Bar the hydrate formed within 2 minutes. For pressures of 55-65Bar the hydrate formed within 4 minutes.

When hydrate crystals were seen in the water the response by pressure increase was immediate. This was seen in setup A. To avoid memory effect between the formations the subsequent procedure was done and tested. It showed no signs of memory effect.

1) The valves connecting the model to the pump cylinders were shut.
2) The still water was replaced by water holding at least 30°C.
3) The valve out to atmospheric pressure was opened and kept open for at least 30 min.

5-5: Hydrate formation data for vacuumed distilled water.

No.	Diff. Pressure (Bar)	Temperature (°C)	Formation
1	145	0.6	Yes
2	145	0.6	Yes
3	145	0.6	Yes
4	145	0.6	Yes
5	145	5.6	Yes
6	140	10.0	Yes
7	140	6.3	Yes
8	140	6.0	Yes

5-6: Hydrate formation data for non-vacuumed distilled water.

No.	Diff. Pressure (Bar)	Temperature (°C)	Formation
1	145	6.5	Yes
2	140	5.5	Yes
3	130	6.0	Yes
4	140	9.5	Yes
5	140	1.1	Yes
6	130	2.4	Yes
7	80	1.2	Yes
8	80	5.6	Yes
9	80	4.6	Yes
10	75	5.3	Yes
11	55	2.9	Yes
12	65	4.5	Yes
13	100	1.5	Yes

As seen by the 21 experiments from table 5-5 and 5-6 flow and turbulence was a key-factor for successfully initiate the crystallization, but not a necessity. Time was also crucial for non-flow formation. But why was it so? From the three hypotheses in section 1.6 the common denominator is clusters to combine to overcome the critical size associated with the Gibbs free energy barrier. It is believed that the turbulence and mixing of fluids contribute to make the probability of clusters gathering at a point higher and the "kink" often needed in crystallization effects (such as supersaturated salt solutions, super-cooled water etc.) was given by the movement of the fluids. The reasoning is based on the same mechanisms as in for example elementary statistical mechanics theory. On average the molecules are at a certain distance from each other, these positions have the largest probability. The molecules have fluctuations around their equilibrium point. The probability that these fluctuations cause molecules to cluster together at one point is low but still it happens (Lillestøl, et al., 2006).

5.3 Hydrate formation characteristics in the micro-model

One interesting fact to consider was where the hydrate formed firstly in the system. It has not been observed that this happened in the field of view, even though all parts of the model have been under observation during primary formation. That is, hydrate growth initially starting in the field of view and spreading outwards has not been seen, whereas the growth coming from outside of the field of view was the norm. Prior to visual hydrate formation in setup B (no leakage), it was always observed a characteristic fluid displacement, see section 0. Upon checking pressure communication between the cylinders when the fluid displacement was occurring and/or right after fluid displacement but still before visual hydrate growth, communication was not found (except for one time, Figure 38). This suggests that the growth in the porous network was initiated from plug generation in vicinity to or in the inlet ports/tubing.

The coiled tubing did not prevent hydrate plug as intended, although one successful gas injection was made with setup B. This is attributed more to luck and randomness than anything else. This indicates that the plug might also be in the part of the model covered by the aluminum frame. On the other hand, it worked excellent as a heat exchanger and reservoir for fluids. Pressure drop upon hydrate formation has not been observed. The small volume of the model compared to pump cylinders and tubing is the cause of this.

5.4 Hydrate appearance at different pressures

One of the objectives was to see if one can distinguish visually between hydrate formed at high and low driving forces in this type of micro-model. Figure 43 gives the visual evidence of the structural differences. Faceted crystals, sharp edges and strait lines is observed at high driving forces, as shown in the right picture in Figure 43, whereas low driving forces gave a much smoother edge following the methane-water interface before formation, see Figure 42.

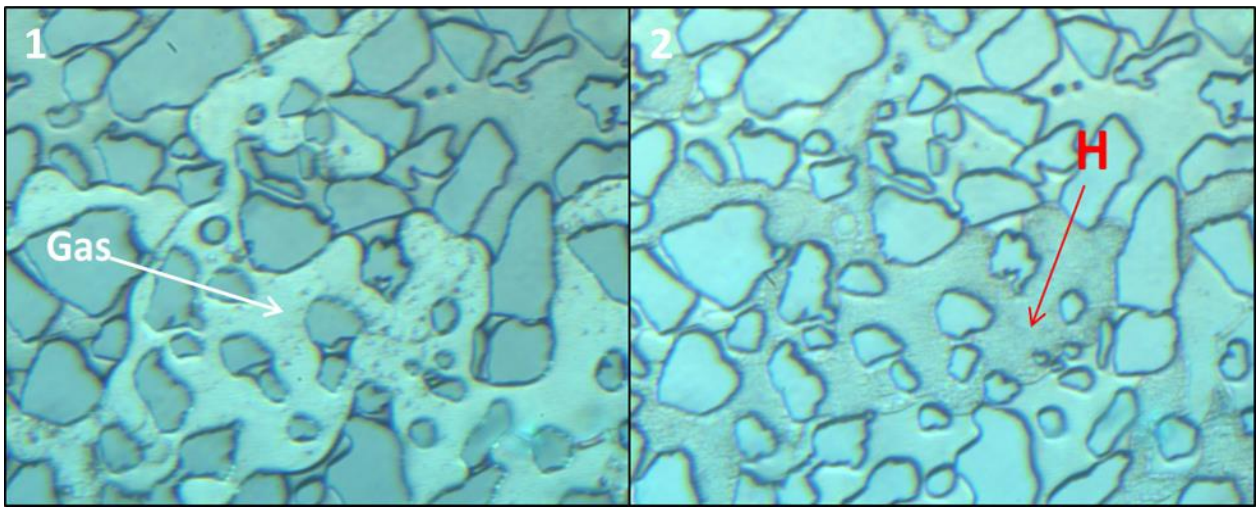

Figure 42: The same field of view before and after hydrate formation and total gas consumption. Upon comparing the gas-water interface with the hydrate layer edge one find that they almost overlap. There will always be some displacement of the gas-water interface during hydrate formation due to gas consumption.

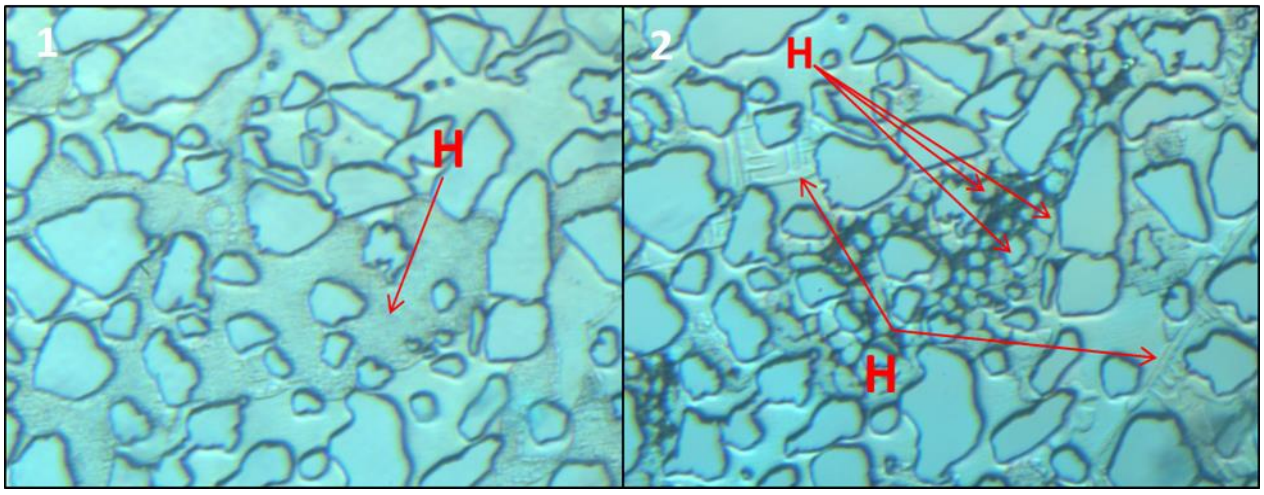

Figure 43: Hydrate formed at 41bar and 3.9°C to the left, shows s grainy but homogenous surface. In the right picture (same field of view) hydrate at 0.6°C and 145bar, and columnar/faceted crystals are seen. Particulate crystals have formed a cluster (three red arrows). These crystals can be hard to detect since they resemble the grains of the model but smaller.

Hydrate formation at low driving forces is a slow process and gas consumption could take days. At high driving forces of 145bar and 0.6°C the gas consumption was mostly done within 3 hours. How the hydrate film developed at varying driving forces was very different. At low driving forces of 41bar and 3.9°C, the hydrate growth started as a black grainy structure slowly merging through the gas phase from the interface. Nearly none fluid displacement took place, see Figure 44.

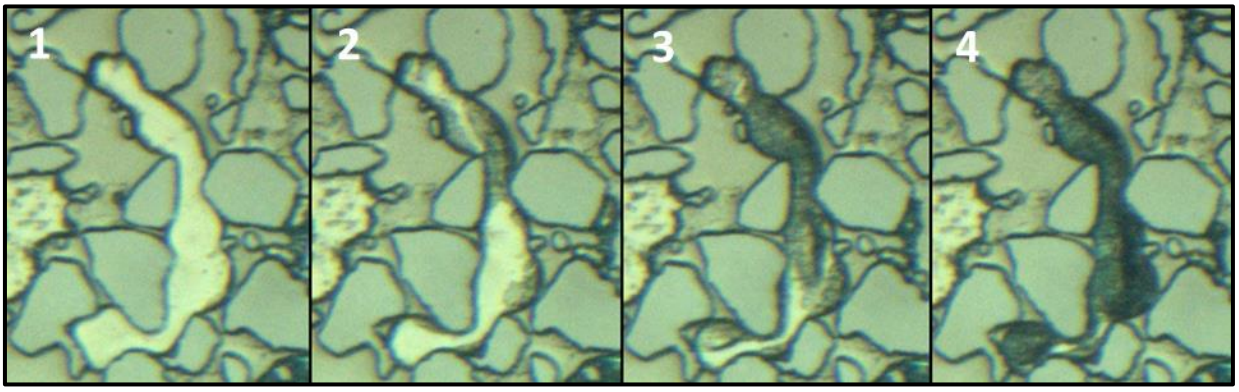

Figure 44: Typical hydrate film growth development at low driving forces of 3.9°C and 41bar. This process was in the course of 4 minutes.

In Figure 45 a typical development of hydrate film growth at high driving forces is visualized. It was a very chaotic event when hydrate started to grow at these conditions. Gas and water were displaced by each other rapidly by local capillary pressure differences; see 0 and Gaydos, et al. (1993). Comparing the interference pattern in Figure 45 with the one of water and gas, they have an opposite developmetn to each other. Weheras, the water film drianing away and getting thinner the thin film in Figure 45 is getting thicker. This proved that the thin film is a part of the hydrate crystallization in the case of high driving forces after fluid flow. A simultaneous crystallization sets in before the water has time to drain away. Water film drainage took 2 minutes (Figure 31) and the crystallization started immediately. Water and gas were then consumed. The crystal/film creates a lower chemical potential towards the itself resulting in water transportation from the free water phase. The film growth under strong driving forces occurs in two different ways; from gas-water interface and inwards as in Figure 44 and by thin film thickening as described in Figure 45. The average growth rate of the thickness of the film could be calculated but serves no purpose in this thesis**.** The furher development is an even growth and thickening of the film leading to a darker area, see Figure 46 picture 4.

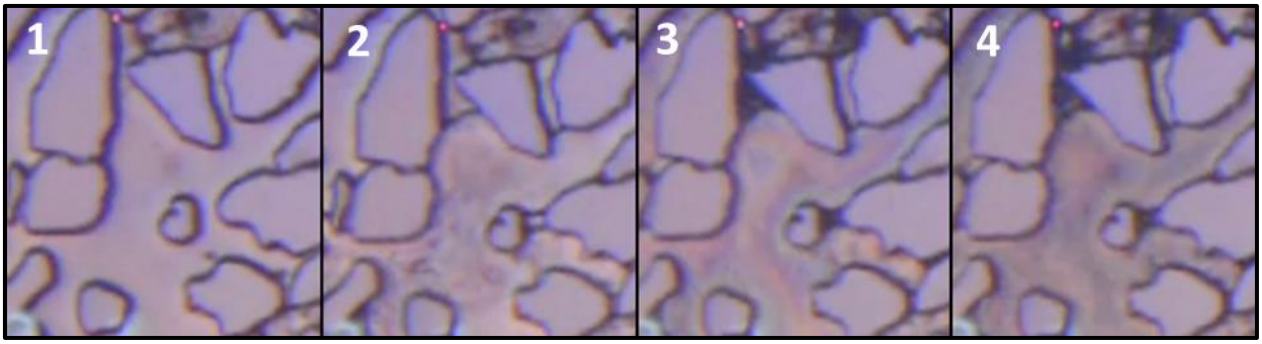

Figure 45: Typical hydrate film growth at high driving forces, 0.6°C and 145bar. First water is displaced by gas (picture 2 from the left), then hydrate film crystallization starts and interference pattern is observed (picture 3). Areas which are red/pink in picture 3 turns black/dark/grey in picture 4. The pictures are still photos from video and have a time span of 55 seconds.

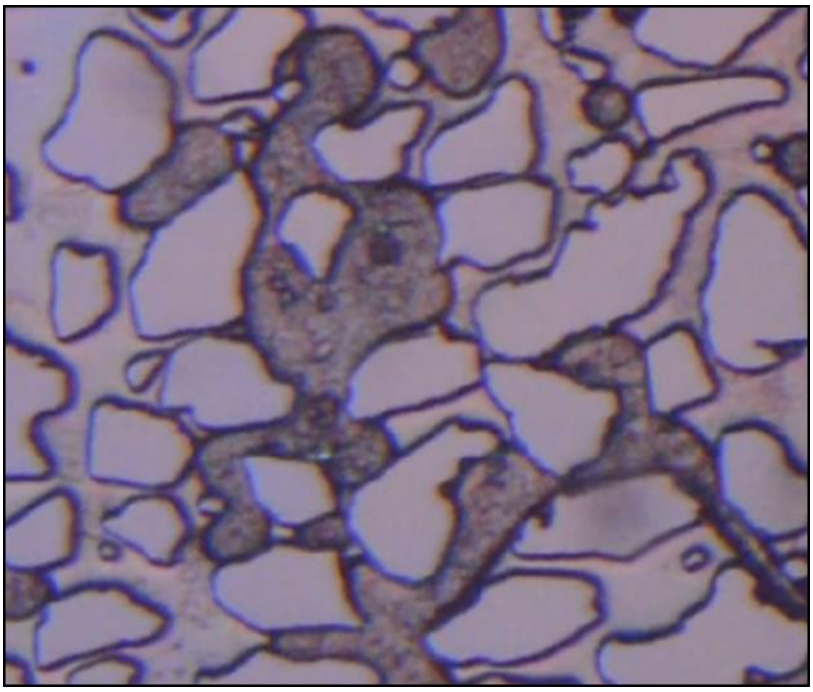

Figure 46: Under high driving forces when a thin water film has crystallized the whole film tend to evenly grow and getting darker over the whole surface simultaneously.

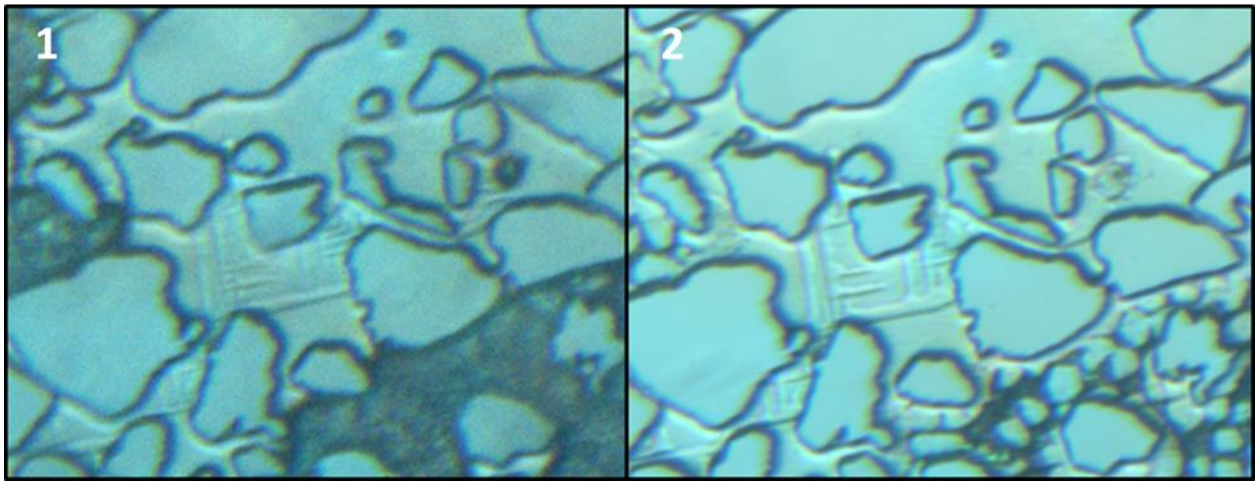

Figure 47: Hydrate crystals under 0.6°C and 145bar. It is shown here that a continued growth of the crystals occur, possibly due to methane migration through the water from the free gas phase under the hydrate film (black area), as described in 2.1 and by Katsuki, et al. (2007).

In Figure 47 the continued growth of the hydrate crystal is evident. This can be a recrystallization effect as described by Hauge, et al. (2015) or by a gas migration throug water as discussed by (Katsuki, et al., 2007). By the development of the gas bubbles near by the latter is most likely. The thermodynamic drive towards the crystals creates an osmotic gradient of methane towards the crystal.

Homogenous hydrate growth and growth into the water phase was not observed in this work. Sun, et al. (2010) did formation in bulk and Tohidi, et al. (2001) with an open pore-network to the surrounding methane gas of 400bar and channel depth and width of 50µm or larger. The supply of methane was continous in both cases but not in this work. Tohidi, et al. (2001) had an experimental pressure of about 4 times as high, which clearly increases the aquaeous methane saturationn significantly. The micro-model in this thesis was constrained by a vertical depth of 25µm which are considered as a small pore in regular Berea sandstone. Katsuki, et al. (2007), used a closed model with straight rectangular channels. They saturated the water with methane at 1K above hydrate equilbrium and observed hydrate growth into the water phase but not homogenoues growth starting in the water phase. Ohmura, et al. (2005), also saturated the water with methane before formation and found hydrate growing into the water phase irrespective of pressures up to 100bar. Therefore, the porous network, methane supply, the etching depth and under-saturation of methane in the aqueous phase, might be reasons for not observing growth in or into the water phase.

While experiments done by others have verified that hydrate growth is initiated in the largest pores first, this has not been seen here. Initial growth has been uniformly distributed. This is attributed to three things mainly.

- The small etching depth of 25µm which was a lot smaller than most of the pores in the micro-model, see Figure 20
- Gas tends to fill the large pores
- The pore sizes are larger than the reported pore size that cause an inhibiting effect on hydrate growth

5.5 The memory effect

All experiments from setup A and B showed that as long as there are visual hydrate crystals left in the water, hydrate crystallization will be an instant effect occurring close to or on the theoretical equilibrium line.

Two runs with setup B where the hydrate was dissociated by 21°C for two hours and the pressure were kept at 145bar were done. The temperature was then brought down to 0.6°C but no hydrate formed. The induction time lasted for 6 hours until the pressure was regulated rapidly down to 135bar and back up to 145bar to create a flow, agitation and turbulence. This was enough get a flow through the model that set off visual hydrate growth. As with crystallization of other substances a “kink” is needed.

Even though the pressure is high and the temperature low there is no guarantee for hydrate formation. The already formed hydrate crystals have shown in every instance that they cause hydrate to form when the system is brought into the theoretical forming conditions. This was exploited and made it possible to trace the three-phase-equilibrium line, see section 0. From this one can conclude that the memory effect definitely have roots in hydrate crystals or structures in the water.

5.6 Water displacement upon hydrate crystallization

Since water is incompressible the pressure is reduced significantly in the water phase upon hydrate formation in surrounding areas. Gas expands as a result of the pressure difference and displaces the water. These areas are not as local as heat and mass transfer locality. The pressure propagates rather quickly through the water phase and the snakelike movement of gas displacing water, was often seen before formation. In Figure 48 the interface crystallizes immediately and the gas does not expand into the whole pore-volume as free gas would.

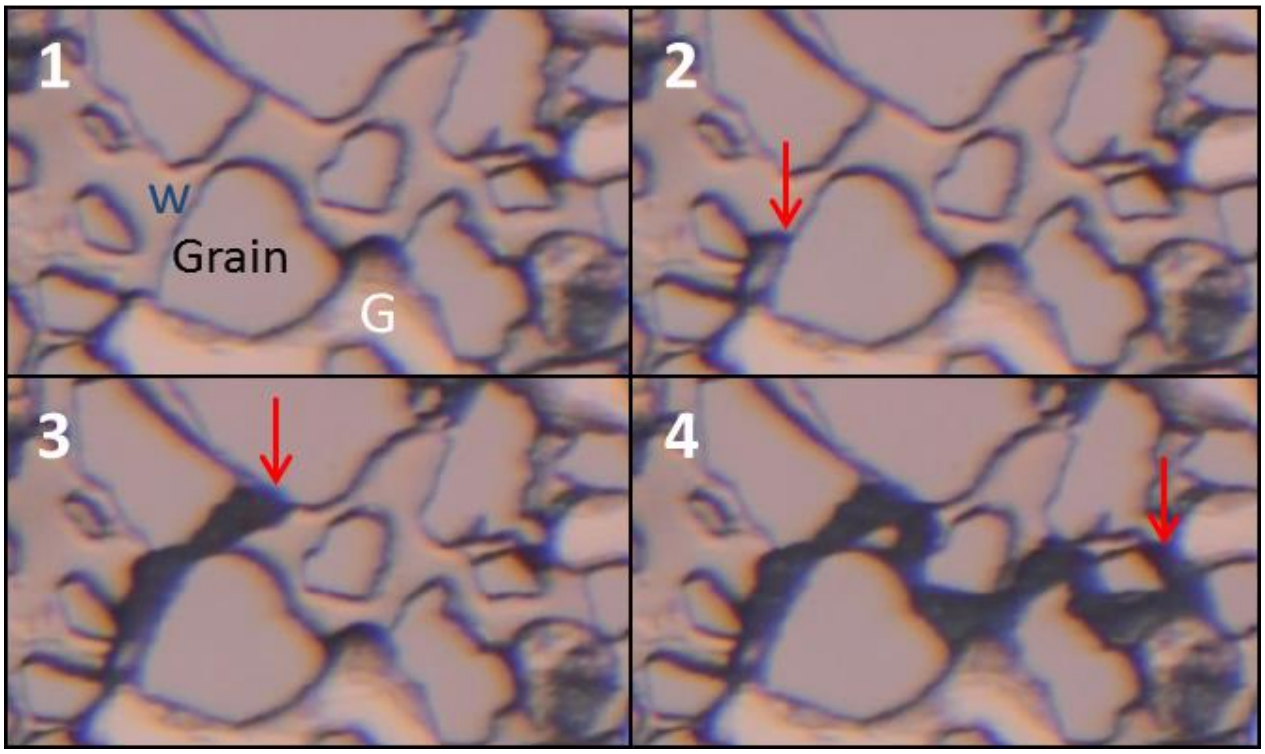

Figure 48: A typical water displacement when hydrate is crystallizing marked by the red arrow. The gas-water interface crystallizes immediately and therefore gets the characteristic pathway.

5.7 Layered hydrate

The assumption that this model is a 2D network, and one phase fills the entire pore space vertically (except of bounded water) has turned out to be a misconception. When only gas and water are present this most probably is true based on visual observation. When hydrate is introduced there exists a phase that connects the two because both phases are needed for growth of the hydrate. It is reasonable to assume that the gas is on top of the hydrate film based on gravity segregation and by evidence in **Figure 49**. The possibility that gas also be beneath the hydrate film in certain occasions should not be neglected. Further work is needed on this topic.

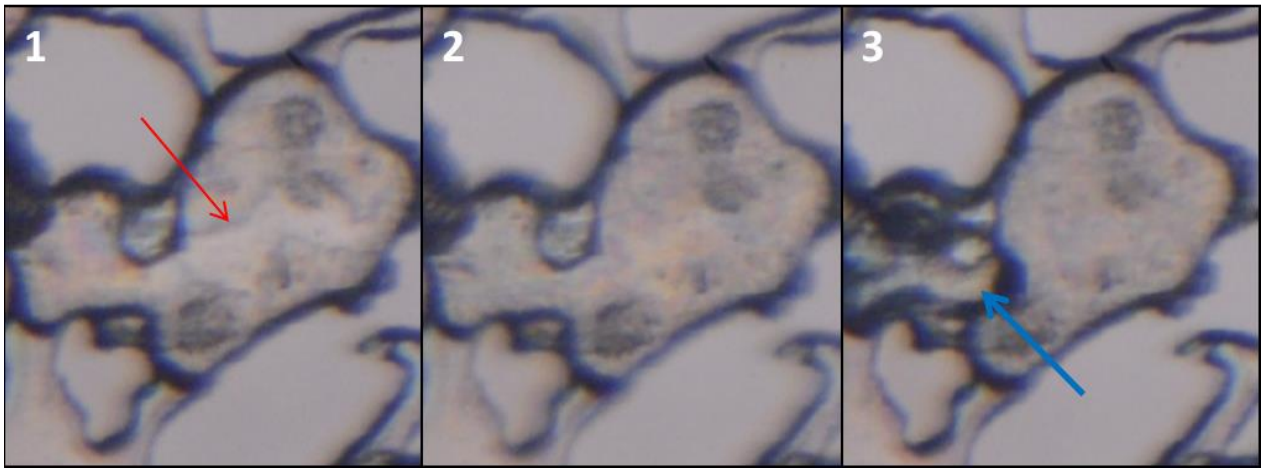

Figure 49: At maximum magnification it was possible to differentiate by the top and bottom (25µm) inside the micro-model by changing the depth of the focus. Notice that the edges of the grains are diffuse while the interference patterns are sharper. This revealed that the initial crystallization was at the bottom on the silicon wafer. This was captured under high driving forces, 140 bar and 0.4^{o}C.

In picture 1 of Figure 49, crystallization has started and the front (red arrow) is advancing inwards. Since no interference pattern is observed before crystallization (too thin film) this points to a water transport along the hydrate film. By comparing the interference pattern with the smooth interference pattern from water films and by the behavior of this advancing front (live view), it is certain that this is a hydrate film. In picture 2 the silicon surface is covered with a thin film. In picture 3, a water droplet (blue arrow) has emerged onto the thin hydrate film already established. One knows its water because it is transparent while the edges are black due to coarser hydrate crystals and interface with methane. This points to a rather complex and layered nature of hydrate growth depending on water and gas supply.

5.8 Finding the equilibrium line

Before reading this subchapter the reader is notified that the permeability of hydrate plugs was tested on several occasions during the three-phase-equilibrium tracing. During the course of a three hour test with 50bar differential pressure across the model, but within hydrate stability zone, no pressure change in either of the transducers was detected.

The three phase equilibrium was traced by controlling the pressure one bar at a time at a set temperature. The temperatures ranged from 0.6℃ to 16℃. The idea was to see if there is a detectable shift in the three-phase-equilibrium line from the vacuumed to non-vacuumed water, the same effect as with thermodynamic inhibitors. If it was possible to do this and get reliable results comparable to literature values was also an important point. It turned out to be difficult and very time consuming. The biggest problem was plugging. The pressure was regulated at the set temperature to observe melting or formation. To detect one or the other at least 30 min of constant pressure and temperature was required. A picture was taken when the desired pressure was reached and one taken after the 30 minutes and compared. The goal was to observe the gas water interface, and see if a hydrate film started to grow or the gas bubble decreased in size. This worked quite well! But for every pressure where growth was observed the hydrate plug had to be melted by a decrease of 15-20 bars (to make it a quick process). Then the model was pressurized one bar below the latter to detect growth or no growth. The pressure was recorded at visual formation. This means that the true equilibrium lies within one bar down. It was important to not keep the pressure below the equilibrium line for too long since the formation relied solely on memory effect.

The plugging turned out to cause more troubles. The initial hydrate growth started most likely in the tubes or in the part of the model covered by the aluminum frame. This plug is impermeable and once it had formed the model did not longer respond to pressure change. Keeping in mind that bigger hydrate crystals has a lower chemical potential than smaller once and that the volume of the model is so small, it is reasonable to believe that the plug sucks water and gas from both sides and reducing the pressure inside the model down to equilibrium. This in turn makes the recorded growth pressure some bars higher than the true equilibrium. The most accurate equilibrium measurements would be to detect when the plugging occurs. This could be done but there was is not enough time. It should be noted that some data points where there were no sign of visual hydrate growth in the field of view, plugging was detected by loss of pressure communication with the model.

Yang, et al. (2001),see section 2.1, performed dissociation to trace the three phase equilibrium line. How this in specific was done is not mentioned in the article but they point out that plugging may cause uncertainties. Their values are most likely a little lower than a the true equilibrium. This because the pressure needed to melt the plug is below the equilibrium. From Figure 50 it is clear that their pressure values match CSMgem values or are lower, whereas the

pressure values of this work are a little above. The dissociation data of Katsuki, et al. (2008) are plotted in Figure 50, but their points are too spread and few to be weighted here.

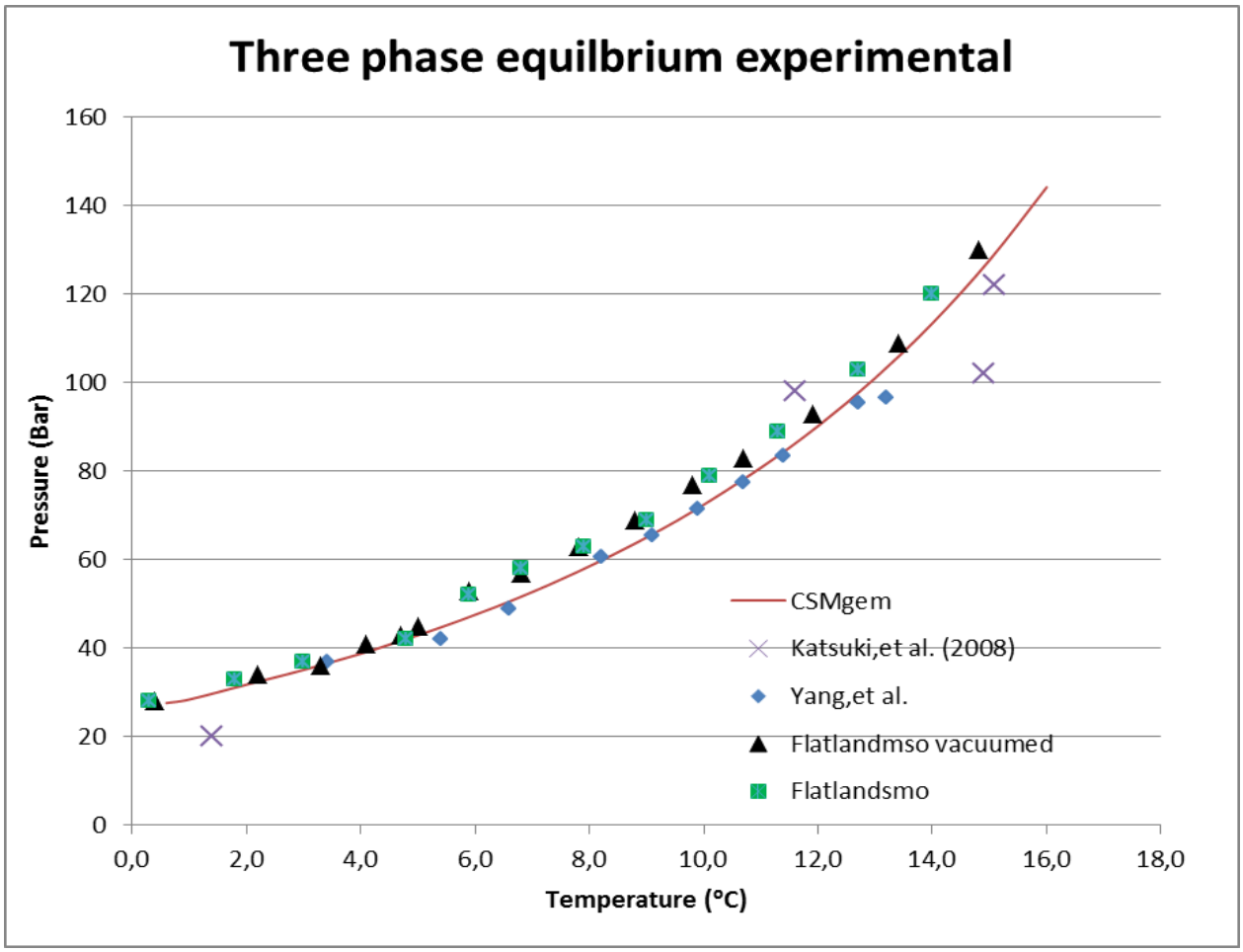

Figure 50: Three-phase-equilibrium data.

In Figure 51, the experimental data with the uncertainites of +0.6°C and -1 bar are plotted. On average the values lays a little below the CSMGem line. This supports the findings of Turner, et al. (2005), section 2.1, that no inhibiting effect is detectable of poresizes larger than 0.12µm when including the uncertainties of the thermocouple.

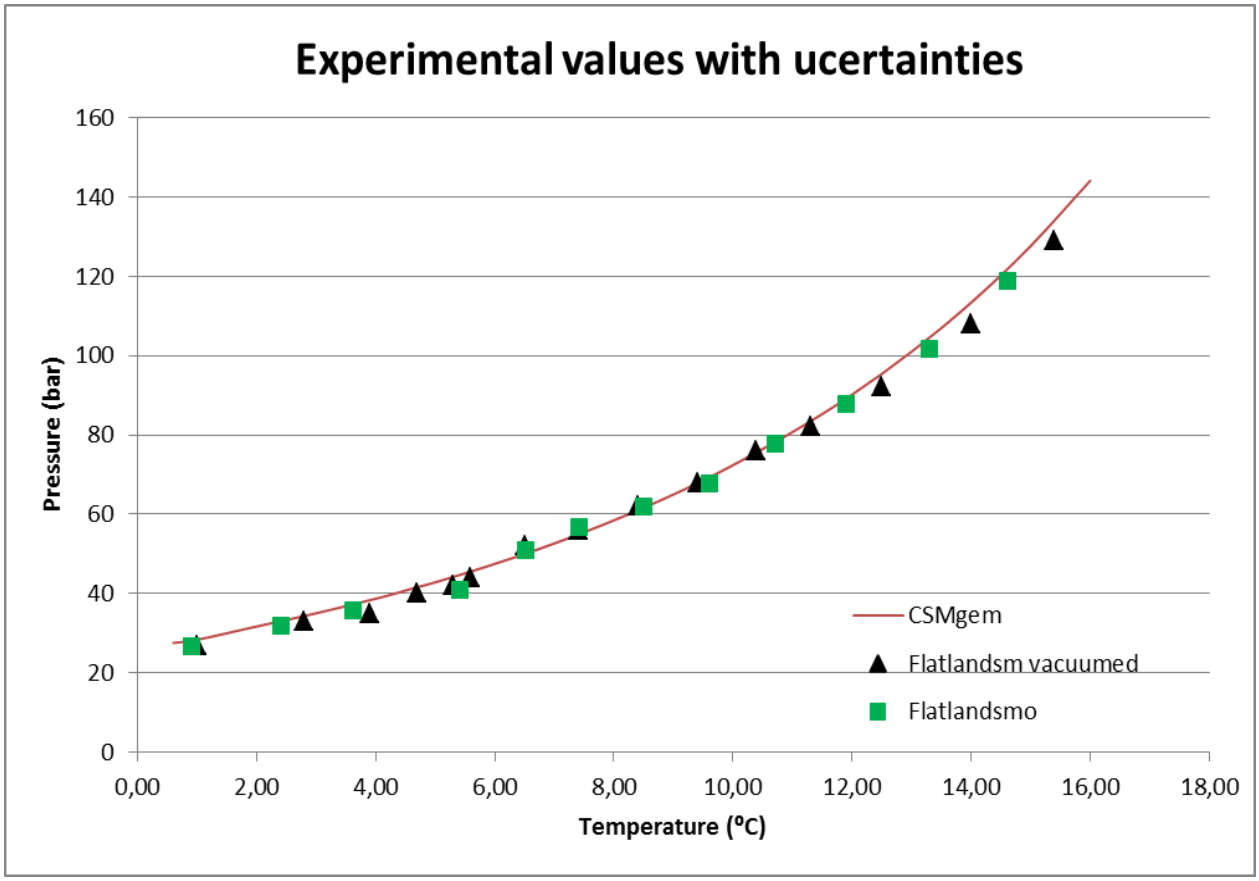

Figure 51: Experimental three-phase-equilibrium data with uncertainties of +0.6°C and -1bar. The data fits well the theoretical data of CSMGem for a bulk system. Note that 1 bar is subtracted since hydrate formation is detected so the true equilibrium is lower.

5.9 Dissociation

5.9.1 Dissociation by pressure decrease

Dissociation has not been the focus in this thesis but still some important points have to be made. Although the hydrate starts to melt at a well-defined line, there are some hydrate crystals that seem more stable than others. Video studies have showed that the hydrate films with gas underneath and the hydrate films and crystals in direct contact with a free gas phase dissociate first. Films and crystals that are completely surrounded by water will be the last ones to melt. The melt-down of these are initiated by a free gas phase creating a contact or by gas bubbles forming at the edge or underneath the film. Once the hydrate is in direct contact with the free gas phase the melt process is relatively quick. At first glance it seems unlikely since the pressure in the water phase is slightly lower than in the gas phase. This pressure difference is caused by the capillary forces. The dissociation is most likely due to the mobility of gas versus mobility of water in this pore network. The water surrounding the hydrate seems to be quite immobile. The free gas phase is clearly the most mobile phase and displaces the water. In places where water are capillary trapped the heat and mass transfer will be limited by diffusion and local temperature gradients, respectively. When the hydrate is introduced to the free gas phase mass can commence and heat transported with it. These results match the ones of Katsuki, et al. (2008) in section 2.2.

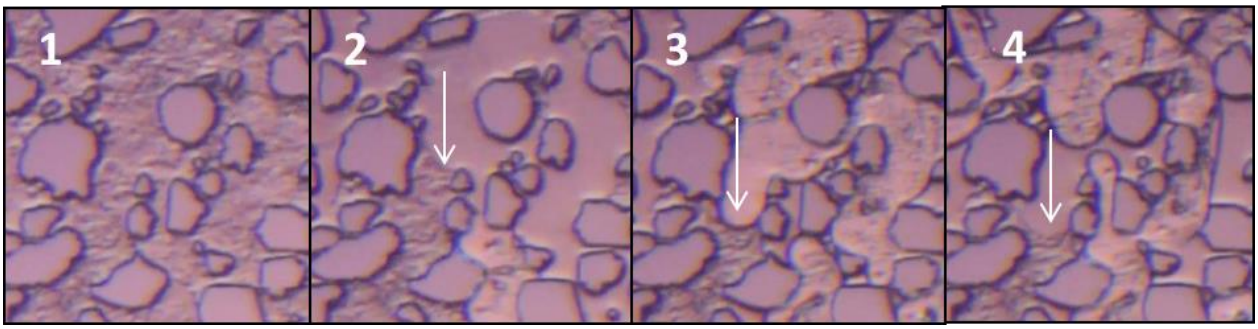

Figure 52: Picture 1: A hydrate film was completely submerged in water. Picture 2: Pressure was reduced and hydrate started to melt. Gas was continuously flowing. Picture 3: A gas bubble achieved contact with the hydrate film and further melting of the hydrate-film-edge could commence. Picture 4: The gas bubble retracted (due to flow) and the melting stopped. One can even see that the edge of the hydrate film was curved similar to the methane-water interface. This sequence is taken from a video and the time span from Picture 1-4 is 70 seconds. This shows that mass and heat transfer via the mobile gas phase is the main cause of hydrate dissociation upon pressure reduction.

5.9.2 Dissociation by heating

The hydrate dissociation by temperature increase had some different characteristics than by pressure decrease. The immobile water did not prevent dissociation and gas release and the hydrate layer melted more evenly, see Figure 53. An area with only gas present was picked because it shows the even dissociation better. The heat transport is believed to be the key of this behavior. Due to the high thermal conductivity of the silicon wafer the heat from the still water will be transported to the hydrate via the silicon wafer and thereby melting the hydrate from beneath.

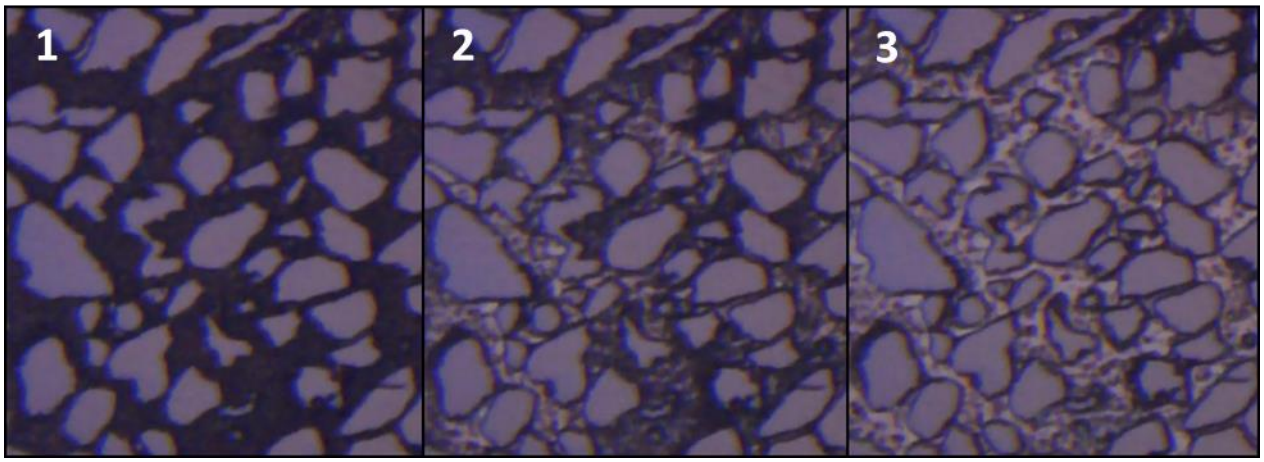

Figure 53: Dissociation by temperature increase. The hydrate film melts more evenly throughout the layer.

5.10 Cementation

The hydrate seemed to have as many grain contacts as not. Whether these grain contacts are considered as cementation is unclear from the literature, but there is not observed a water layer between the hydrate and grains. Therefore, it is assumed that these contacts are of cementing nature in this thesis. Seemingly, the driving forces did not affect cementation. Grain contact was achieved at both high and low driving forces. The number of grain contacts at different conditions is not quantified here.

When hydrate were dissociated with 15-20bar below equilibrium, high flow paths of alternating gas and water were present. The hydrate film stayed in place until it had melted. The hydrate layer exhibited the property as a mechanical hindrance for flow.

6 Conclusions

- There is no indication that vacuumed water promotes hydrate growth more than non-vacuumed water when the flow and turbulence is high. When measuring the equilibrium line no significant differences between the two were found.
- No effect by vacuuming the water with regards to hydrate formation was found. A capillary inhibition or promotion was not observed. This is explained by partial pressure of oxygen and nitrogen at atmospheric pressure being low compared to a system under high pressure with methane as the only free gas.
- Turbulence and flow was an important factor for initiating the hydrate growth process. In 21 of 21 experiments with flow and turbulence, hydrate was formed within 4 minutes. The growth was immediate when the driving forces were high and the visual growth was observed within minutes for low. The result is relevant for gas migration through a reservoir creating flow conditions or in pipelines.
- Significant hysteresis effect for hydrate formation and reformation was observed. If the system of methane and water was brought into hydrate forming conditions or well within at static conditions (non-flow), the growth process had a long induction time of several hours or did not start at all. If a memory effect was present then hydrate would start to crystallize at the three-phase-stability curve. Once the crystallization process has begun it would not stop until the mass transport ceased or the system was brought out of the stability area.
- Hydrate growth from the interface between gas and water into the water phase was not observed, but a continued growth of an already grown crystal surrounded by only water was seen. This continued growth was likely due to methane dissolving and migrating through the water phase. All hydrate growth seems to be occurring at the water-methane interface and continues into the free gas phase.
- At low driving forces a black hydrate film encapsulated the gas phase slowly. At higher driving forces a thin water film appeared within the gas phase and crystallized first and then the film grows evenly throughout the gas phase.
- Thin film interference was used to detect thin hydrate films upon crystallization.
- Faceted and particulate crystals were observed as well as hydrate films or layers. Dendritic crystals have not been observed in this work.
- A characteristic of dissociation by pressure reduction was that hydrate needed to be in direct contact with a free gas phase to melt. Mass transport through via the mobile gas phase was pointed out to be a key factor. By temperature increase the hydrate melted more evenly due to heat transport through the silicon wafer.

- Visual evidence of confirmed hydrate cementation on the micro-model surface and it seemed to be independent of the pressure and temperature conditions.

7 Future Work

- More elaborate dissociation study.
- Replication of three-phase-equilibrium experiment with calibrated thermometer, by plug detection and by dissociation data.
- CO_2 hydrate formation at high driving forces, around 145 bar and below 1^oC, to compare with methane hydrate. Possibly visual detection of hydrate growth into water phase.
- CO_2 three-phase-equilibrium study.
- Do a study on plugging to detect whether the plug is located in the tubes or in the covered part of the model.
- CO_2-CH_4 exchange, if this is possible. This can possibly be done with filing the model and tubes with water and then inject methane by a flow path between the two ports on the short side. Once the hydrate has formed, CO_2 can be injected diagonally form the two ports that is water filled. Is there visual differences and will the crystals change?
- Do hydrate studies in micromodels with etching depth of 5µm to see whether this reveals more about the layered nature of hydrate films.
- Use a microscope with a larger magnification and investigate cementation effect and the layered nature of the hydrate.
- Find at which pressure and temperature methane hydrate crystals are growing from- and into the water phase.
- More investigation on vertical placement of hydrate film by the use of focusing the microscope at maximal magnification.
- Investigate the effect of cooling rate. This can be done having the micro-model pressurized with methane and water and only air in the chamber. Then cool down water by another low temperature bath to desired level or by ice and water in a bucket, and pour it into the chamber. Or by a much more effective low-temperature bath.
- A visual study of diffusion would be interesting and of importance. To see how/if diffusion is constrained by the vertical depth of 25µm and by the pore-network would be beneficial when discussing gas transport through water and water films, and water transport in a static situation. This can be done by flowing water with visual tracers on the short side of the model at lowest rate possible. Then achieve a static system and observe the tracers as they diffuse through to the other end of the model. If the model is filled with tracers initially, water without tracers can be injected from one of the other ports on the opposite side to the point where a small amount of tracers are left.

8 Appendix

8.1 Experimental table values for three-phase-equilibrium line.

8-1: Vacuumed distilled water

T (^{o}C)	P(Bar)
0,4	28
2,2	34
3,3	36
4,1	41
4,7	43
5,0	45
5,9	53
6,8	57
7,8	63
8,8	69
9,8	77
10,7	83
11,9	93
13,4	109
14,8	130

8-2: Non-vacuumed distilled water

T (^{o}C)	P(Bar)
0,3	28
1,8	33
3,0	37
4,8	42
5,9	52
6,8	58
7,9	63
9,0	69
10,1	79
11,3	89
12,7	103
14,0	120

9 Bibliography

Agency, I. E., 2015. *India Energy Outlook,* Paris: IEA PUBLICATIONS.

Anon., 2015. *www.aqualab.com.* [Online] Available at: http://www.aqualab.com/education/what-is-water-activity/ [Accessed 24 August 2015].

Anon., n.d. *https://dornsife.usc.edu.* [Online] Available at: https://dornsife.usc.edu/assets/sites/336/imgs/Water-Molecule.png

Azom, 2011. *www.Azom.com.* [Online] Available at: http://www.azom.com/article.aspx?ArticleID=4765 [Accessed 27 september 2015].

BIRKEDAL, K. A., 2013. *Empirical and Numerical Evaluation of Mechanisms in Gas Production from CH4-Hydrates – Emphasis on Kinetics, Electrical Resistivity, Depressurization and CO2-CH4 Exchange. PhD Thesis.* s.l.:University of Bergen.

Bishnoi, P. R. & Natarajan, V., 1993. *Thermodynamics and nucleation kinetics of gas hydrates,* Calgary: Chemical and Petroleum Engineering, University of Calgary.

Brandon, D. & Kaplan, W. D., 2008. *Microstructural Characterization of Materials.* 2nd ed. Sussex: John Wiley & Sons.

Buchgraber, M., Castanier, L. & Kovscek, A., 2012. *Microvisual Investigation of Foam Flow in Ideal Fractures: Role of Fracture Aperture and Surface Roughness.* San Antonio, Texas, Society of Petroleum Engineers.

Bylov, M. & Rasmussen, P., 1997. experimental determination of refractive index of gas hydrate. *Chemical Engineering Science,* 52(19), pp. 3295-3301.

Chandler-Horowitz, D. & Amirtharaj, P. M., 2005. High-accuracy, midinfrared (450cm−1⩽ω⩽4000cm−1) refractive index values of silicon.. *Journal of Applied physics,* Volume 97.

Clennell, M. B. et al., 1999. Formation of natural gas hydrates in marine sediments 1. Conceptual model of gas hydrate growth conditioned by host sediment properties. *Journal of Geophysical research,* 104(B10), pp. 22,985-23,003.

Daisuke, K., Ryo, O., Takao, E. & Hideo, N., April, 2006. Formation, growth and ageing of clathrate hydrate crystals in a porous medium. *Philosophical Magazine,* 21 Aug, 86(12), pp. 1753-1761.

DAVIES, S. R., Sloan, D. E., Sum, A. K. & Koh, C. A., 2010. n Situ Studies of the Mass Transfer Mechanism across a Methane Hydrate Film Using High-Resolution Confocal Raman Spectroscopy. *Journal of Physical Chemistry,* 114(2), pp. 1173-1180.

EngineeringToolBox, n.d. *EngineeringToolBox.com.* [Online] Available at: http://www.engineeringtoolbox.com/refractive-index-d_1264.html [Accessed 7 September 2015].

EngineeringToolbox, n.d. *www.EngineeringToolbox.com.* [Online] Available at: http://www.engineeringtoolbox.com/linear-expansion-coefficients-d_95.html [Accessed 27 september 2015].

Englezos, P., Kalogerakis, N., Dholabhai, P. & Bishnoi, P., 1987. Kinetics of Formation of Methane and Ethane Gas Hydrates. *Chemkcal Engineering Science,* 42(11), pp. 2647-2658.

Everett, D., 1961. The thermodynamics of frost damage to porous solids. *Transactions of the Faraday society,* Issue 57, pp. 1541-1551.

Gaydos, J., Li, D. & Neumann, A. W., 1993. Implications of the phase rule for capillary systems containing surfaces and three-phase contact lines with surface and linear constraint relations. *Colloid & Polymer Science,* 271(8), pp. 715-725.

Handa, Y. P. & Stupin, D., 1992. Thermodynamic Properties and Dlssociation Characteristics of Methane and Propane Hydrates in 70-Å-Radius Silica gel pores. *The Journal of Physical Chemistry,* 96(21), pp. 8599-8603.

Hauge, L. et al., 2015. Eperimental verification of pore-level hydrate formation mechanisms in silicon micromodels. In: *Laboratory Imaging of CO2 Flow and Storage in Hydrates and Saline Aquifers.* Bergen: University of Bergen, Norway.

Haynes, W., Bruno, T. J. & Lide, D. R., 2015. *Handbook of Chemistry and Physics.* 96th- Internet version ed. s.l.:CRC Press.

Hornbrook, J., Castanier, L. & Pettit, P., 1991. *Observation of Foam/Oil interactions in a New High-Resolution micromodel.* Dallas, TX, Society of Petroleum Engineers.

Høyland, M. D., 2014. *Measurements and visualization of hydrate growth in porous media..* Bergen: Master thesis: Department of Physics and Technology, University of Bergen..

Jiang, G., Wu, Q. & Zhan, J., 2010. Experimental studies of the formation and dissociation of methane hydrate in loess. *Journal of Natural Gas Chemistry,* 19(3), pp. 217-223.

Kashchieva, D. & Firoozabadi, A., 2003. Induction time in crystallization of gas hydrates. *Journal of Crystal Growth,* Issue 250, pp. 499-515.

Katsuki, D., Ohmura, R., Ebinuma, T. & Narita, H., 2007. Methane hydrate crystal growth in a porous medium filled with methane-saturated liquid water. *Philosophical Magazine,* 87(7), pp. 1057-1069.

Katsuki, D., Ohmura, R., Ebinuma, T. & Narita, H., 2008. Visual observation of dissociation of methane hydrate crystals in a glass micro model: Production and transfer of methane. *AIP-Journal of Applied physics,* Volume 104.

Kim, H.-J., Kim, Y.-Y., Lee, K.-w. & Park, S.-H., 2011. A distributed Bragg reflector porous silicon layer for optical interferometric sensing of organic vapor. *Sensors and Actuators B: Chemical ,* 155(2), pp. 673-678.

Kvamme, B., 2014. *PTEK232: Fundamentals of Natural Gas Hydrates and Practical Implications.* Bergen: University of Bergen.

Kvamme, B., 2015. Feasibility of simultaneous CO2 storage and CH4 production from natural gas hydrate using mixtures of CO2 and N2. *Canadian Journal of Chemistry*, 1 january, pp. 897-905.

Lillestøl, E., Hunderi, O. & Lien, J. R., 2006. *Generell fysikk for universiteter og høgskoler.* 2 ed. s.l.:Universitetsforlaget.

Lourdes Martinez de Baños, M., Carrier, O., Bouriat, P. & Broseta, D., 2015. Droplet-based milli fluidics as a new tool to investigate hydrate crystallization: Insights into the memory effect. *Chemical Engineering Science,* Volume 123, pp. 564-572.

Makogon, Y., Holditch, S. A. & Makogon, T., 2007. Natural gas-hydrates - Apotetial energy source for the 21st Century. *Journal of Petroleum Science and Engineering,* 56(1-3), pp. 14-31.

Mekala, P., Babu, P., Sangwai, J. S. & Linga, P., 2014. Formation and Dissociation Kinetics of Methane Hydrates in Seawater and Silica Sand. *Energy & Fuels,* Volume 28, pp. 2708-2716.

Millam, J., Klos, K. & Sommerville, I. D., n.d. *http://www.reasons.org/.* [Online] Available at: http://www.reasons.org/articles/water-designed-for-life-part-2-of-7 [Accessed 23 03 2015].

Mines, C. S. o., 2009. *Center for Hydrate Research.* [Online] Available at: http://hydrates.mines.edu/CHR/Software.html [Accessed 19 12 2015].

Mirshafieyan, S. S. & Guo, J., 2014. Silicon colors: spectral selective perfect light absorption in single layer silicon films on absorption in single layer silicon films on. *Optics Express,* 22(25).

Miyawa, J. H. & Schulman, S. G., 2001. Ultraviolet-Visible Spectrophotometry . In: L. Ohannesian & A. J. Streeter, eds. *Handbook of Pharmaceutical Analysis.* New York, Basel: Taylor & Francis e-library.

Nerheim, A., T.M, S. & Samuelsen E, J., 1994. *Laser Light Scattering Studies of Natural Gas Hydrates.* New Orleans, LA, USA, SPE.

Ohmura, R. et al., 2005. Clathrate hydrate crystal growth in liquid water saturated with a guest substance: Observations in a methane + water system. *Crystal grwoth & design,* 5(3), pp. 953-957.

Ormestad, H., 2009. *Store Norske Leksikon.* [Online] Available at: https://snl.no/varmeledning

Radhakrishnan, R., Demurov, A., Herzog, H. & Trout, B. L., 2003. A consistent and verifiable macroscopic model for the dissolution of liquid CO2 in water under hydrate forming conditions.. *Energy Convesrsion & Management,* Volume 44, pp. 771-780.

Rangel-German, E. & Kovscek, A. R., 2006. A micromodel investigation of two-phase matrix-fracture transfer mechanism. *WATER RESOURCES RESEARCH,* Volume 42.

Sachs, W. & Meyn, V., 1994. *Pressure and temperature dependence of the surface tension in the system natural gas/water. Principles of investigation and the first precise experimental data for pure methan/water at 25 C up to 46.8 MPa,* Clausthal-Zellerfeld, Germany: ELSEVIER- Science.

Selley, R. C., 1998. *Elemetns of Petroleum Geology.* 2nd ed. San Diego: ACADEMIC PRESS.

Semiconductor, V., n.d. *www.virginiasemi.com.* [Online] Available at: http://www.virginiasemi.com/pdf/Basic%20Mechanical%20and%20Thermal%20Properties%20of%20Silicon.pdf
[Accessed 12 12 2015].

Servio, P. & Englezos, P., 2003. Morphology of Methane and Carbon Dioxide Hydrates Formed from Water Droplets. *AIChE Journal,* 49(1), pp. 269-276.

Sloan, E. D., 1998. *Clathrate Hydrates of Natural Gases.* 2nd ed. ed. New York: Marcel Decker, Inc..

Sloan, E. D. & Koh, C. A., 2008. *Clathrate Hydrates of Natural Gases.* 3rd ed. ed. Boca Raton, FL 33487-2742: CRC Press, Taylor & Francis Group.

Stillinger, F. H., 1980. Water Revisited. *Science,* 209(4455), pp. 451-457.

Sun, C. Y. et al., 2010. Studies on hydrate film growth. *Royal Society of Chemistry,* Volume 106, pp. 77-100.

Taylor, C. E. & Kwan, J. T., 2004. *Advances in the study of Gas Hydrates.* 1st ed. New York: Kluwer Academic/Plenum Publishers.

Tohidi, B., Anderson, R., Clennel, B. M. & Burgass, R. W., 2001. Visual observation of gas-hydrate formation and disssociaton in synthetic porous media by means of glass micromodels. *Geology,* 29(9), pp. 867-870.

Turner, D. J., Cherry, R. S. & Sloan, E. D., 2005. *Sensitivity of methane hydrate phase equilibra to sediment pore size,* Colorado: Elsevier-Science Direct.

Uchida, T. et al., 2004. Decomposition of methane hydrates in sand, sandstone, clays, and glass beads. *JOURNAL OF GEOPHYSICAL RESEARCH,* Volume 109.

Waite, W., Winters, W. & Mason, D., 2004. Methane hydrate formation in partially water saturated Ottawa sand. *American Mineralogist,* 89(8-9), pp. 1202-1207.

Wallis, G. & Pomerantz, D. I., 1969. Field Assisted Glass-Metal Sealing. *Journal of Applied Physics,* 40(10), pp. 3946-3949.

Yang, S., Cho, S., Lee, H. & Lee, C., 2001. Measurement and prediction of phase equilibria for water + methane in hydrate forming conditions. *Fluid Phase equilibria,* 185(1-2), pp. 53-63.

Zatsepina, O. Y. & Buffet, B., 1998. Thermodynamic conditions for the stability of gas hydrate in the seafloor. *Journal of Geophysical research*, 10 October, pp. 24127-24139.